In presenting the dissertation as a partial fulfillment of the requirements for an advanced degree from the Georgia Institute of Technology, I agree that the Library of the Institution shall make it available for inspection and circulation in accordance with its regulations governing materials of this type. I agree that permission to copy from, or to publish from, this dissertation may be granted by the professor under whose direction it was written, or, in his absence, by the dean of the Graduate Division when such copying or publication is solely for scholarly purposes and does not involve potential financial gain. It is understood that any copying from, or publication of, this dissertation which involves potential financial gain will not be allowed without written permission.

VISCOUS FLUID FLOW UNDER THE INFLUENCE OF A RESONANT ACOUSTIC FIELD

A THESIS

Presented to

The Faculty of the Graduate Division

by

Kenneth Rodman Purdy

In Partial Fulfillment

of the Requirements for the Degree

Doctor of Philosophy in the

School of Mechanical Engineering

Georgia Institute of Technology

June, 1963

78
12 R

VISCOUS FLUID FLOW UNDER THE INFLUENCE OF A RESONANT ACOUSTIC FIELD

Approved:

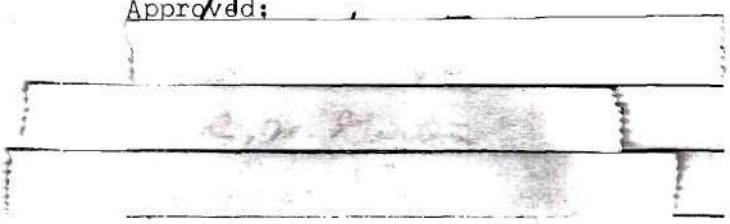

Date approved by Chairman: 5-21-63

ACKNOWLEDGMENTS

The author is indebted to the many individuals who have contributed to the success of this work. In particular, he would like to express his sincere appreciation to his Thesis Co-advisors, Dr. Thomas W. Jackson and Dr. C. W. Gorton for their continued encouragement and advice and to Dr. Henderson C. Ward, who served as a member of the thesis committee. The research collaboration with Mr. C. C. Oliver was an experience for which the author will always feel grateful. He would also like to express his gratitude to Dr. J. M. Spurlock for his contributions to this work.

An extreme debt of gratitude is owed to his parents for their continued guidance and to Mr. L. P. Ordway, who made the author's undergraduate education possible. His deepest appreciation goes to his wife and children for their infinite patience and their unending source of strength.

Finally, the author would like to express his appreciation to E. I. du Pont de Nemours, Inc., for a Summer Research Grant and to the National Science Foundation, for a Science Faculty Fellowship.

TABLE OF CONTENTS

LIST OF TABLES

LIST OF ILLUSTRATIONS

LIST OF ILLUSTRATIONS (Continued)

SUMMARY

The effect of a resonant acoustic field on laminar internal flow was investigated analytically and experimentally. The analytical study was concerned with two-dimensional compressible flow between infinite parallel plates. Sanders (3), in a recent experimental investigation, showed that the density variation of a gas (air) in a resonant acoustic field is essentially the same as that which is predicted by first order acoustics. Therefore, the influence of sound was introduced into the governing equations by: (i) assuming that the density variation of a gas is the same as that predicted by first order acoustics and (ii) assuming that the compression-rarefaction process is isentropic.

The governing equations were obtained by: (i) assuming that the properties of the fluid may be expressed as the sum of a time-mean component and a time-dependent component (this is the same technique which is used in the treatment of turbulent flow and was proposed for periodic laminar flow by Lin (2)); (ii) assuming the orders of magnitude for the characteristic values of the properties; and, (iii) performing an order of magnitude analysis of the dimensionless form of the continuity and momentum equations for two-dimensional flow and the time average of these equations. This technique reduced the governing equations to a set of four linear, partial differential equations; two governing the time-dependent velocity components and two governing the time-mean velocity components. The time-dependent velocity components, the time-mean velocity components, and the stream function were obtained for a first approximation utilizing these equations.

The theoretical analysis predicted the presence of standing vortices in the channel both with and without through flow. The vortices were one-quarter wavelength long and the thickness of the larger vortices (the ratio of the width of a large vortex to the half width of the channel) was shown to be solely a function of the parameter M/M_o^2, where M is the Mach number based on the average through-flow velocity and M_o is the Mach number based on the maximum amplitude of the x-component of the time-dependent velocity.

The experimental investigation was concerned with circular tube flow since it was found that channel flow (in conjunction with a resonant acoustic field) could not be satisfactorily approximated by a rectangular duct. This study utilized tobacco smoke as a tracer in atmospheric air and an axial beam of light to visualize the flow field in a circular tube. With this system the existence of standing vortices was verified and the thickness of the larger vortices was shown to be solely (at least to the accuracy of the measurements that were made) a function of the parameter M/M_o^2.

Finally, the experimental heat transfer data of Jackson (1) and Eastwood (2) were qualitatively explained in the region of flow where the average through-flow velocity was less than the maximum amplitude of the time-dependent x-component of velocity. In addition, the threshold level data of Eastwood (the sound level below which sound no longer affects the local heat transfer rate in a horizontal isothermal tube) were correlated by $M/M_o^2 \approx 63$.

NOMENCLATURE

Symbol		Units
a	Half width of the channel	ft
a_1	Constant	
a_2	Constant	
A	Constant	
$\bar{A}$	Inside diameter of the bellmouth tube	in
b_1	Constant	
b_2	Constant	
B	Constant	
$\bar{B}$	Minimum diameter of the main-stream flow	in
c	Isentropic speed of sound	ft/sec
c_1	Constant	
c_2	Constant	
c_p	Constant pressure specific heat	$ft^2/sec^2-{}^oR$
C_p	Pressure correction factor	
c_v	Constant volume specific heat	$ft^2/sec^2-{}^oR$
d_1	Constant	
d_2	Constant	
db	Decibels	
e_1	Constant	
e_2	Constant	
E	Constant	
f	Function	
f_1	Function	

f_2	Function	
F_1	Function	
F_2	Function	
F_3	Function	
F_4	Function	
g	Function	
i	$\sqrt{-1}$	
k	Ratio of the specific heats - c_p/c_v	
m_1, m_2	Constants	
M	Mach number based on U	
M_o	Mach number based on U_o	
n	Integer (1,2,3,$\cdots$)	
p	Pressure of a fluid	lb/ft^2
p_1	Time-dependent pressure	lb/ft^2
$\bar{p}$	Time-mean pressure	lb/ft^2
P	Root-mean-square of p_1	microbar
Q	Volumetric flow rate	ft^3/sec
R	Gas constant	$ft^2/sec^2-{}^oR$
s	Entropy	$ft^2/sec^2-{}^oR$
SPL	Sound-pressure level (re 0.0002 μbar)	db
t	Time	sec
T	Absolute temperature of a fluid	^oR
u	X-component of velocity	ft/sec
u_1	Time-dependent component of u	ft/sec
$\bar{u}$	Time-mean component of u	ft/sec

U	Average through-flow velocity based on the mass flow rate	ft/sec
U_o	Maximum amplitude of $\|u_1\|$	ft/sec
$\bar{U}$	Characteristic velocity for $\bar{u}$	ft/sec
v	Y-component of velocity	ft/sec
v_1	Time-dependent component of v	ft/sec
$\bar{v}$	Time-mean component of v	ft/sec
V_o	Characteristic velocity for v_1	ft/sec
$\bar{V}$	Characteristic velocity for $\bar{v}$	ft/sec
w	Mass flow rate	lb-sec/ft
x	Space coordinate	ft
X	X-component of the body force	lb/ft^3
X_1, X_2	Functions	
y	Space coordinate	ft
Y	Y-component of the body force	lb/ft^3
Y_1, Y_2	Functions	
z	Space coordinate	

Greek Symbols

γ_m	Vortex size	
δ	$2\,\delta_{ac}/\lambda$ or a number much less than one	
δ_{ac}	A.C. boundary layer thickness	ft
θ	Order of magnitude	
λ	Wavelength	ft
μ	Dynamic viscosity of a fluid	$lb\text{-}sec/ft^2$
ν	Kinematic viscosity of a fluid	ft^2/sec^2

π	3.14159	
ρ	Density of a fluid	$lb\text{-}sec^2/ft^4$
ρ_1	Time-dependent component of ρ	$lb\text{-}sec^2/ft^4$
$\bar{\rho}$	Time-mean component of ρ	$lb\text{-}sec^2/ft^4$
ψ	Stream function	ft^2/sec
ω	Circular frequency	ft/ft-sec

Subscripts

o	Time mean of the property at x = 0, y = a
1n	Fourier coefficient (n = 1,2,3,...)

CHAPTER I

INTRODUCTION AND HISTORICAL BACKGROUND

Statement of Intent

The intent of this investigation is to conduct an analytical and an experimental study of the effect of a resonant acoustic field upon the laminar flow of a compressible fluid. The results of these studies are then to be used to qualitatively explain the local variations in heat transfer rates which have been experimentally determined by Jackson, et al., (1, 2).

Acoustic Fields

Although a knowledge of the properties of an acoustic field is not necessary to follow the analysis to be presented in Chapter II, it is felt that a summary of the salient characteristics of acoustic fields will be helpful in understanding the significance of the assumptions which will stem from first order acoustics. The model which will be used to illustrate these characteristics is shown in Figure 1. It consists of an ideal,

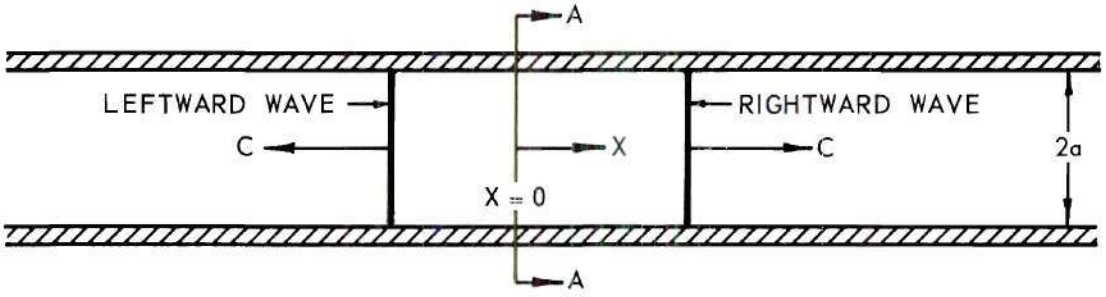

Figure 1. Plane Wave Channel.

inviscid gas between infinite, parallel plates which are separated by a distance 2a. This model will be used again in Chapter II; however, the ideal gas will then be assumed to be a Newtonian fluid.

It can be shown that a small pressure or velocity disturbance travels with the isentropic speed of sound. For an ideal gas this is

$$c^2 \equiv \left.\frac{\partial p}{\partial \rho}\right|_s = k\,RT = k\,p/\rho \quad . \tag{1.1}$$

Two such waves are shown in Figure 1; one wave is shown traveling to the left, a leftward wave, and the other is shown traveling to the right, a rightward wave. These plane waves which travel in the x-direction are governed by the one-dimensional wave equation. (The wave equation is derived in detail in Appendix A.) The velocity wave equation is

$$\frac{\partial^2 u_1}{\partial t^2} = c_o^2 \frac{\partial^2 u_1}{\partial x^2} \quad . \tag{1.2}$$

Similar equations may also be written for density and pressure waves. They all express the behavior of the deviation of velocity, density and pressure from their undisturbed or time-mean values. That is, the true velocity, density and pressure are expressed as the sum of a time-mean and a time-dependent component as follows:

$$u(x,t) = \bar{u}(x) + u_1(x,t) \tag{1.3a}$$

$$\rho(x,t) = \bar{\rho}(x) + \rho_1(x,t) \tag{1.3b}$$

$$p(x,t) = \bar{p}(x) + p_1(x,t) \tag{1.3c}$$

where the bar superscript denotes the time-mean and the subscript "1"

denotes the deviation of the property from its mean value. In the illustrations to be given here the fluid is assumed to be "stagnant," $\bar{u}(x) = 0$, and therefore the time-mean density and pressure will be constant and equal to ρ_o and p_o, respectively. By their definition, acoustic waves are such that $u_1 \ll c_o$, $\rho_1 \ll \rho_o$ and $p_1 \ll p_o$ and finally, the speed of sound in the wave equation is based on ρ_o and p_o and therefore $c_o^2 = k\, p_o/\rho_o$.

The general solution to the velocity wave equation is of the form

$$u_1(x,t) = F_1(x - c_o t) + F_2(x + c_o t) \tag{1.4}$$

where F_1 and F_2 are arbitrary functions of their arguments. $F_1(x - c_o t)$ represents a rightward wave and $F_2(x + c_o t)$ represents a leftward wave. To illustrate the properties of acoustic waves, two examples will now be given.

Example 1. The first example will consist of plane velocity waves which are being generated by a diaphragm at plane A-A that is oscillating with a simple harmonic motion such that the velocity, u_1, at $x = 0$, is

$$u_1(0,t) = - U_o \cos(\omega t) \tag{1.5}$$

The solution of the wave equation for this case is

For $0 \leq x$

$$F_1(x - c_o t) = \text{REAL}\left[- U_o \exp\left\{- i \frac{\omega}{c_o} (x - c_o t)\right\}\right] \tag{1.6a}$$

$$F_2(x + c_o t) = 0 \tag{1.6b}$$

or

$$u_1(x,t) = - U_o[\cos(\omega x/c_o) \cos(\omega t) + \sin(\omega x/c_o) \sin(\omega t)] \quad (1.6c)$$

and for $0 \geq x$

$$F_1(x - c_o t) = 0 \quad (1.7a)$$

$$F_2(x + c_o t) = \text{REAL}\left[- U_o \exp\left\{- i \frac{\omega}{c_o} (x + c_o t)\right\}\right] \quad (1.7b)$$

or finally

$$u_1(x,t) = - U_o[\cos(\omega x/c_o) \cos(\omega t) - \sin(\omega x/c_o) \sin(\omega t)] \quad (1.7c)$$

It should be noted that the leftward waves have been omitted in the region for which x is greater than zero and that the rightward waves have been omitted in the other half of the channel. These omissions assume that there are no reflected waves in the infinite channel. The velocity wave pattern is shown graphically in Figure 2. The wavelength, λ, of the velocity wave is the value of x for which

$$\frac{\omega x}{c_o} = 2\pi$$

or

$$\lambda \equiv \frac{2\pi c_o}{\omega} \quad . \quad (1.8)$$

Example 2. The second example will consist of both leftward and rightward velocity waves of the same strength throughout the entire channel and such that

$$u_1(0,t) = - U_o \cos(\omega t) \quad (1.5)$$

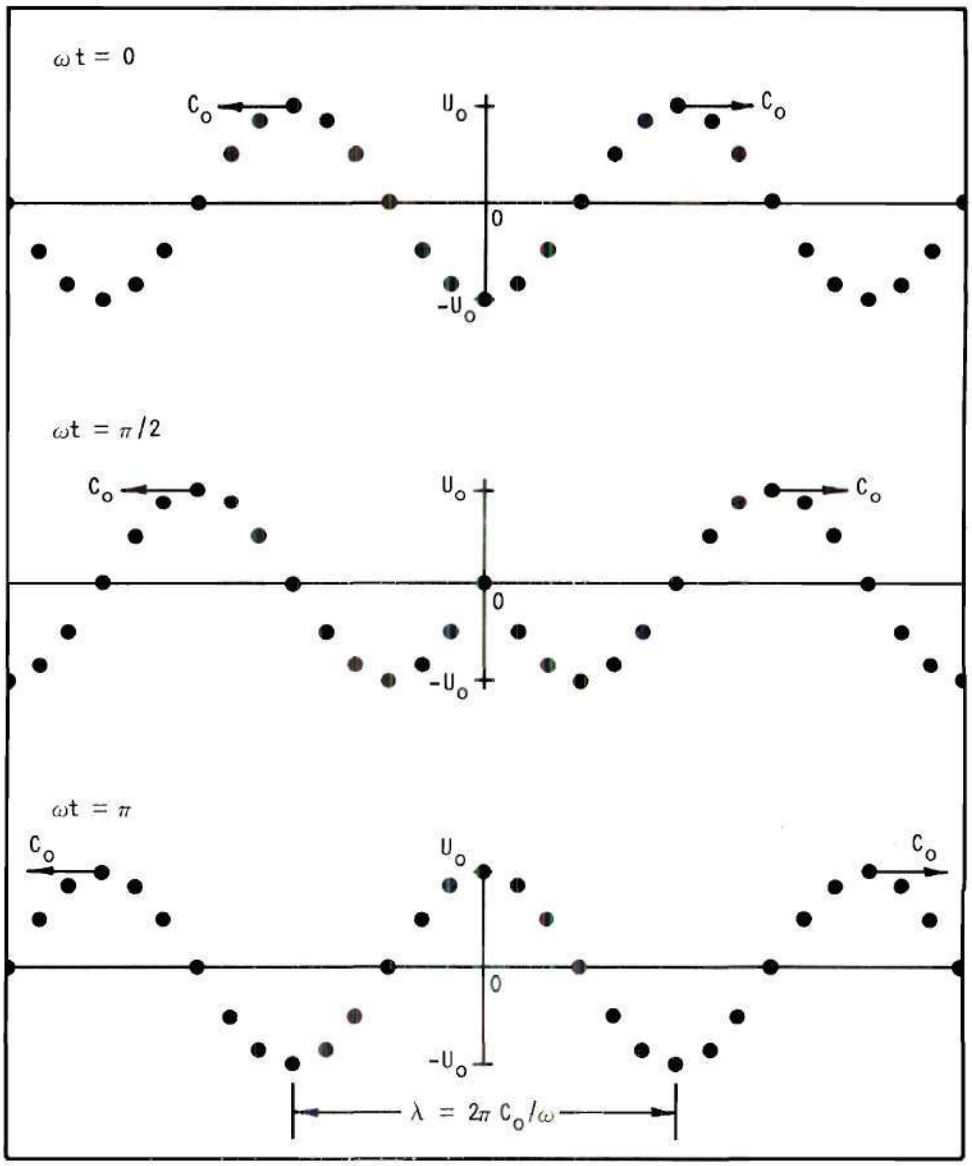

Figure 2. Velocity Wave Pattern for Example 1.

The solution for this case is

$$F_1(x - c_o t) = \text{REAL}\left[-\frac{U_o}{2} \exp\left\{-i \frac{\omega}{c_o}(x - c_o t)\right\}\right] \qquad (1.9a)$$

$$F_2(x + c_o t) = \text{REAL}\left[-\frac{U_o}{2} \exp\left\{-i \frac{\omega}{c_o}(x + c_o t)\right\}\right] \qquad (1.9b)$$

or finally

$$u_1(x,t) = -U_o \cos(\omega x/c_o) \cos(\omega t) \qquad (1.9c)$$

The pressure distribution may now be determined from the reduced momentum equation (equation A.26) as follows:

$$\frac{\partial p_1}{\partial x} = -\rho_o \frac{\partial u_1}{\partial t} = -\rho_o \omega U_o \cos(\omega x/c_o) \sin(\omega t)$$

or after integrating with respect to x

$$p_1(x,t) = -\rho_o c_o U_o \sin(\omega x/c_o) \sin(\omega t) \qquad (1.10)$$

The density may be determined from the reduced continuity equation (equation A.28) as follows:

$$\frac{\partial \rho_1}{\partial t} = -\rho_o \frac{\partial u_1}{\partial x} = -\frac{\rho_o \omega U_o}{c_o} \sin(\omega x/c_o) \cos(\omega t)$$

or after integrating with respect to t

$$\rho_1(x,t) = -\rho_o M_o \sin(\omega x/c_o) \sin(\omega t) \qquad (1.11)$$

where

$$M_o \equiv U_o/c_o \ . \qquad (1.12)$$

The velocity, density and pressure represented in dimensionless form are

$$u_1'(x',t') \equiv u_1/U_o = -\cos(\pi x')\cos(\pi t') \qquad (1.13)$$

$$p_1'(x',t') \equiv p_1/p_o = -M_o \sin(\pi x')\sin(\pi t') \qquad (1.14)$$

$$\rho_1'(x',t') \equiv \rho_1/\rho_o = -M_o \sin(\pi x')\sin(\pi t') \qquad (1.15)$$

where $x' \equiv 2x/\lambda$ and $t' \equiv \omega t/\pi$. (1.16)

It can be seen from equations 1.13, 1.14 and 1.15 that the deviation in the property values will be small (the wave will be an acoustic wave) if the Mach number, M_o, is small. The pressure distribution in a resonant channel is shown in Figure 3 for various dimensionless positions and times. It should be noted from this figure that the pressure has its maximum deviation from the mean pressure at the positions labeled "L". These positions are referred to as pressure loops whereas the positions where the pressure deviation is zero are referred to as pressure nodes and are labeled "N" in Figure 3.

A logical question which should be asked at this point is, how well do these equations from one-dimensional acoustics predict the properties of a real gas? This question has been answered in part by Sanders (3) who has these concluding remarks:

> Because of the fluctuating brightness of the arc lamp, the output of the photomultiplier-shlieren constructed for acoustic measurement varied erratically, and in order to obtain accurate measurements, the vibrating knife edge was introduced to permit the continuous determination of the sensitivity. The average sensitivity was 7 amps/gm/cm^3, and it was possible to detect (in air) AC density differences with amplitudes as small as 10^{-9} gm/cm^3. This means that a fractional density difference of 10^{-4} can be measured with a 1% precision. The space resolution of this instrument is limited by the

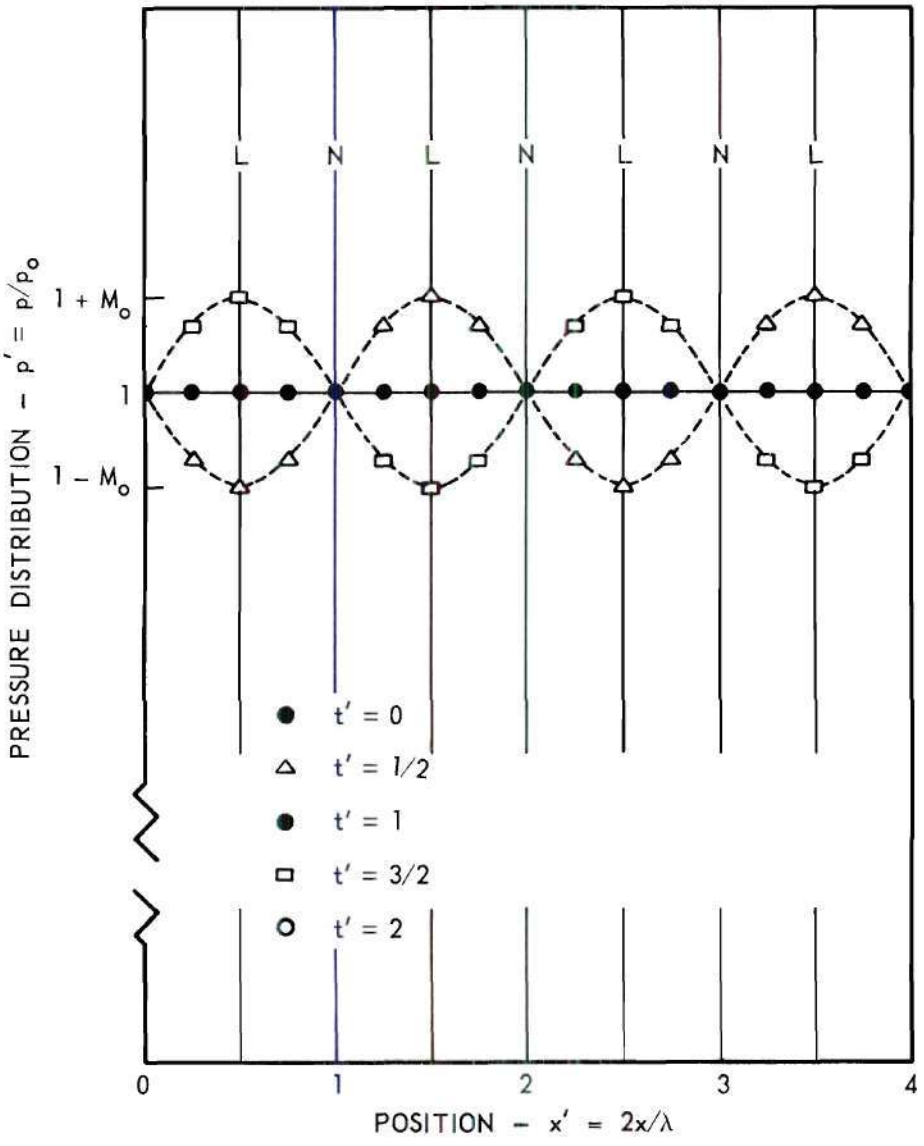

Figure 3. Pressure Distribution in a Resonant Channel.

diffraction taking place at the defining aperture, so that details of the density distribution smaller than 0.03 cm cannot be resolved.

The photomultiplier-schlieren was first employed to investigate the acoustic field within a rectangular resonant tube. The density difference profiles were determined for a series of resonances with frequencies between 348 and 5080 cps and with intensities from 84 to 144 decibels. In all cases, the experimental results were in excellent agreement with the one dimensional standing wave predicted by first order acoustics.

Therefore, the density deviations have been shown experimentally to be essentially the same as those predicted by equation 1.15. Although the velocity of sound for a small disturbance is very accurately predicted by assuming that the compression-rarefaction process is isentropic and Sanders has shown that the deviations in pressure are also accurately predicted by equation 1.14, equation 1.13 is not a sufficient representation of the velocity fluctuations since a viscous gas must satisfy the no-slip boundary condition.

In view of Sanders' studies, it will be assumed that the pressure and density distributions in a viscous, ideal gas are adequately represented by equations 1.14 and 1.15, respectively. The velocity distribution for such a gas will be determined in Chapter II.

Historical Background

Two very excellent reviews of the literature pertinent to the work being presented here have been given by Sanders (3) and Fand (4) and, therefore, it would be superfluous to give a complete review here. Sanders' review is primarily concerned with the phenomena that occur in a resonant column of air (a Kundt's tube) while Fand's review is devoted to the secondary flows that are generated when a resonant acoustic field interacts with a solid boundary. Since these reviews exit, only the literature directly associated with the present study will be given.

In 1883 Lord Rayleigh (5) presented the first analytical explanation of the steady circulations that were experimentally observed when a fluid was subjected to vibratory motion. His opening remarks are very interesting and they will be quoted here to emphasize the insufficiency of first-order acoustic theory when one is attempting to explain real fluid effects.

> Experimenters in Acoustics have discovered more than one set of phenomena apparently depending for their explanation upon the existence of regular currents of air resulting from vibratory motion, of which theory has as yet rendered no account. This is not, perhaps, a matter for surprise, when we consider that such currents, involving as they do circulation of the fluid, could not arise in the absence of friction, however great the extent of vibration. And even when we are prepared to include in our investigations the influence of friction, by which the motion of fluid in the neighbourhood of solid bodies may be greatly modified, we have no chance of reaching an explanation, if, as usual, we limit ourselves to the supposition of infinitely small motion and neglect the squares and higher powers of the mathematical symbols by which it is expressed.

Thus, in Rayliegh's opinion, the steady circulations can only be predicted analytically when the fluid motion is assumed to be governed by the viscous equations of motion (Navier-Stokes equations).

The third problem in his paper, related to the circulations observed by Dvorak (6) in Kundt's tubes, was a special case of the problem that will be presented in Chapter II. He investigated the case for which there was no through flow in the direction of the sound waves. The problem to be presented here will consider through flow and, therefore, Rayleigh's problem will be a special case—that of no through flow.

Rayleigh's initial premise, that the compression-rarefaction process is isothermal, was not defended by him. The isothermal process requires a low frequency vibratory motion and this introduces non-linear terms in the equation of motion that he did not consider. Rayleigh's solution was

corrected on this point when Westervelt (7), in 1953, resolved the problem with the assumption that the process is isentropic rather than isothermal.

Both Rayleigh and Westervelt predicted that the mean motion of the fluid, as shown in Figure 4, is from the velocity loops to the velocity nodes along the wall and vice-versa near the plane of symmetry.

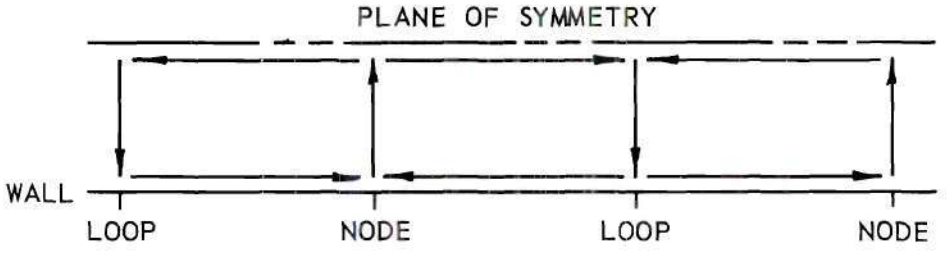

Figure 4. Rayleigh's Circulation Patterns.

The first experimental verification of Rayleigh's solution was accomplished by Andrade (8) in 1931. Andrade was interested in studying the flow patterns in a resonant tube by introducing foreign particle tracers. He analytically investigated the behavior of spherical particles in the presence of a vibrating viscous medium by using Koenig's (9) expression for the ratio of the maximum velocities, or of the maximum amplitudes of motion, of a spherical particle in vibrating air. This analysis showed that tobacco smoke particles in air follow the vibratory air motion to within 0.12 per cent for a frequency of 2000 cps and to within 0.042 per cent for a frequency of 1200 cps. Thus for frequencies less than approximately 2000 cps tobacco smoke will serve as an excellent tracer.

Andrade obtained some very good photographic data of the streamlines in a resonant tube by using a mixture of tobacco smoke and air. The agreement with the patterns predicted by Rayleigh was excellent when one considers that Rayleigh's solution was for channel flow.

Figure 5, a reproduction from Andrade's paper, compares the results of his photographic streamline patterns, shown on the right-hand side of the figure, with those from Rayleigh's modified solution, shown on the left-hand side. The stream numbers are not intended to be the same. It should also be noted that Andrade verified the direction of rotation predicted by Rayleigh.

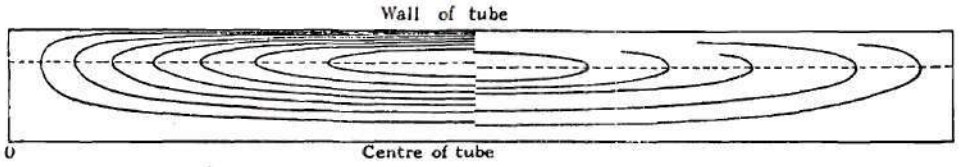

Figure 5. Comparison of Andrade's and Rayleigh's Streamline Patterns.

Resonant ducts reached engineering significance in the early 1950's when increasing demands for higher jet afterburner performance increased the occurrence and intensity of screeching combustion. The Lewis Laboratory Staff (10) has given an excellent summary of preliminary investigations into the characteristics of combustion screech in ducted burners. They concluded that screech in jet afterburners, a resonance phenomena which usually results in rapid destruction of the combustor shell and other combustor parts shortly after its onset, is linked to the transverse mode of acoustic resonance while the screaming effects in rocket engines have generally been correlated with the closed-closed pipe organ or the longitudinal mode of oscillation.

With this stimulus Jackson, Harrison and Boteler (11) conducted an experimental study of the effect of the longitudinal mode of resonant

acoustic vibrations on combined forced and free convection in a vertical, isothermal tube during 1954 and 1955. A more comprehensive program to study the effects of resonant acoustic fields on viscous fluid flow and convective heat transfer was initiated by Jackson in 1958. This study was primarily concerned with resonant longitudinal sound waves in a horizontal isothermal tube. The following effects on convective heat transfer were obtained by Jackson, et al. (1) and Eastwood (2).

1. For Reynolds numbers less than 33,000 the local heat transfer coefficient varied periodically with axial position in the tube as shown in Figure 6. The period of this variation was one half the wavelength of the impressed sound field. Local increases and decreases of up to 300 per cent occurred in the heat transfer coefficient with the maximum values of the local coefficient occurring at the velocity loops and the minimum values occurring at the velocity nodes. Sound threshold values, sound pressure levels below which no noticeable change in the heat transfer characteristics occurs, were found to increase with increasing Reynolds numbers. Only slight increases (30 per cent) were obtained in the overall heat transfer coefficient.

2. For Reynolds numbers greater than 40,000 a radical change in the local characteristics took place. The resonant sound field no longer increased the local coefficients as shown in Figure 7. The local coefficients still vary periodically in the axial direction; they still have the same period; but the position of the maximum value of the local coefficient has shifted to the velocity node and the minimum value has shifted to the velocity loop. This shift was accompanied by a radical lowering of the sound threshold level as shown in Figure 8. The overall heat transfer

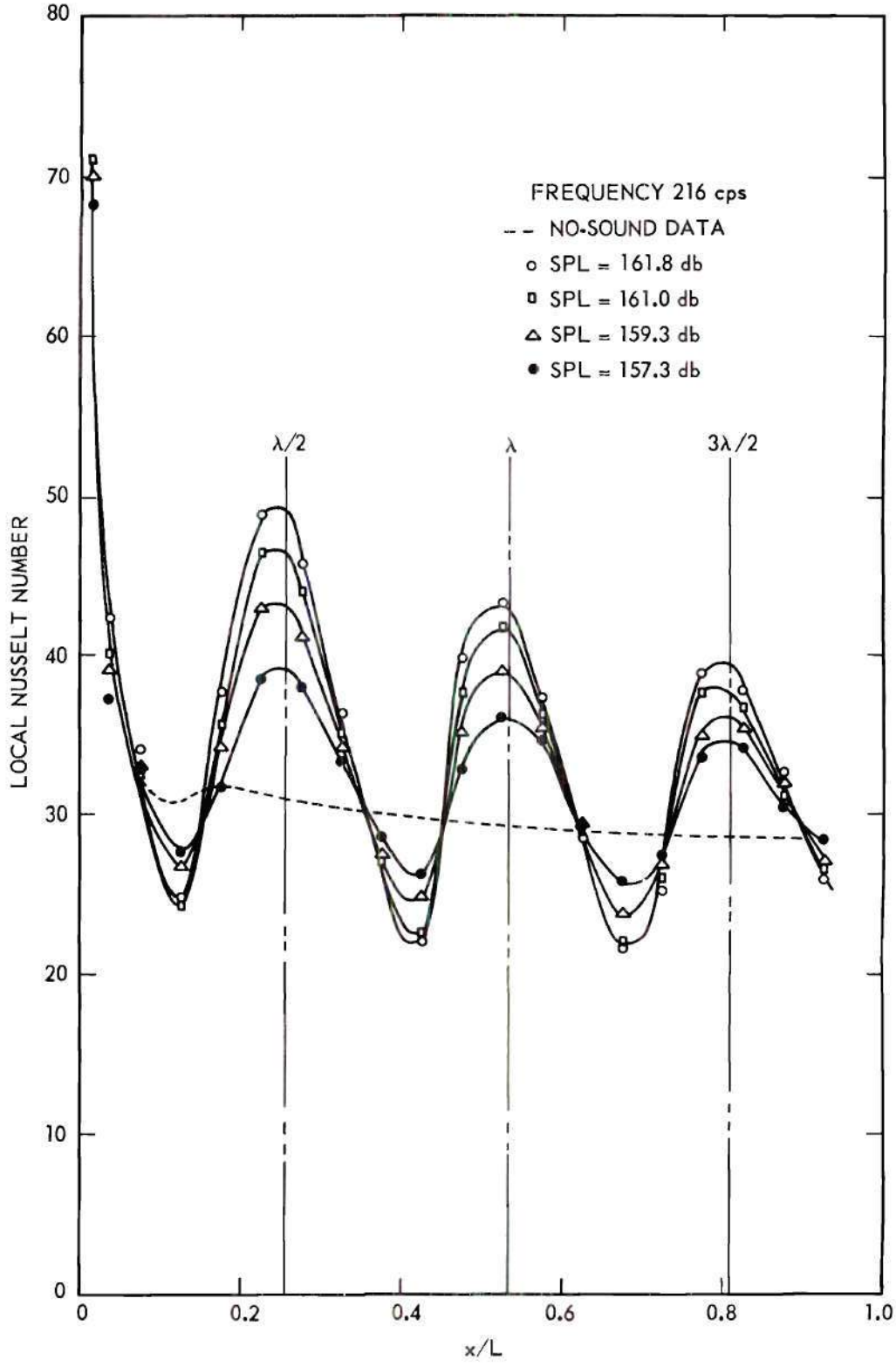

Figure 6. Local Nusselt Numbers Versus x/L for Various Sound-Pressure Levels, Reynolds Number ≈ 11,600.

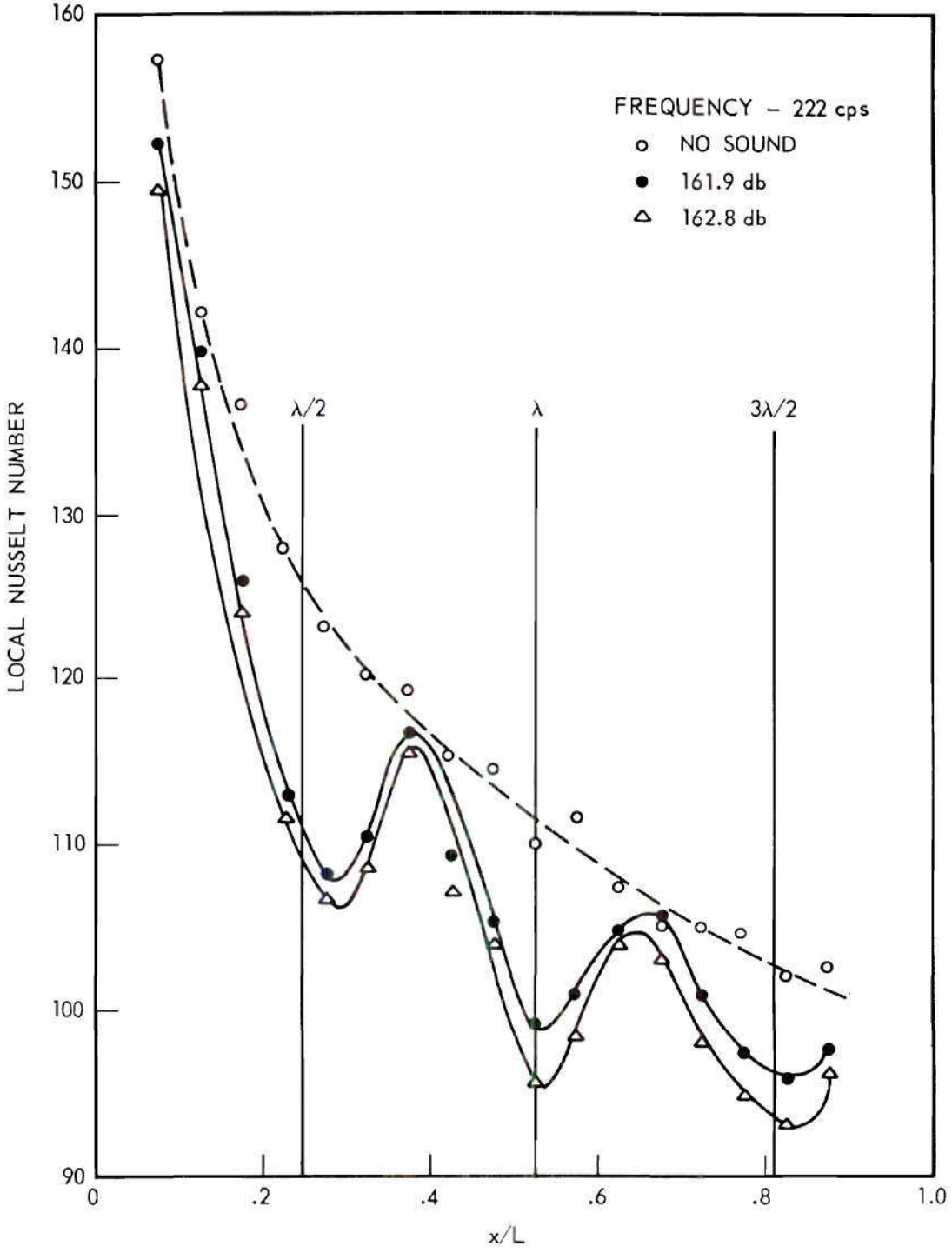

Figure 7. Local Nusselt Numbers Versus x/L for Various Sound-Pressure Levels, Reynolds Number ≈ 49,600.

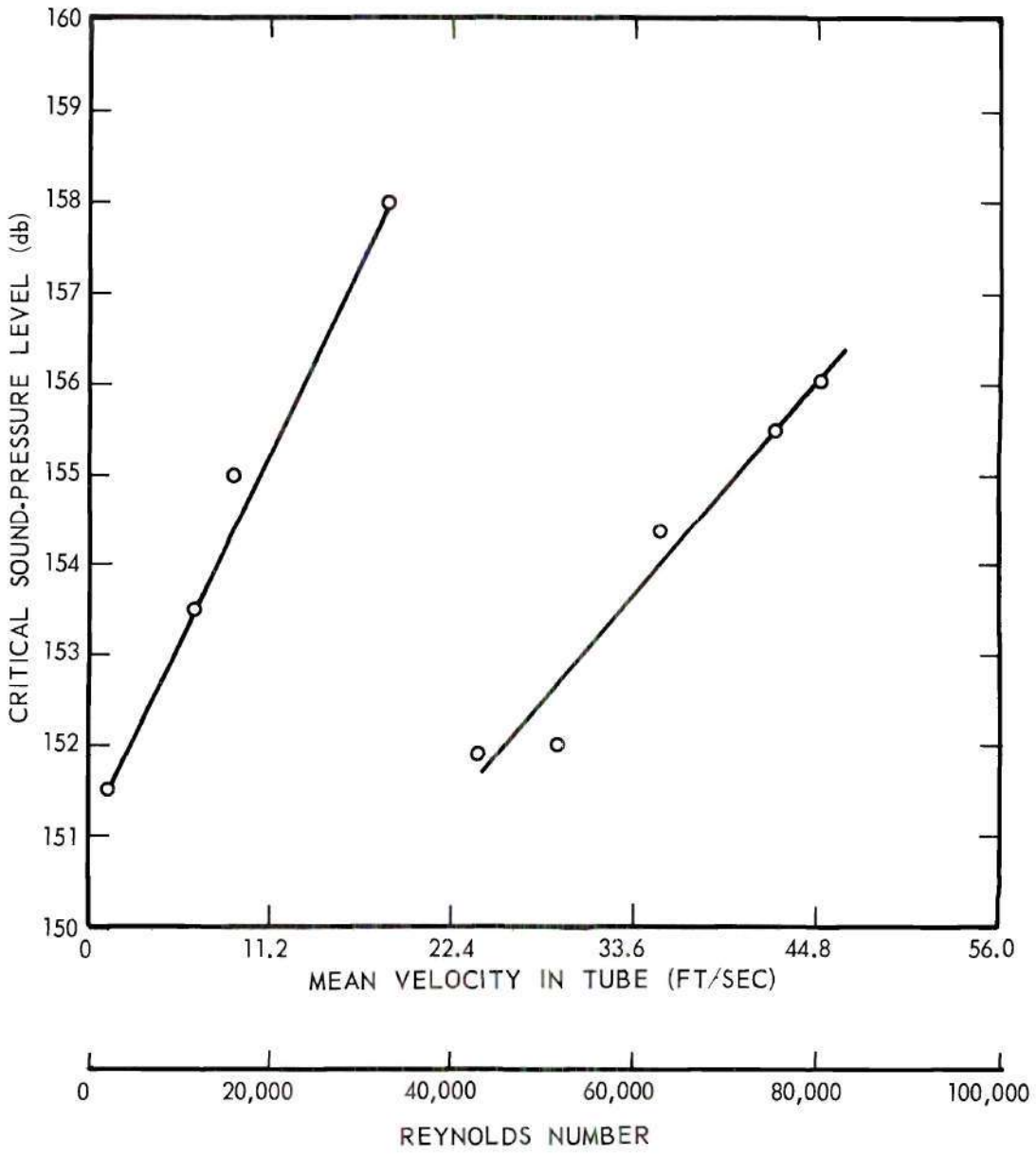

Figure 8. Critical Sound-Pressure Level Versus Reynolds Number.

coefficient was reduced in all cases for Reynolds numbers greater than 40,000 and less than 100,000.

It should be pointed out that the tube from which the above results were obtained had a 3.86 inch inside diameter, had a ten foot length and it had a bellmouth entrance so that the flow was neither hydrodynamically nor thermally developed. It can be concluded from the foregoing remarks that Jackson has uncovered two distinctly different phenomena; one associated with laminar flow and the other with turbulent flow.

Purpose and Scope

The purpose of this dissertation is to analytically predict the velocity field that is produced when resonant longitudinal sound waves are impressed upon laminar channel flow. The results of the analytical study will be qualitatively checked by a visualization study of resonant tube flow. The results of these studies will then be used to qualitatively explain the variations in the local heat transfer coefficients that were obtained by Jackson for laminar flow.

CHAPTER II

ANALYTICAL INVESTIGATIONS

Mathematical Statement of the Problem

The mathematical model of the problem as shown in Figure 9 consists of "fully" developed laminar flow between infinite parallel plates which are separated by a distance 2a. The fluid is assumed to be a viscous, ideal gas. Superimposed upon this flow is a resonant acoustic

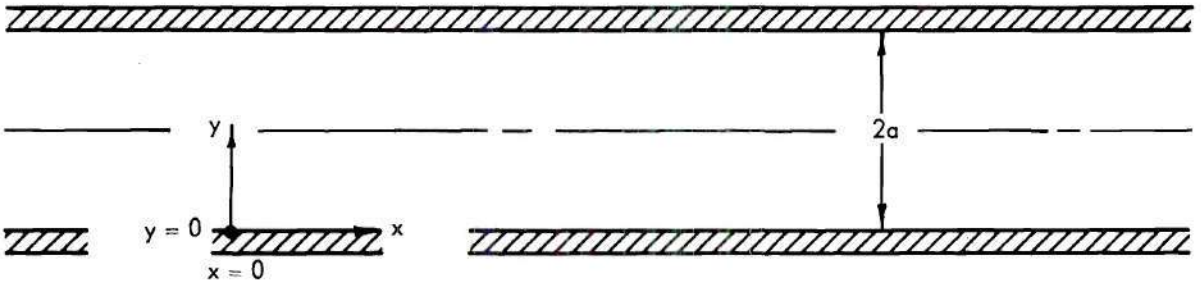

Figure 9. Model of the Flow System.

field (with a pressure node at x = 0). The flow is assumed to be independent of the z-direction but dependent upon time. For this model, the equations which govern the fluid motion are:

Continuity

$$\frac{\partial \rho}{\partial t} + \frac{\partial}{\partial x}(\rho u) + \frac{\partial}{\partial y}(\rho v) = 0 \qquad (2.1)$$

Momentum

$$\rho \left[\frac{\partial u}{\partial t} + u \frac{\partial u}{\partial x} + v \frac{\partial u}{\partial y}\right] = X - \frac{\partial p}{\partial x} \tag{2.2}$$

$$+ \frac{\partial}{\partial x}\left[\mu \left\{2 \frac{\partial u}{\partial x} - \frac{2}{3}\left(\frac{\partial u}{\partial x} + \frac{\partial v}{\partial y}\right)\right\}\right] + \frac{\partial}{\partial y}\left[\mu \left\{\frac{\partial u}{\partial y} + \frac{\partial v}{\partial x}\right\}\right]$$

and

$$\rho \left[\frac{\partial v}{\partial t} + u \frac{\partial v}{\partial x} + v \frac{\partial v}{\partial y}\right] = Y - \frac{\partial p}{\partial y} \tag{2.3}$$

$$+ \frac{\partial}{\partial y}\left[\mu \left\{2 \frac{\partial v}{\partial y} - \frac{2}{3}\left(\frac{\partial u}{\partial x} + \frac{\partial v}{\partial y}\right)\right\}\right] + \frac{\partial}{\partial x}\left[\mu \left\{\frac{\partial u}{\partial y} + \frac{\partial v}{\partial x}\right\}\right]$$

Reduction of the Governing Equations

Assumptions

In order to reduce the governing equations, the following assumptions are made:

(A1) It is assumed that the pressure may be written as the sum of a time-mean component $\bar{p}(x,y)$ and a periodic component $p_1(x,y,t)$. It is further assumed that $p_1(x,y,t)$ is directly related to the resonant acoustic field and is, therefore, periodic in both time t and position x. Thus

$$p(x,y,t) = \bar{p}(x,y) + p_1(x,y,t) \tag{2.4}$$

(A2) The density is also assumed to consist of a time-mean component $\bar{\rho}(x,y)$ and a periodic component $\rho_1(x,y,t)$, such that

$$\rho(x,y,t) = \bar{\rho}(x,y) + \rho_1(x,y,t) \tag{2.5}$$

For the flows to be considered, the spatial variations in density are assumed to have only a small effect upon the flow and, therefore, the time-mean density, $\bar{\rho}(x,y)$, is considered to be constant and equal to ρ_o.

(A3) The viscosity of the fluid is assumed to be constant and equal to μ_o.

(A4) Following Lin (12), it is assumed that the x-velocity component, $u(x,y,t)$, and the y-velocity component, $v(x,y,t)$, may be separated into time-mean and time-periodic components as follows:

$$u(x,y,t) = \bar{u}(x,y) + u_1(x,y,t) \tag{2.6}$$

and

$$v(x,y,t) = \bar{v}(x,y) + v_1(x,y,t) \tag{2.7}$$

In these equations the bar represents the time-mean and the subscript "1" refers to the periodic component.

(A5) The body forces are assumed to be negligible, i.e., $X = Y = 0$.

(A6) In order to perform an order of magnitude analysis it is necessary to introduce dimensionless forms of each of the properties in the governing equations. In addition, it is necessary to assume an order of magnitude for various quantities. A discussion of the dimensionless properties denoted by prime superscripts and the orders of magnitude listed below is given in Appendix B.

Dimensionless Variables.

$$x = \lambda/2\, x' \tag{2.8a}$$

$$y = \delta_{ac}\, y' \tag{2.8b}$$

$$t = \pi/\omega\, t' \tag{2.8c}$$

$$\bar{u} = \bar{U}\, \bar{u}' \tag{2.8d}$$

$$u_1 = U_o\, u_1' \tag{2.8e}$$

$$\bar{v} = \bar{V}\, \bar{v}' \tag{2.8f}$$

$$v_1 = V_o\, v_1' \tag{2.8g}$$

$$\bar{p} = p_o\, \bar{p}' \tag{2.8h}$$

$$p_1 = \rho_o c_o U_o\, p_1' \tag{2.8i}$$

$$\bar{\rho} = \rho_o\, \bar{\rho}' \tag{2.8j}$$

$$\rho_1 = \rho_o M_o\, \rho_1' \tag{2.8k}$$

$$\mu = \mu_o\, \mu' \tag{2.8l}$$

Orders of Magnitude.

$$\theta\left(\frac{\partial}{\partial x'}, \frac{\partial}{\partial y'}, \frac{\partial}{\partial t'}, \bar{u}', u_1', \bar{v}', v_1', \bar{p}', p_1', \bar{\rho}', \rho_1', \mu'\right) = 1 \tag{2.8m}$$

$$\theta\left(2\,\delta_{ac}/\lambda\ ,\ U_o/c_o\ ,\ \bar{U}/U_o\right) = \delta \tag{2.8n}$$

where

$$\delta_{ac} \equiv \sqrt{2\nu_o/\omega} \tag{2.9}$$

Method of Reduction

Under the foregoing assumptions the reduced governing equations can be obtained as follows:

Step 1. The time-dependent continuity equation is obtained by retaining only the terms in the dimensionless continuity equation (Appendix B,

equation B.15), which are of the order of magnitude of one. This results in the following dimensional equation

$$\frac{\partial \rho_1}{\partial t} + \rho_o \left\{\frac{\partial u_1}{\partial x} + \frac{\partial v_1}{\partial y}\right\} = 0 \qquad (2.10)$$

Step 2. The time-mean continuity equation is obtained by taking the time average over one period of the dimensionless continuity equation. This results in the following dimensional equation:

$$\frac{\partial \bar{u}}{\partial x} + \frac{\partial \bar{v}}{\partial y} = -\frac{1}{\rho_o}\left\{\frac{\partial}{\partial x}\left(\overline{\rho_1 u_1}\right) + \frac{\partial}{\partial y}\left(\overline{\rho_1 v_1}\right)\right\} \qquad (2.11)$$

Step 3. The time-dependent momentum equations are obtained by retaining only the terms in the dimensionless momentum equations (Appendix B, equations B.21 and B.22), which are of the order of magnitude of $1/\delta$. This results in the following dimensional equations:

$$\frac{\partial u_1}{\partial t} + \frac{1}{\rho_o}\frac{\partial p_1}{\partial x} = \nu_o \frac{\partial^2 u_1}{\partial y^2} \qquad (2.12)$$

and

$$\frac{\partial p_1}{\partial y} = 0 \qquad (2.13)$$

Step 4. Elimination of the pressure terms in the dimensionless momentum equations is accomplished by

(a) noting that $\frac{\partial^2 p'}{\partial x' \partial y'} = \frac{\partial^2 p'}{\partial y' \partial x'}$ and

(b) performing the following mathematical operations:

$$\frac{\lambda}{2\,\delta_{ac}} \frac{\partial}{\partial y'} \{\text{Equation B.21}\} - \frac{\partial}{\partial x'} \{\text{Equation B.22}\} \qquad (2.14)$$

Step 5. The time-mean momentum equation is obtained by first taking the time average over one period of equation 2.14 and then by retaining only the terms which are of the order of magnitude of $1/\delta$. This results in the following dimensional equation:

$$\mu_o \frac{\partial^3 \bar{u}}{\partial y^3} = \frac{\partial}{\partial y} \left[\overline{\rho_1 \frac{\partial u_1}{\partial t} + \rho_o \left(u_1 \frac{\partial u_1}{\partial x} + v_1 \frac{\partial u_1}{\partial y} \right)} \right] \qquad (2.15)$$

Solution of the Governing Equations

Method of Solution

Time-Dependent Solution. The equations to be solved for the time-dependent velocities $u_1(x,y,t)$ and $v_1(x,y,t)$ and the corresponding boundary conditions are

Continuity

$$\frac{\partial \rho_1}{\partial t} + \rho_o \left\{ \frac{\partial u_1}{\partial x} + \frac{\partial v_1}{\partial y} \right\} = 0 \qquad (2.10)$$

Momentum

$$\nu_o \frac{\partial^2 u_1}{\partial y^2} - \frac{\partial u_1}{\partial t} = \frac{1}{\rho_o} \frac{\partial p_1}{\partial x} \qquad (2.12)$$

Boundary Conditions

$$y = 0 : \quad u_1 = 0 , \quad v_1 = 0 \qquad (2.16a)$$

$$y = a : \frac{\partial u_1}{\partial y} = 0 , \quad v_1 = 0 \tag{2.16b}$$

The conditions at y = 0 correspond to the no-slip and solid-boundary conditions and the conditions at y = a correspond to the symmetry condition.

Equation 2.12 is a linear partial differential equation. The following is an outline of a method which may be used to solve this equation.

Step 1. Since the imposed resonant acoustic field has a circular frequency of ω, it is desirable to express the time-dependent components of density and pressure in the form of a Fourier series as follows:

$$\rho_1(x,y,t) = \text{REAL}\left[\sum_{n=1}^{\infty} \rho_{1n}(x,y)\, \exp(-in\omega t)\right] \tag{2.17}$$

and

$$p_1(x,y,t) = \text{REAL}\left[\sum_{n=1}^{\infty} p_{1n}(x,y)\, \exp(-in\omega t)\right] \tag{2.18}$$

Step 2. The time-dependent components of velocity will also be expressed in the form of Fourier series as follows:

$$u_1(x,y,t) = \text{REAL}\left[\sum_{n=1}^{\infty} u_{1n}(x,y)\, \exp(-in\omega t)\right] \tag{2.19}$$

$$v_1(x,y,t) = \text{REAL}\left[\sum_{n=1}^{\infty} v_{1n}(x,y)\, \exp(-in\omega t)\right] \tag{2.20}$$

Step 3. The foregoing expressions for density, pressure, and velocity are substituted into the time-dependent continuity and momentum

equations (equations 2.10, 2.12 and 2.13), and the factors of $\exp(-in\omega t)$, for $n = 1,2,3,\cdots$, are then equated to zero. This results in the following set of linear partial differential equations:

Factors of $\exp(-i\omega t)$

$$\frac{\partial u_{11}}{\partial x} + \frac{\partial v_{11}}{\partial y} = \frac{i\omega}{\rho_o} \rho_{11} \tag{2.21}$$

$$\nu \frac{\partial^2 u_{11}}{\partial y^2} = - i\omega\, u_{11} + \frac{1}{\rho_o} \frac{\partial p_{11}}{\partial x} \tag{2.22a}$$

and

$$\frac{\partial p_{11}}{\partial y} = 0 \tag{2.22b}$$

Factors of $\exp(-i2\omega t)$

$$\frac{\partial u_{12}}{\partial x} + \frac{\partial v_{12}}{\partial y} = \frac{i2\omega}{\rho_o} \rho_{12} \tag{2.23}$$

$$\nu_o \frac{\partial^2 u_{12}}{\partial y^2} = - i2\omega\, u_{12} + \frac{1}{\rho_o} \frac{\partial p_{12}}{\partial x} \tag{2.24a}$$

and

$$\frac{\partial p_{12}}{\partial y} = 0 \tag{2.24b}$$

Etc.

The solution to the above set of equations requires that the time-dependent components of density and pressure be known. The details of a

solution for a particular form of ρ_1 and p_1 are given in the section entitled "A Solution of the Time-Dependent Equations."

Time-Mean Solution. The equations to be solved for the time-mean velocities $\bar{u}(x,y)$ and $\bar{v}(x,y)$ and the corresponding boundary conditions are

Continuity

$$\frac{\partial \bar{u}}{\partial x} + \frac{\partial \bar{v}}{\partial y} = -\frac{1}{\rho_o}\left\{\frac{\partial}{\partial x}\left(\overline{\rho_1 u_1}\right) + \frac{\partial}{\partial y}\left(\overline{\rho_1 v_1}\right)\right\} \tag{2.11}$$

Momentum

$$\mu_o \frac{\partial^3 \bar{u}}{\partial y^3} = \frac{\partial}{\partial y}\left[\overline{\rho_1 \frac{\partial u_1}{\partial t} + \rho_o\left(u_1 \frac{\partial u_1}{\partial x} + v_1 \frac{\partial u_1}{\partial y}\right)}\right] \tag{2.15}$$

Boundary Conditions

$$y = 0: \quad \bar{u} = 0, \quad \bar{v} = 0 \tag{2.25a}$$

$$y = a: \quad \frac{\partial \bar{u}}{\partial y} = 0, \quad \bar{v} = 0 \tag{2.25b}$$

and

$$\text{for all } x: \quad \int_{y=0}^{a} \rho_o \bar{u}\, dy = \text{Constant} \tag{2.25c}$$

The first two conditions are no-slip and symmetry, respectively. The third condition requires a steady through flow in the x-direction and forms the basic difference between this study and the previous studies of Rayleigh (5) and Westervelt (7) which considered the special case of no through flow.

The foregoing equations may be solved by direct integration. The details of the solution are given in the section entitled "A Solution of the Time-Mean Equations."

A Solution of the Time-Dependent Equations

Additional Assumptions. In addition to the six assumptions given previously, the following assumptions are made:

(A7) The time-dependent component of pressure, $p_1(x,y,t)$, is assumed to be the same as the periodic component of pressure in a stationary inviscid fluid which is undergoing resonant acoustic vibrations (see equation 1.14, Chapter I). Thus $p_1(x,y,t)$ is given by

$$p_1(x,t) = \text{REAL}\left[-i\,\rho_o\,c_o\,U_o\,\sin(\omega x/c_o)\,\exp(-i\omega t)\right] \qquad (2.26)$$

This expression for p_1 was chosen not only because of its simplicity, but because the order of magnitude analysis showed that $\frac{\partial p_1}{\partial y} \ll \frac{\partial p_1}{\partial x}$. This implies that the pressure outside the "A.C." boundary layer is impressed upon this layer and is essentially unchanged with respect to the y-direction. Sanders (3) has shown experimentally, that the density variations and thus the pressure variations in a viscous gas undergoing resonant acoustic vibrations were the same as those in an inviscid gas.

(A8) In order to eliminate $\rho_1(x,y,t)$ from the foregoing equations it is now necessary to assume a relationship between the density and the pressure of the fluid. The time-mean density-pressure variation will be omitted from this analysis and, therefore, only the relationship between the density and the pressure during the compressions and rarefactions of the fluid will be considered. In addition to the assumption that the fluid is an ideal gas, it is also assumed that the compression-rarefaction process

is isentropic, i.e.

$$\rho = p/RT \ , \quad c_p = \text{constant} \tag{2.27}$$

$$p\rho^{-k} = \text{constant} = p_o\rho_o^{-k} \tag{2.28}$$

(A9) The time-dependent components of velocity are assumed to be sufficiently represented by

$$u_1(x,y,t) = \text{REAL}\,[u_{11}(x,y)\ \exp(-i\omega t)] \tag{2.29}$$

$$v_1(x,y,t) = \text{REAL}\,[v_{11}(x,y)\ \exp(-i\omega t)] \tag{2.30}$$

(A10) Finally, the complex coefficient of the x-component of velocity, $u_{11}(x,y)$, is assumed to be of the form

$$u_{11}(x,y) = X_1(x)\cdot Y_1(y) \ . \tag{2.31}$$

In this context $X_1(x)$ and $Y_1(y)$ represent complex functions of x and y.

Evaluation of ρ_{1n} and p_{1n}. Assumptions A7 and A8 will now be used to evaluate ρ_{1n} and p_{1n} for $n = 1,2,3,\cdots$.

If

$$p_1(x,t) = \text{REAL}\,[-\,i\ \rho_o\ c_o\ U_o\ \sin\,(\omega x/c_o)\ \exp(-i\omega t)] \tag{2.26}$$

then

$$p_{11} = -\,i\ \rho_o\ c_o\ U_o\ \sin\,(\omega x/c_o) \tag{2.32a}$$

$$p_{1n} = 0 \qquad \text{for} \qquad n = 2,3,4,\cdots \tag{2.32b}$$

If the time-mean variations in pressure are neglected, i.e. $\bar{p}(x,y) = p_o$, then the isentropic relationship between density and pressure yields

$$p\rho^{-k} = (p_o + p_1)(\rho_o + \rho_1)^{-k} = p_o\rho_o^{-k}$$

or

$$(1 + p_1/p_o)(1 + \rho_1/\rho_o)^{-k} = 1$$

If $(1 + \rho_1/\rho_o)^{-k}$ is expanded in a binomial series and only the terms which are of the order of magnitude of δ or larger are retained, then the following expression is obtained:

$$p_1 \approx k \frac{p_o}{\rho_o} \rho_1 \quad .$$

The sound wave propagation speed, c, for isentropic compressions and rarefactions in an ideal gas is given by

$$c^2 = k \frac{p}{\rho}$$

and, therefore,

$$p_1(x,t) \approx c_o^2 \rho_1(x,t) \tag{2.33}$$

and

$$\rho_1(x,t) = p_1/c_o^2 = \text{REAL}\,[-i\,\rho_o M_o \sin(\omega x/c_o)\exp(-i\omega t)] \tag{2.34}$$

and finally

$$\rho_{11} = - i \rho_o M_o \sin (\omega x/c_o) \tag{2.35a}$$

$$\rho_{1n} = 0 \quad \text{for} \quad n = 2,3,4,\cdots. \tag{2.35b}$$

Solution for $u_{11}(x,y,t)$. Under the foregoing assumptions equation 2.22 becomes

$$\nu_o X_1 \cdot Y_1'' = - i\omega X_1 \cdot Y_1 - i\omega U_o \cos (\omega x/c_o) \tag{2.36}$$

The prime notation in equation 2.36 represents differentiation with respect to the appropriate independent variable. This equation may be further simplified by first dividing by $\nu_o X_1(x)$ and then by rearrangement. This yields

$$Y_1'' + i \frac{\omega}{\nu_o} Y_1 = - i \frac{\omega}{\nu_o} U_o \cos (\omega x/c_o)/X_1 \quad . \tag{2.37}$$

Equation 2.37 produces a paradoxical situation unless

$$Y_1'' + i \frac{\omega}{\nu_o} Y_1 = E \equiv e_1 + i e_2 \tag{2.38a}$$

and

$$- i \frac{\omega}{\nu_o} U_o \cos (\omega x/c_o)/X_1 = E \tag{2.38b}$$

where $E \equiv e_1 + i e_2$ is a complex constant which must be determined. Solving equation 2.38b for $X_1(x)$ results in

$$X_1(x) = - \frac{i}{E} \frac{\omega}{\nu_o} U_o \cos (\omega x/c_o) \quad . \tag{2.39}$$

Equation 2.38a can now be solved for $Y_1(y)$ as follows:

1. Complementary solution for $Y_1(y)$. The total differential equation to be solved is

$$Y_1'' + i \frac{\omega}{\nu_o} Y_1 = 0 \quad . \tag{2.40}$$

The corresponding auxiliary equation is

$$m^2 + i \frac{\omega}{\nu_o} = 0 \tag{2.41}$$

and the roots of equation 2.41, as determined from complex variable theory, are

$$m_1 = \sqrt{\omega/2\nu_o}\,(1 - i) \quad , \tag{2.42a}$$

and

$$m_2 = -\sqrt{\omega/2\nu_o}\,(1 - i) \quad . \tag{2.42b}$$

The complementary function, therefore, is

$$Y_1^c(y) = A \exp\left[(1 - i)\, y'\right] + B \exp\left[-(1 - i)\, y'\right] \tag{2.43}$$

where

$$A \equiv a_1 + i\, a_2 \quad ,$$

$$B \equiv b_1 + i\, b_2 \quad ,$$

and

$$y' = y/\sqrt{\frac{2\nu_o}{\omega}} = y/\delta_{ac} \quad .$$

2. Particular solution for $Y_1(y)$. A particular solution of equation 2.38a is

$$Y_1^p(y) = - i \frac{\nu_o}{\omega} E \quad . \tag{2.44}$$

The general solution for $Y_1(y)$ is equal to the sum of the complementary and particular solutions, i.e.

$$Y_1(y) = A \exp [(1 - i) y'] + B \exp [- (1 - i) y'] \tag{2.45}$$

$$- i \frac{\nu_o}{\omega} E \quad .$$

An expression for $u_{11}(x,y)$ is finally obtained by substituting the solutions for $X_1(x)$ and $Y_1(x)$ into equations 2.31. This gives

$$u_{11}(x,y) = - U_o \cos (\omega x/c_o)$$

$$\{1 + i \frac{\omega}{\nu_o} \frac{A}{E} \exp [(1 - i) y'] + i \frac{\omega}{\nu_o} \frac{B}{E} \exp [- (1 - i) y']\} \ ,$$

or if by definition

$$A' \equiv i \frac{\omega}{\nu_o} \frac{A}{E} = a_1' + i \, a_2'$$

and

$$B' \equiv i \frac{\omega}{\nu_o} \frac{B}{E} = b_1' + i \, b_2'$$

then

$$u_{11}(x,y) = - U_o \cos(\omega x/c_o) \{1 + A' \exp[(1 - i) y'] + B' \exp[-(1 - i) y']\} \quad . \tag{2.46}$$

The combination of equations 2.29 and 2.46 gives the following expression for the time-dependent velocity $u_1(x,y,t)$:

$$\begin{aligned} u_1(x,y,t) = - U_o \cos(\omega x/c_o) [&\cos(\omega t) \\ &+ a_1' \exp(y') \cos(\omega t + y') \\ &+ a_2' \exp(y') \sin(\omega t + y') \\ &+ b_1' \exp(-y') \cos(\omega t - y') \\ &+ b_2' \exp(-y') \sin(\omega t - y')] \quad . \end{aligned} \tag{2.47}$$

If the no-slip and symmetry boundary conditions are applied to equation 2.47, then the following expressions for a_1', a_2', b_1' and b_2' can be obtained by solving the resulting system of four linear algebraic equations:

$$a_1' = - \{2 + 2 \exp(2a/\delta_{ac})[2 \cos^2(a/\delta_{ac}) - 1]\}/DEN \quad , \tag{2.48a}$$

$$a_2' = - \{4 \sin(a/\delta_{ac}) \cos(a/\delta_{ac}) \exp(2a/\delta_{ac})\}/DEN \quad , \tag{2.48b}$$

$$b_1' = - 1 - a_1' \quad , \tag{2.48c}$$

and

$$b_2' = - a_2' \quad , \tag{2.48d}$$

where

$$DEN \equiv 2 + 4[2 \cos^2(a/\delta_{ac}) - 1] \exp(2a/\delta_{ac}) + 2 \exp(4a/\delta_{ac}) \quad . \tag{2.48e}$$

For air at normal temperatures and pressures and for the frequencies and channel thicknesses which are being considered here, the quantity a/δ_{ac} is very much larger than one. Thus an excellent approximation to the foregoing coefficients which will greatly simplify the time-mean solution is obtained by assuming that terms which are of the order of magnitude of $\exp(-a/\delta_{ac})$ are zero. This yields the following approximate expressions for the four coefficients:

$$a_1' = a_2' = b_2' = 0 \quad , \tag{2.49a}$$

and

$$b_1' = -1 \quad . \tag{2.49b}$$

Therefore, the periodic component of the x-velocity is

$$u_1(x,y,t) = -U_o \cos(\omega x/c_o) \left[\cos(\omega t) - \exp(-y') \cos(\omega t - y')\right] \quad . \tag{2.50}$$

Solution for $v_{11}(x,y)$. The coefficient, $v_{11}(x,y)$, can now be determined from equation 2.21 as follows:

After rearranging equation 2.21, it may be written as

$$\frac{\partial v_{11}}{\partial y} = i\omega \rho_{11}/\rho_o - \frac{\partial u_{11}}{\partial x} \quad . \tag{2.51}$$

If the approximate coefficients given in equations 2.49a and 2.49b are substituted into equation 2.46, then the following equation for $u_{11}(x,y)$ is obtained:

$$u_{11}(x,y) = - U_o \cos (\omega x/c_o)\left[1 - \exp [-(1 - i)\, y']\right] . \qquad (2.52)$$

This in conjunction with equation 2.35a gives

$$\frac{\partial v_{11}}{\partial y} = \omega M_o \sin (\omega x/c_o) \exp [-(1 - i)\, y'] . \qquad (2.53)$$

Integration of equation 2.53 with respect to y yields

$$v_{11}(x,y) = - 1/2\, \omega\, \delta_{ac}\, M_o\, (1 + i) \sin (\omega x/c_o) \exp[-(1 - i)\, y'] \qquad (2.54)$$
$$+ f_1(x) + i\, f_2(x) ,$$

or finally by substituting equation 2.54 into equation 2.30 the expression for $v_1(x,y,t)$ becomes

$$v_1(x,y,t) = f_1(x) \cos (\omega t) + f_2(x) \sin (\omega t) \qquad (2.55)$$
$$- (\omega\, \delta_{ac}\, M_o/2) \exp (-y') \sin (\omega x/c_o) \cdot$$
$$\left[\{\cos (y') - \sin (y')\} \cos (\omega t)\right.$$
$$\left. + \{\cos (y') + \sin (y')\} \sin (\omega t)\right] .$$

If the no-slip boundary condition is applied to equation 2.55 then the following expressions for $f_1(x)$ and $f_2(x)$ are obtained:

$$f_1(x) = f_2(x) = (\omega\, \delta_{ac}\, M_o/2) \sin (\omega x/c_o) , \qquad (2.56)$$

and, therefore,

$$v_1(x,y,t) = (\omega\, \delta_{ac}\, M_o/\sqrt{2}) \sin (\omega x/c_o) \cdot \qquad (2.57)$$
$$[\cos (\omega t - \pi/4) - \exp (-y') \cos (\omega t - \pi/4 - y')] .$$

Dimensionless Form of the Time-Dependent Velocities. For resonant acoustic vibrations the circular frequency ω is related to the wavelength such that

$$\omega = 2\pi c_o/\lambda \quad , \tag{2.58}$$

and therefore

$$\omega x/c_o = 2\pi x/\lambda = \pi x' \quad ,$$

and

$$\omega \delta_{ac} M_o = 2\pi \delta_{ac} U_o/\lambda = \pi \delta U_o \quad .$$

If these expressions are substituted into equations 2.50 and 2.57 then the time-dependent velocities in dimensionless form become

$$u_1'(x',y',t') = -\cos(\pi x')\,[\cos(\pi t') - \exp(-y')\cos(\pi t' - y')] \quad , \tag{2.59}$$

and

$$v_1'(x',y',t') = (\pi/\sqrt{2})\sin(\pi x')\,[\cos(\pi t' - \pi/4) - \exp(-y')\cos(\pi t' - \pi/4 - y')] \quad , \tag{2.60}$$

where

$$u_1' = u_1/U_o$$

and

$$v_1' = v_1/(U_o\delta) \quad .$$

It is interesting to note that the choice of the characteristic time-dependent velocities U_o and $U_o \delta$ produces dimensionless velocities $u_1'(x',y',t')$ and $v_1'(x',y',t')$ which are of the order one. Thus the previous choice of U_o as the characteristic time-dependent x-velocity was correct and the characteristic y-velocity, V_o, should be $U_o \delta$.

A Solution of the Time-Mean Equations

The time-mean velocities $\bar{u}(x,y)$ and $\bar{v}(x,y)$ will now be determined from the following governing equations:

Continuity

$$\frac{\partial \bar{v}}{\partial y} = - \frac{\partial \bar{u}}{\partial x} - \frac{1}{\rho_o} \left[\frac{\partial}{\partial x} \left(\overline{\rho_1 u_1} \right) + \frac{\partial}{\partial y} \left(\overline{\rho_1 v_1} \right) \right] \tag{2.61}$$

Momentum

$$\frac{\partial^3 \bar{u}}{\partial y^3} = \frac{1}{\nu_o} \frac{\partial}{\partial y} \left[\overline{\frac{\rho_1}{\rho_o} \frac{\partial u_1}{\partial t} + u_1 \frac{\partial u_1}{\partial x} + v_1 \frac{\partial u_1}{\partial y}} \right] \tag{2.62}$$

Boundary Conditions

$$y = 0 : \quad \bar{u} = 0 , \quad \bar{v} = 0 \tag{2.25a}$$

$$y = a : \quad \frac{\partial \bar{u}}{\partial y} = 0 , \quad \bar{v} = 0 \tag{2.25b}$$

$$\text{all } x : \quad \int_{y=0}^{a} \rho_o \, \bar{u} \, dy = \text{constant} \tag{2.25c}$$

Solution for $\bar{u}(x,y)$. Substitution of equations 2.34, 2.50 and 2.57 into equation 2.62 yields

$$\frac{\partial^3 \bar{u}}{\partial y^3} = \frac{U_o^2}{2\, c_o \delta_{ac}^2} \sin(2\omega x/c_o) \cdot \frac{\partial}{\partial y}\left\{\exp(-y')\,[3\cos(y') - \sin(y') - \exp(-2y')]\right\} . \tag{2.63}$$

Equation 2.63 is a linear partial differential equation of the form

$$\frac{\partial^3 \bar{u}}{\partial y^3} = f(x)\cdot g(y)$$

for which the solution is

$$\bar{u}(x,y) = f(x) \int_0^y \int_0^{y_2} \int_0^{y_1} g(y_o)\, dy_o dy_1 dy_2 + F_1(x)\frac{y^2}{2} + F_2(x)\, y + F_3(x) ,$$

where

$$f(x) = \frac{U_o^2}{2\, c_o \delta_{ac}^2} \sin(2\omega x/c_o)$$

and

$$g(y) = \frac{\partial}{\partial y}\left\{\exp(-y')\,[3\cos(y') - \sin(y') - \exp(-y')]\right\} ,$$

or finally

$$\bar{u}(x,y) = \frac{U_o}{8c_o} \sin(2\omega x/c_o)\left\{-4\, y'^2 + 2\, y' + 3 - \exp(-y')\,[2\cos(y') + 6\sin(y') + \exp(-y')]\right\} + F_1(x)\frac{y^2}{2} + F_2(x)\, y + F_3(x) . \tag{2.64}$$

If the no-slip boundary condition is applied to equation 2.64 then it is seen that $F_3(x) = 0$.

Solution for $\bar{v}(x,y)$. The y-component of the time-mean velocity can now be determined by substituting equations 2.34, 2.50, 2.57 and 2.64 into equation 2.61. This yields

$$\frac{\partial \bar{v}}{\partial y} = -\frac{U_o^2 \omega}{4c_o^2} \cos(2\omega x/c_o) \left\{-4y'^2 + 2y' + 3 \right. \tag{2.65}$$

$$\left. - \exp(-y')[2\cos(y') + 7\sin(y') + \exp(-y')]\right\}$$

$$+ \frac{U_o^2 \omega}{4c_o^2} \exp(-y')\sin(y') - F_1'(x)\frac{y^2}{2} - F_2'(x)\, y \quad .$$

The prime notation on $F_1(x)$ and $F_2(x)$ represents the derivative of these functions with respect to x. Integration of equation 2.65 with respect to y yields the following expression for $\bar{v}(x,y)$:

$$\bar{v}(x,y) = -\frac{U_o^2 \omega \delta_{ac}}{8c_o^2} \left\{\cos(2\omega x/c_o)\left[-\frac{8}{3}y'^3 + 2y'^2\right.\right. \tag{2.66}$$

$$+ 6y' + \exp(-y')\{9\cos(y')$$

$$\left. + 5\sin(y') + \exp(-y')\}\right]$$

$$\left. + \exp(-y')[\cos(y') + \sin(y')]\right\}$$

$$- F_1'(x)\frac{y^3}{6} - F_2'(x)\frac{y^2}{2} + F_4(x) \quad .$$

If the solid-boundary condition is applied to equation 2.66, then $F_4(x)$ is found to be

$$F_4(x) = \frac{U_o^2 \omega \delta_{ac}}{8c_o^2} [1 + 10 \cos (2\omega x/c_o)] \quad . \qquad (2.67)$$

The functions $F_1(x)$ and $F_2(x)$ must now be determined from the application of equations 2.25b and 2.25c to equation 2.64, i.e. for

$$y = a : \quad \frac{\partial \bar{u}}{\partial y} = 0$$

and for

$$\text{all } x : \quad \int_{y=0}^{a} \rho_o \bar{u} \, dy = \text{constant} = w$$

For these conditions $F_1(x)$ and $F_2(x)$ become

$$F_1(x) = \frac{U_o^2}{8c_o} \sin (2\omega x/c_o) \frac{1}{\delta_{ac}^2} [8 + 9 (\frac{\delta_{ac}}{a})^2 - \frac{27}{2} (\frac{\delta_{ac}}{a})^3] \qquad (2.68)$$

$$- \frac{3w}{\rho_o a^3}$$

and

$$F_2(x) = - \frac{U_o^2}{8c_o} \sin (2\omega x/c_o) \frac{1}{\delta_{ac}} [2 + 9 (\frac{\delta_{ac}}{a}) - \frac{27}{2} (\frac{\delta_{ac}}{a})^2] \qquad (2.69)$$

$$+ \frac{3w}{\rho_o a^2} \quad .$$

The quantity, w, represents the time-mean through-flow rate in the x-direction for one half of the channel. An average through-flow velocity

will now be defined in terms of w as follows:

$$w = \rho_o(\text{Area})(\text{Mean Velocity}) = \rho_o a U$$

or

$$U \equiv \frac{w}{\rho_o a} \quad . \tag{2.70}$$

If the expressions for $F_1(x)$, $F_2(x)$ and U are substituted into the equations for the time-mean velocities, then the following equations are obtained:

$$\begin{aligned}\bar{u}(x,y) = {} & 3U\left[(y/a) - 1/2\ (y/a)^2\right] \\ & - \frac{U_o^2}{8c_o} \sin\left(2\omega x/c_o\right)\left\{\left[9 - \frac{27}{2}\left(\frac{\delta_{ac}}{a}\right)\right]\left[(y/a) - 1/2\ (y/a)^2\right]\right. \\ & \left. - 3 + \exp(-y')\left[2\cos(y') + 6\sin(y') + \exp(-y')\right]\right\}\end{aligned} \tag{2.71}$$

and

$$\begin{aligned}\bar{v}(x,y) = {} & -\left[\frac{2\pi U_o^2}{8c_o}\right]\left[\frac{a}{\lambda}\right]\left[\cos\left(2\omega x/c_o\right)\left\{\right.\right. \\ & \left[9 - \frac{27}{2}\left(\frac{\delta_{ac}}{a}\right)\right]\left[1/3\ (y/a)^3 - (y/a)^2\right] + 6\ (y/a) \\ & - \left(\frac{\delta_{ac}}{a}\right)\left[10 - \exp(-y')\left\{9\cos(y') + 5\sin(y')\right.\right. \\ & \left.\left. + \exp(-y')\right\}\right]\Big\} + \left(\frac{\delta_{ac}}{a}\right)\left[\exp(-y')\left\{\cos(y')\right.\right. \\ & \left.\left.\left. + \sin(y')\right\} - 1\right]\right] \quad .\end{aligned} \tag{2.72}$$

Dimensionless Form of the Time-Mean Velocities. The assumed characteristic velocities $\bar{U}$ and $\bar{V}$ can now be determined from equations 2.71 and 2.72. The velocity $\bar{U}$ must be chosen such that $\bar{u}(x,y)$ will be of the order of magnitude of one. Since U represents the average through-flow velocity, its range of values will be $0 \leq |U| \leq \bar{U}$. Therefore, U is not a suitable choice for $\bar{U}$. The only other possible choice is $\bar{U} = U_o^2/c_o = M_o U_o$. This quantity will only be zero if the sound field does not exist. Thus

$$\bar{U} \equiv M_o U_o \quad . \tag{2.73}$$

The quantity $U/\bar{U}$ will be of the order one only if U/U_o is of the order δ since

$$\frac{U}{\bar{U}} = \frac{U}{M_o U_o} = \frac{U/U_o}{M_o}$$

and $\theta(M_o) = \delta$ and, therefore, if $\theta(\vec{u}) = 1$, then

$$\theta(U/U_o) = \delta \quad .$$

That is, the average through-flow velocity must be small in comparison to the maximum amplitude of the time-dependent x-velocity. The characteristic velocity $\bar{V}$ will be taken as

$$\bar{V} \equiv \frac{U_o^2}{c_o} \frac{a}{\lambda} = U_o M_o \frac{a}{\lambda} \tag{2.74}$$

Equations 2.71 and 2.72 can be written in dimensionless form as

$$\bar{u}'(x',y') = \frac{3U/U_o}{M_o}\left[(y'/a') - 1/2\ (y'/a')^2\right] \qquad (2.75)$$

$$- \frac{1}{8}\sin(2\pi x')\left\{\left[9 - \frac{27}{2a'}\right]\left[(y'/a') - 1/2\ (y'/a')^2\right]\right.$$

$$\left. - 3 + \exp(-y')\left[2\cos(y') + 6\sin(y') + \exp(-y')\right]\right\}$$

and

$$\bar{v}'(x',y') = -\frac{\pi}{4}\left[\cos(2\pi x')\left\{\left[9 - \frac{27}{2a'}\right]\left[1/3\ (y'/a')^3\right.\right.\right. \qquad (2.76)$$

$$\left. - (y'/a')^2\right] + 6\ (y'/a') - \frac{1}{a'}\left[10 - \exp(-y')\{9\cos(y')\right.$$

$$\left.\left. + 5\sin(y') + \exp(-y')\}\right]\right\} + \frac{1}{a'}\left[\exp(-y')\{\cos(y')\right.$$

$$\left.\left. + \sin(y')\} - 1\right]\right] \ ,$$

where

$$\bar{u}' \equiv \bar{u}/(M_o U_o), \quad \bar{v}' \equiv \bar{v}/(M_o U_o\ a/\lambda)$$

and

$$a' \equiv a/\delta_{ac} \ .$$

Time-Mean Stream Function. If the spatial variations in the time-mean density are neglected then an expression for the stream function, $\psi(x',y')$, can be determined as follows:

From the definition of the stream function

$$\bar{u}' = \frac{\partial\psi}{\partial y'}$$

or

$$\psi(x',y') = \psi(x',0) + \int_0^{y'} \bar{u}(x',t)\, dt \tag{2.77}$$

If $\psi(x',0) = 0$, then $\psi(x',y')$ becomes

$$\psi(x',y') = \frac{3(U/U_o)}{2\, M_o} \left[(y'/a')^2 - (y'/a')^3/3\right] a' \tag{2.78}$$

$$+ \frac{a'}{8} \sin(2\pi x') \left\{3\,(y'/a') - \frac{9}{2}\left[1 - \frac{3}{2a'}\right][(y'/a')^2 - \frac{1}{3}(y'/a')^3\right] + \frac{1}{2a'}\left[\exp(-y')\{8\cos(y') + 4\sin(y') + \exp(-y')\} - 9\right]\right\} .$$

Discussion of Results

In order to present a clearer discussion of the results of the analytical investigations, the velocity field will be determined for the following set of property values:

$$\omega = 2000\pi \ \frac{\text{ft}}{\text{ft-sec}} \ (1000 \text{ cps})$$

$$a = 1 \text{ inch}$$

$$\lambda = 12 \text{ inches}$$

$$T_o = 522^\circ \text{ R}$$

$$p_o = 1 \text{ atm}$$

$$\delta_{ac} = 2.552 \times 10^{-3} \text{ inches}$$

$$U/(U_o M_o) = M/M_o^2 = 0 \text{ and } 0.5$$

$$a' \equiv a/\delta_{ac} = 392$$

Time-Dependent Velocity Components

X-Component. The first velocity that will be considered is the x-component of the time-dependent velocity, $u_1'(x',y',t')$. This velocity is given by equation 2.59 as

$$u_1'(x',y',t') = - \cos(\pi x') \left[\cos(\pi t') - \exp(-y') \cos(\pi t' - y')\right] ; \quad (2.59)$$

it satisfies the reduced equation of motion (equation 2.12), the no-slip boundary condition (equation 2.16a) and the symmetry condition (equation 2.16b) to within a quantity that is of the order of magnitude of $\exp(-a')/\delta_{ac}(10^{-166.7})$. The relaxation of the symmetry condition resulted from assuming that terms that were of the order of $\exp(-a')$ were, for all practical purposes, zero. Equation 2.59 is illustrated graphically in Figure 10 for $x' = 0$ and for selected values of t'.

In obtaining the equations which govern the time-dependent velocities only the terms in the dimensionless continuity and momentum equations that were of the highest order of magnitude were retained. The validity of this approach can be demonstrated by solving for the x-component of the time-dependent velocity that results from retaining the terms in the governing equation which are of the two highest orders of magnitude—1 and $1/\delta$ or δ and 1. The solution for $u_1'(x',y',t')$ under this condition can be shown (see Appendix C) to be

$$\begin{aligned} u_1'(x',y',t') = &- \cos(\pi x') \left[\cos(\pi t') - \exp(-y') \cos(\pi t' - y')\right] \\ &+ \frac{M_o}{4} \sin(2\pi x') \left[\sin(2\pi t') + \exp(-\sqrt{2}\, y') \sin(2\pi t' - \sqrt{2}\, y')\right. \\ &\left. - 2 \exp(- y') \sin(2\pi t' - y')\right] \end{aligned} \quad (2.79)$$

or

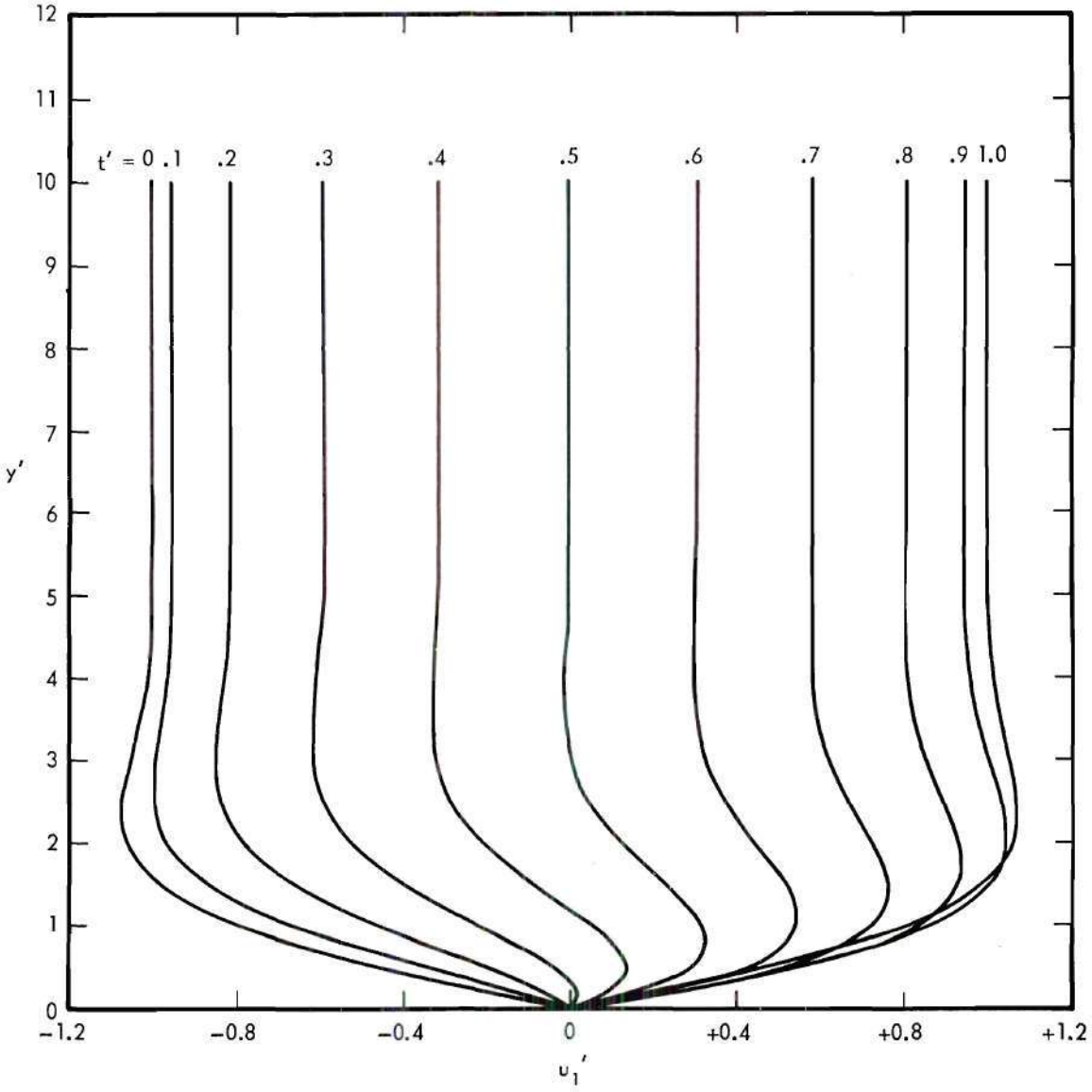

Figure 10. X-Component of the Time-Dependent Velocity (x' = 0).

$$u_1'(x',y',t') = \text{(Equation 2.59)} + \frac{M_o}{4}\{\sin(2\pi x')[\sin(2\pi t') + \exp(-\sqrt{2}\,y')\sin(2\pi t' - \sqrt{2}\,y') - 2\exp(-y')\sin(2\pi t' - y')]\} \quad . \tag{2.80}$$

The acoustic Mach number, M_o, was assumed to be of the order δ in the order of magnitude analysis and, therefore, equation 2.59 should be an excellent approximation to equation 2.80. This can be shown even more clearly when it is noted that a sound-pressure level of 150 db—re 0.0002 microbar—corresponds to $M_o \approx 0.0063$.

Equation 2.59 is the same as the solution for $u_1'(x',y',t')$ that was obtained by both Rayleigh and Westervelt.

Y-Component. The y-component of the time-dependent velocity as given by equation 2.60 is

$$v_1'(x',y',t') = (\pi/\sqrt{2})\sin(\pi x')[\cos(\pi t' - \pi/4) - \exp(-y')\cos(\pi t' - \pi/4 - y')] \quad . \tag{2.60}$$

This equation satisfies the reduced equation of motion (equation 2.13) and the no-slip boundary condition (equation 2.16a). It does not satisfy the symmetry condition (equation 2.16b) since in the order of magnitude analysis the y-momentum equation was of order δ in comparison with the x-momentum equation. This reduced the order of the differential equations by one and, therefore, one of the boundary conditions had to be relaxed. The symmetry condition for v_1' was assumed to be the least important boundary condition and it was felt that this would not appreciably alter the time-mean velocity profiles.

Both Rayleigh and Westervelt were confronted with the same dilemma that has arisen here. Westervelt's y-component of the time-dependent velocity was the same as that given in equation 2.60. Rayleigh, however, circumvented the problem by arbitrarily introducing the term $[1 - y'/a'] \cos(\pi t' - \pi/4)$ in place of the term $\cos(\pi t' - \pi/4)$. Thus his expression for $v_1'(x',y',t')$ was

$$v_1'(x',y',t') = (\pi/\sqrt{2}) \sin(\pi x') [(1-y'/a') \cos(\pi t'-\pi/4) - \exp(-y') \cos(\pi t' - \pi/4 - y')] \quad . \tag{2.81}$$

Equation 2.61 satisfies the no-slip and symmetry boundary conditions but it does not satisfy the reduced continuity equation.

Since equation 2.60 does not involve the introduction of an arbitrary function of y and since Westervelt in his correction of Rayleigh's work used this expression for $v_1'(x',y',t')$, it was decided that the time-mean velocities would be based on the time-dependent velocities as given by equations 2.59 and 2.60.

Equation 2.60 is illustrated graphically in Figure 11 for $x' = 1/2$ and for selected values of t'.

Time-Mean Velocities

X-Component. The x-component of the time-mean velocity as given by equation 2.75 is

$$\bar{u}'(x',y') = \frac{3M}{M_o^2} [(y'/a') - (y'/a')^2/2] - \frac{1}{8} \sin(2\pi x') \left\{ \left[9 - \frac{27}{2a'}\right] [(y'/a') - (y'/a')^2/2] - 3 + \exp(-y') [2 \cos(y') + 6 \sin(y') + \exp(-y)] \right\} \tag{2.75}$$

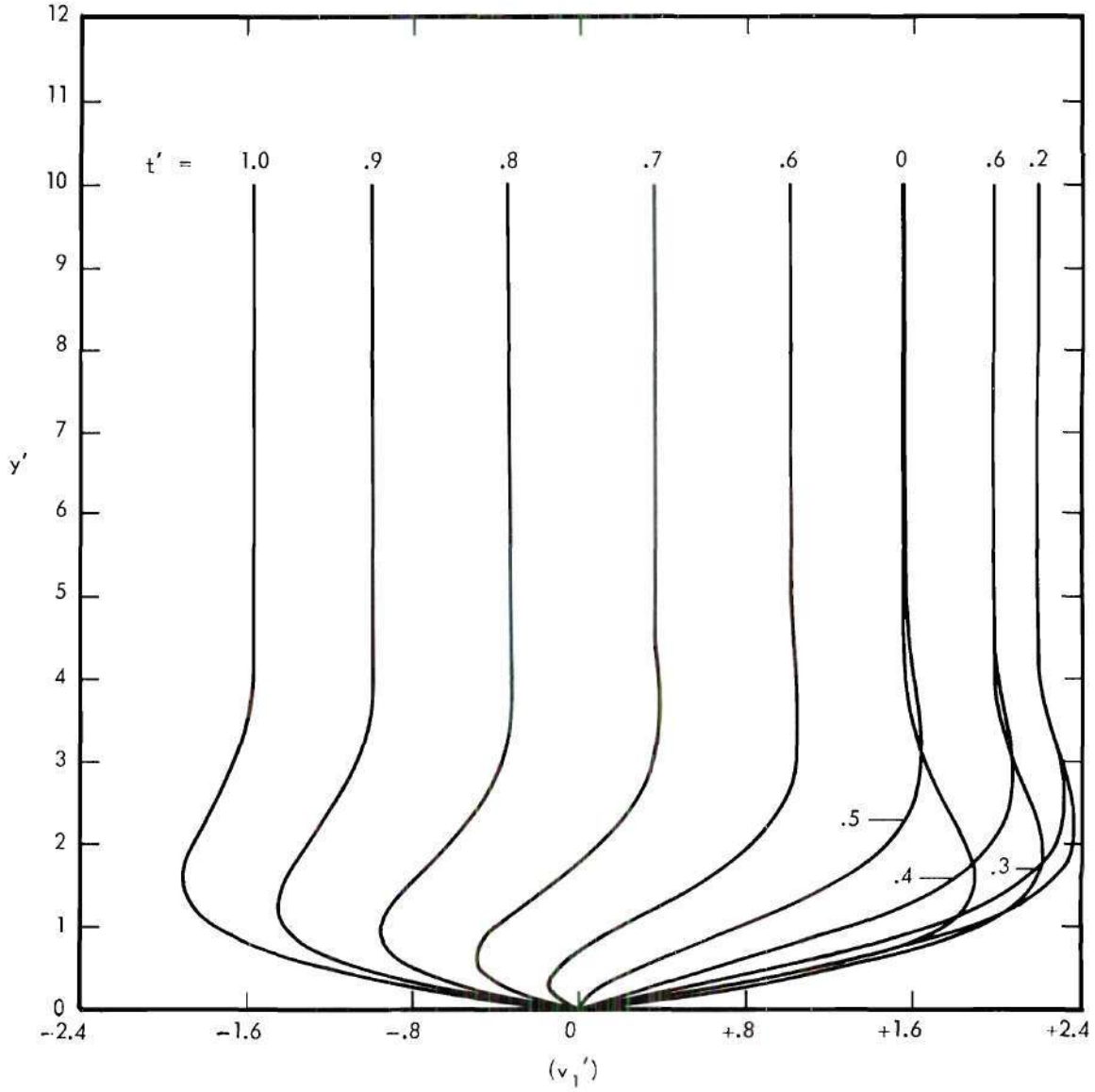

Figure 11. Y-Component of the Time-Dependent Velocity (x' = 1/2).

where

$$M/M_o^2 = (U/U_o)/M_o \quad .$$

Equation 2.75 is illustrated graphically in Figures 12 and 13 for $M/M_o^2 = 0$ and 1/2, respectively.

The first figure shows the velocity profiles which exist in a resonant channel in which there is no through flow, the case which was considered first by Rayleigh and then later by Westervelt. Equation 2.75 can be reduced to Westervelt's solution for the x-component of the time-mean velocity expressed in Eulerian (fixed) coordinates by setting M equal to zero (no through flow) and by neglecting the quantity $27/(2a')$ since it is small in comparison to nine.

Figure 13 shows the x-velocity profiles which exist when a slow through flow is present. It should be noted that there is no back-flow in the region for which $0 \leq x/\lambda \leq 1/4$ and $\delta_{ac} < y < a$. A small back-flow does exist within the A.C. boundary layer and this is shown in the exploded view of the A.C. boundary layer given in Figure 17 (p. 58).

A large back-flow exists throughout the region for which $1/4 \leq x/\lambda \leq 1/2$ and $\delta_{ac} < y$ and, therefore, a standing vortex is present in this region even though there is through flow in the channel. It should also be noted in Figure 17 that the velocity becomes positive again before going to zero at the wall. This results in another very thin vortex adjacent to the wall.

Y-Component. The y-component of the time-mean velocity as given by equation 2.76 is

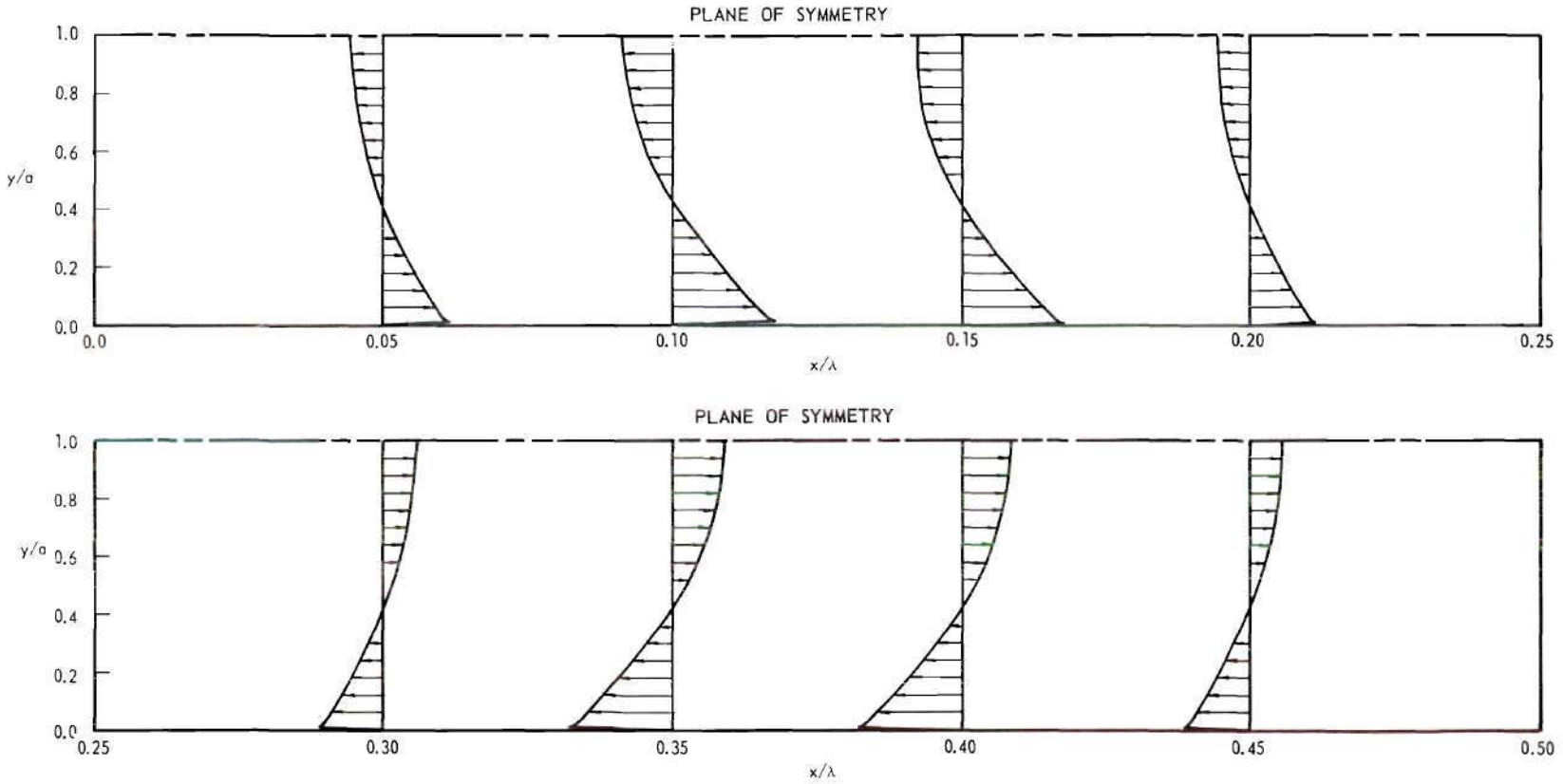

Figure 12. X-Component of the Time-Mean Velocity for $M/M_o^2 = 0$.

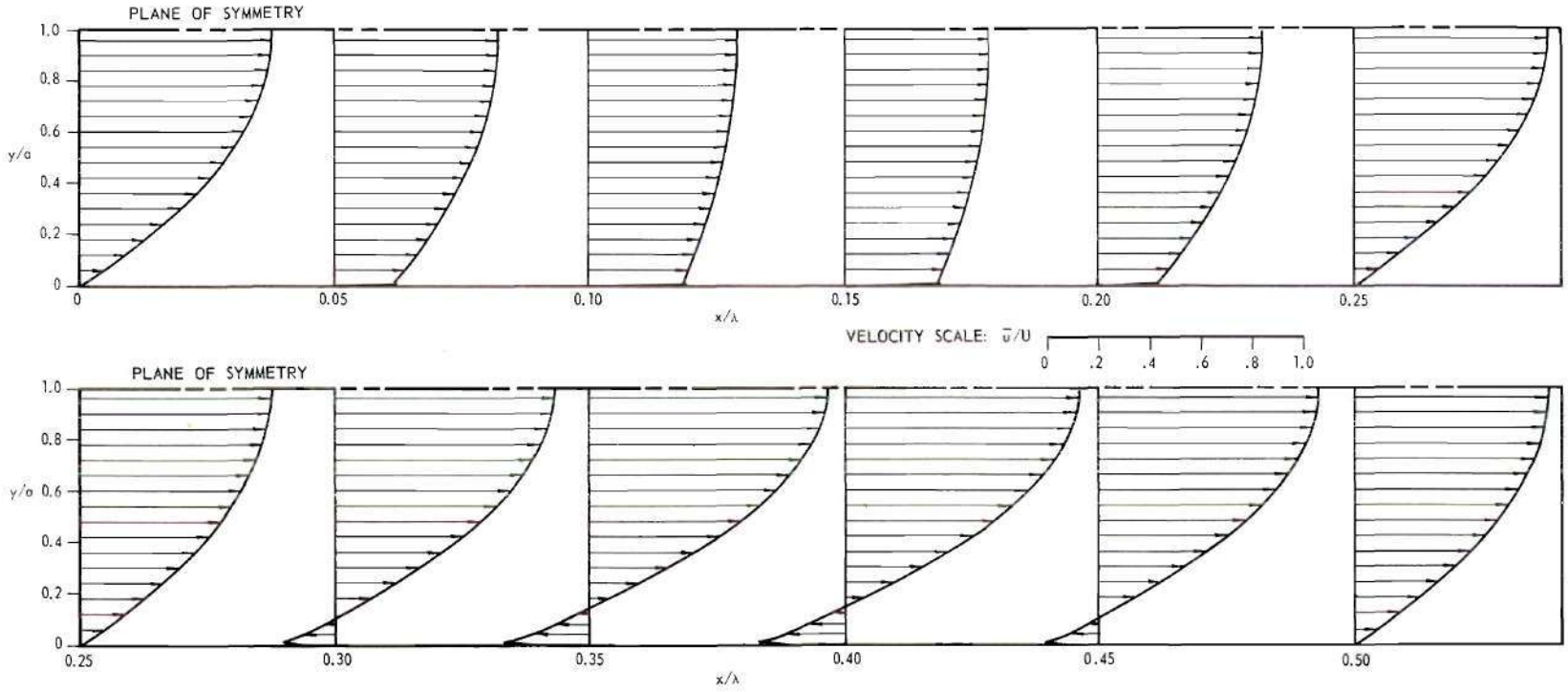

Figure 13. X-Component of the Time-Mean Velocity for $M/M_o^2 = 1/2$.

$$\bar{v}'(x',y') = -\frac{\pi}{4}\Big[\cos(2\pi x')\Big\{\Big[9 - \frac{27}{2a'}\Big][(y'/a')^3/3 - (y'/a')^2] + 6\,(y'/a') - \frac{1}{a'}\,[10 - \exp(-y')\{9\cos(y') + 5\sin(y') + \exp(-y')\}]\Big\} + \frac{1}{a'}\,[\exp(-y')\{\cos(y') + \sin(y')\} - 1]\Big] \tag{2.76}$$

where $\bar{v}' \equiv \bar{v}/(M_o U_o\, a/\lambda)$ and the characteristic velocity is $\bar{V} \equiv U_o M_o \frac{a}{\lambda}$. It was assumed in the order of magnitude analysis that $\bar{V}$ was small in comparison to $\bar{U}$ and $\bar{U}$ was shown to be $U_o M_o$. This means that if these assumptions are to be satisfied then the half width of the channel should be small in comparison to the wavelength of the acoustic waves. The necessity of this restriction has been shown experimentally by Andrade, Jackson (13), and the present flow visualization study.

It is also of interest to note that $\bar{v}'$ does not depend upon the through-flow velocity U. Equation 2.76 is illustrated graphically in Figure 14.

Time-Mean Stream Function

The time-mean stream function as given by equation 2.78 is

$$\psi(x',y') = \frac{3M}{2M_o^2}\,[(y'/a')^2 - (y'/a')^3/3]\,a' + \frac{a'}{8}\sin(2\pi x')\Big\{3\,(y'/a') - \frac{9}{2}\Big[1 - \frac{3}{2a'}\Big][(y'/a')^2 - (y'/a')^3/3] + \frac{1}{2a'}\,[\exp(-y')\{8\cos(y') + 4\sin(y') + \exp(-y')\} - 9]\Big\}\,. \tag{2.78}$$

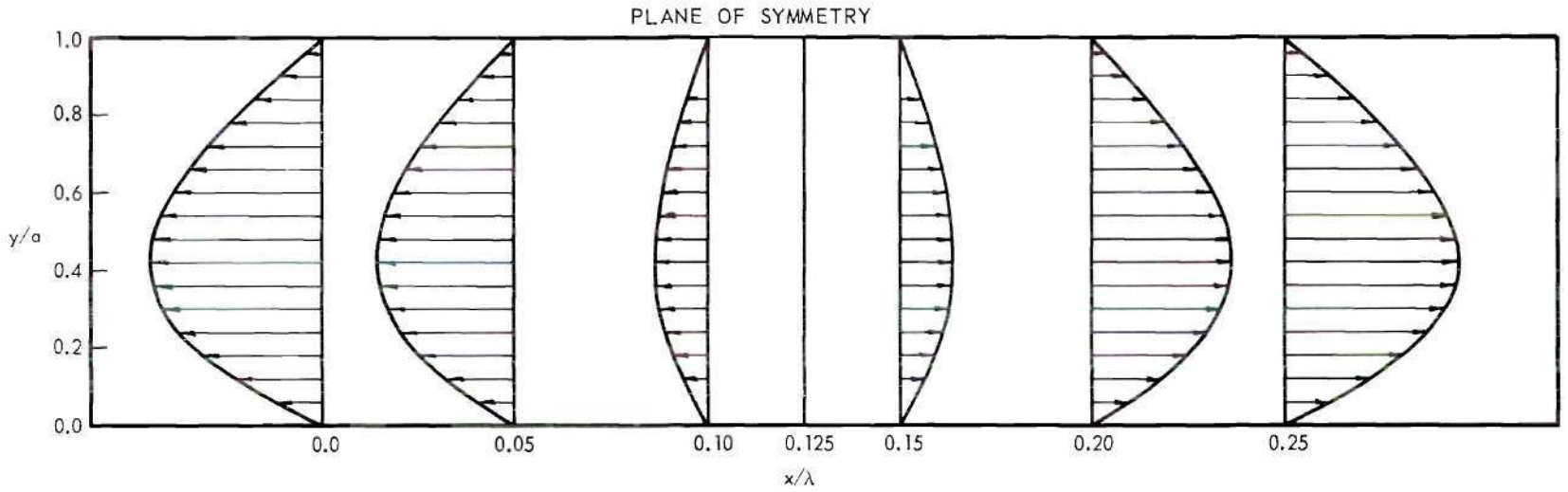

Figure 14. Y-Component of the Time-Mean Velocity.

The stream function is shown graphically in Figures 15 and 16 for $M/M_o^2 = 0$ and 1/2, respectively. Figure 15 represents the streamline pattern that is formed in a stagnant (no through flow) resonant channel. This is the case which was considered by Rayleigh and Westervelt. It can be seen from Figure 15 that there are four large vortices in a one half wavelength section of channel. It should be pointed out that there are also four very thin vortices in this section adjacent to the walls which have not previously been reported in the literature. The details of the smaller vortices are shown in Figure 17 for the case of a slow through flow.

Thickness of the Main-Vortices. For the case of through flow that is shown in Figures 16 and 17 it is seen that the streamline pattern is repeated in one half wavelength sections and that each of these sections contain six standing vortices; four very thin vortices adjacent to the walls and two thick vortices (main vortices). The thickness of the four vortices next to the walls is approximately 0.003 inch and is, therefore, very small in comparison to the half width of the channel.

The thickness of the two main vortices can be determined by: (i) setting the stream function (equation 2.78) equal to zero and (ii) solving the resulting cubic equation in y'/a' for its largest root. The two smaller roots of this equation correspond to the wall and to the thicknesses of the four vortices adjacent to the walls.

An excellent approximation to the largest root can be obtained, when the maximum main-vortex thickness is greater than 0.1 a', by neglecting the terms in the stream function which are of the order of magnitude of $\exp(-y')$ and $1/a'$. With this approximation the thickness of the main vortices (the

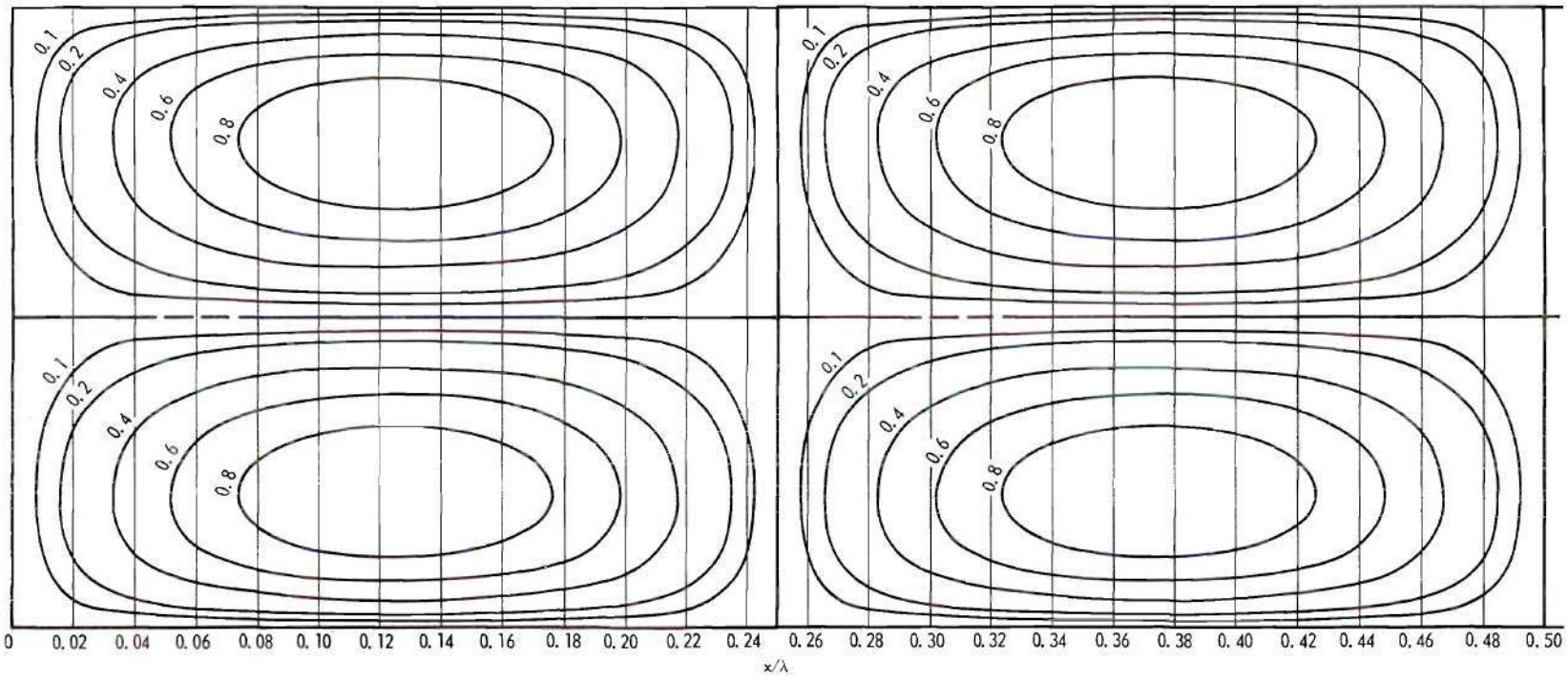

Figure 15. Time-Mean Stream Function for $M/M_o^2 = 0$.

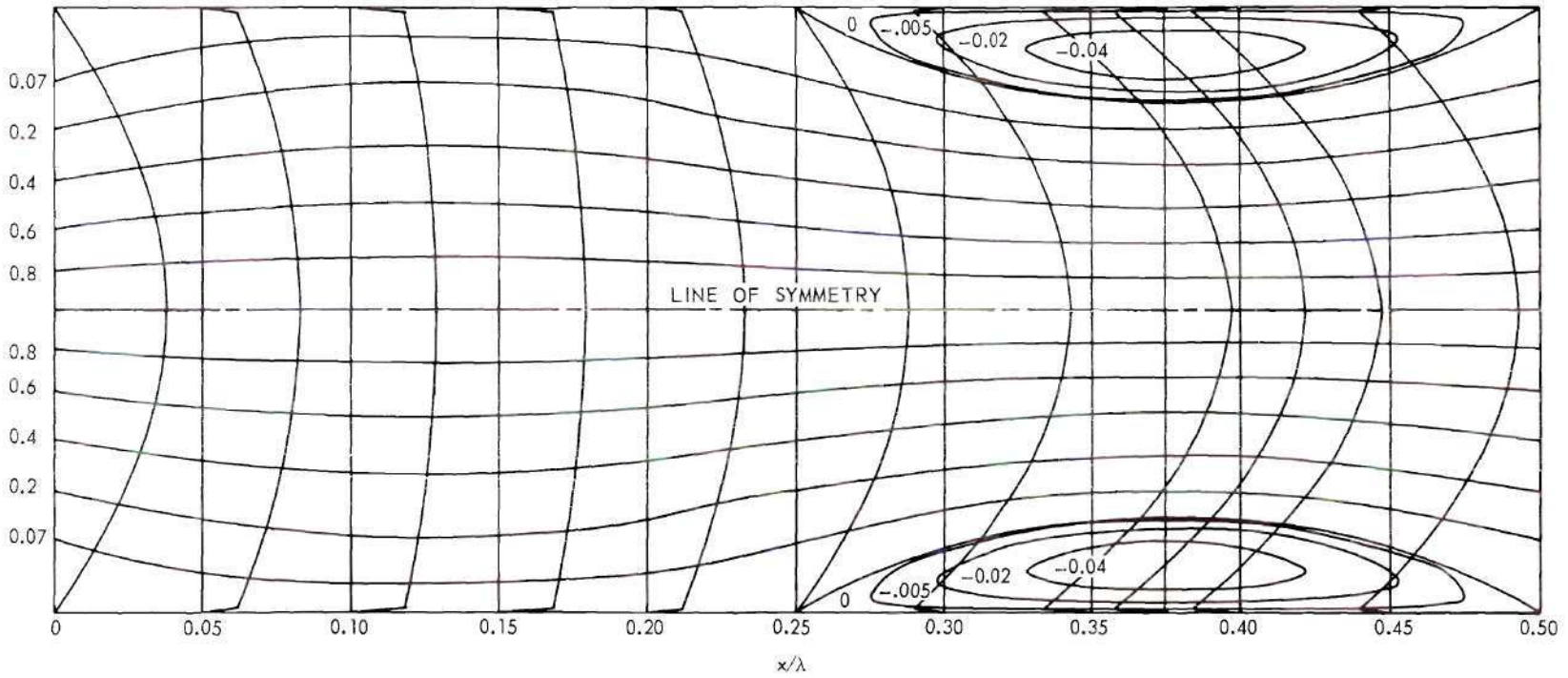

Figure 16. Time-Mean Stream Function for $M/M_o^2 = 1/2$.

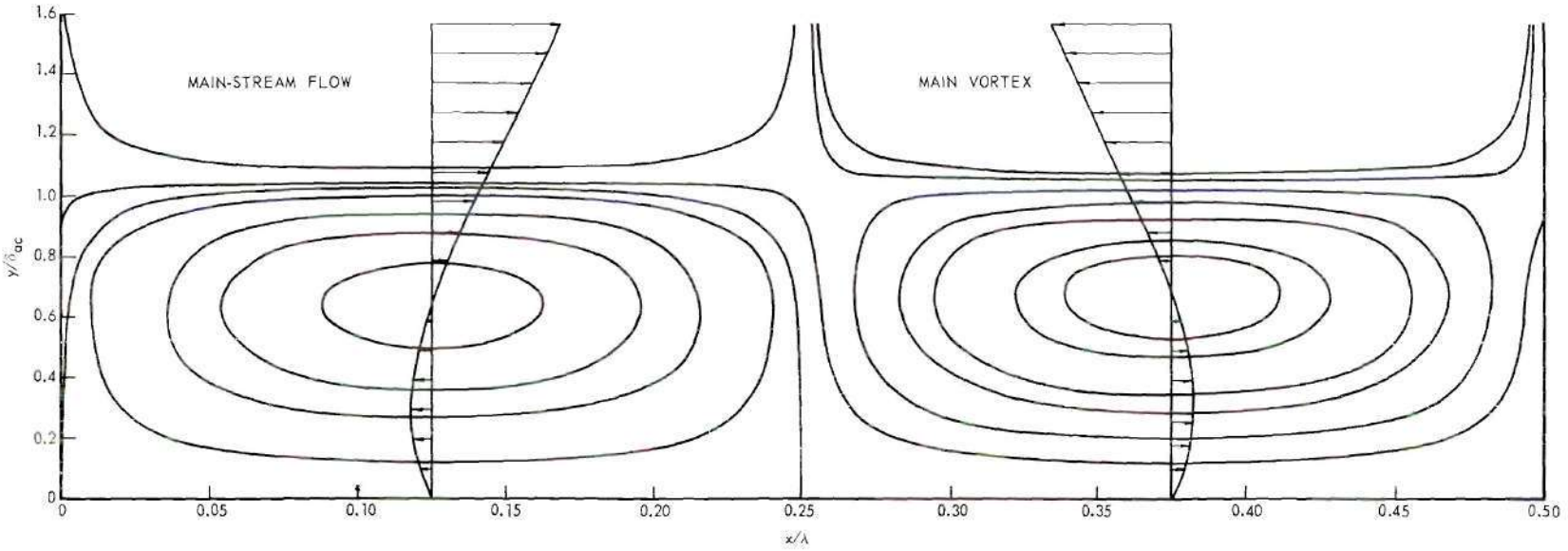

Figure 17. Time-Mean Stream Function for $M/M_o^2 = 1/2$ Showing Details of the Wall Vortices.

largest value of $y'/a' \equiv \gamma_x'$ for which the stream function is equal to zero) is given by

$$\gamma_x' = \frac{3}{2} - \left[\frac{9}{4} - 2/\left\{1 - \frac{8}{3}\left\{\frac{M}{M_o^2}\right\} \csc(2\pi x')\right\}\right]^{1/2} \qquad (2.82)$$

where $M \equiv U/c_o$ and $M_o \equiv U_o/c_o$.

The maximum value of γ_x' occurs when

$$x' = m - 1/4 , \qquad m = 0, \pm 1, \pm 2, \cdots$$

and, therefore, the maximum thickness of the main vortices (γ_m) is given by

$$\gamma_m = \frac{3}{2} - \left[\frac{9}{4} - 2/\left\{1 + \frac{8}{3}\left\{\frac{M}{M_o^2}\right\}\right\}\right]^{1/2} . \qquad (2.83)$$

It should be noted that the maximum thickness of the main vortices is, to a first approximation, solely a function of the parameter M/M_o^2. This is shown graphically in Figure 18.

Region of Applicability

The region of applicability of the solution will now be determined by reconsidering the order of magnitude assumptions which were made in view of the solutions that have been obtained for the time-dependent and time-mean velocities.

In order to reduce the governing equations the following orders of magnitude were assumed for each of the characteristic velocities:

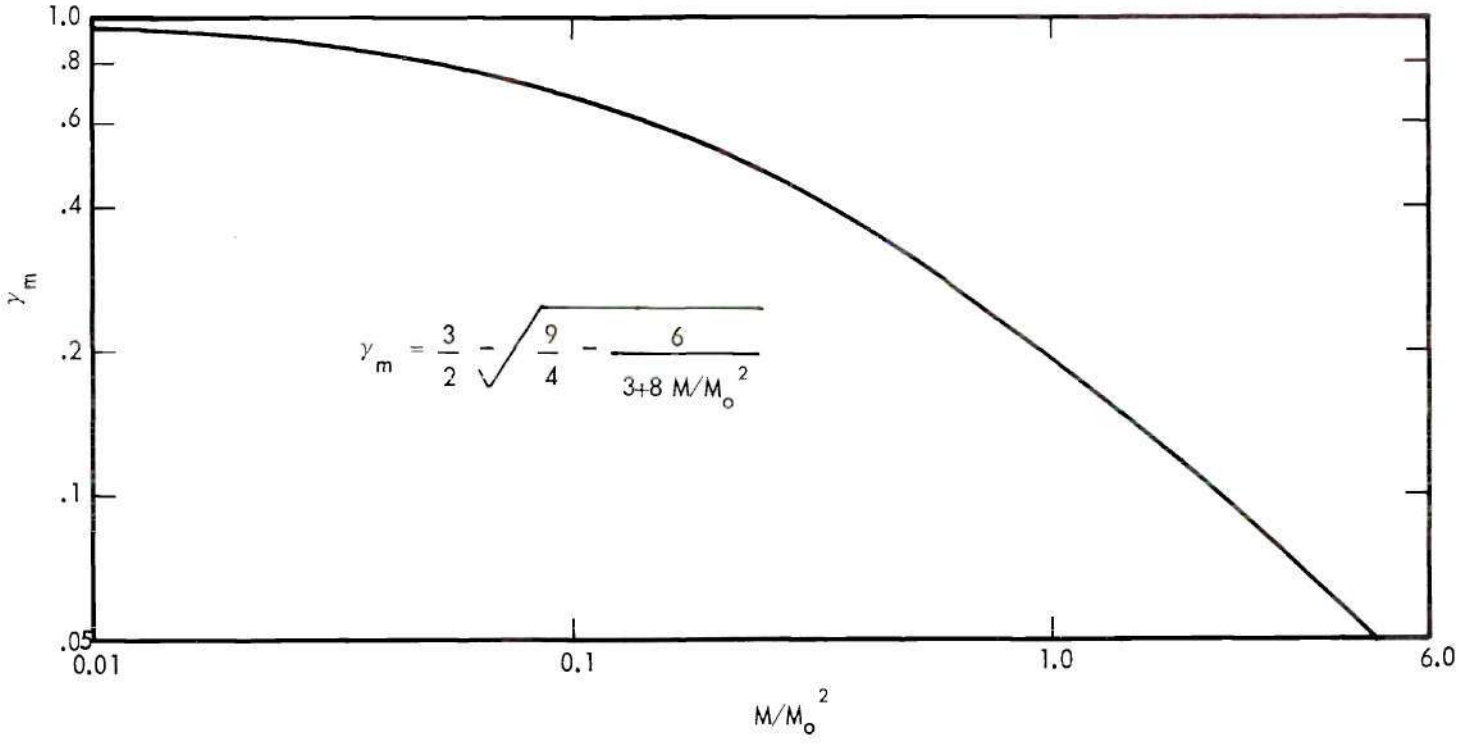

Figure 18. Maximum Thickness of the Main Vortices Versus M/M_o^2.

$$\theta(U_o/c) = \delta$$

$$\theta(V_o/U_o) = \delta$$

$$\theta(\bar{U}/U_o) = \delta$$

$$\theta(\bar{V}/U_o) = \delta^2$$

The characteristic velocities that were obtained from the velocity solutions are

$$U_o = U_o$$

$$V_o = U_o \delta \qquad \text{or} \qquad V_o/U_o = \delta$$

$$\bar{U} = U_o M_o \qquad \text{or} \qquad \bar{U}/U_o = M_o$$

$$\bar{V} = U_o M_o \frac{a}{\lambda} \qquad \text{or} \qquad \bar{V}/U_o = M_o \frac{a}{\lambda}$$

and, therefore, the original order of magnitude assumptions will be satisfied if $\theta(M_o) = \delta$ and $\theta(a/\lambda) = \delta$. This means that the half width of the channel should be small in comparison to the wavelength of the acoustic waves.

Another term should also be considered in this discussion. If $\bar{u}'(x',y)$ is to be of order one, then $|U/\bar{U}|$ must be less than or equal to one, i.e.

$$|U/(U_o M_o)| \leq 1$$

or

$$|M| \leq M_o^2 \quad .$$

This means that this solution does not predict the effect of very small intensities of sound on laminar channel flow and, therefore, the condition of no sound is not a special case of this solution. It is interesting to note that the time-mean x-component of velocity for no sound is nevertheless the same as that for fully-developed channel flow (Couette flow).

The region of applicability may be summarized by stating that the flow must satisfy the following conditions:

$$M_o \ll 1$$

$$|M| \leq M_o^2$$

$$a/\lambda \ll 1 \quad .$$

CHAPTER III

EXPERIMENTAL INVESTIGATIONS

Instrumentation and Equipment

Geometry

Before the analytical study that was presented in Chapter II was undertaken a preliminary flow visualization study was conducted to determine if a resonant acoustic field will produce a time-mean secondary flow. Since Jackson's heat transfer experiments had been conducted for a circular tube it seemed logical to use a circular tube for the preliminary flow visualization study. The qualitative results of this investigation, as shown in Figure 19, demonstrated that secondary time-mean flow does exist and that the flow seems to be periodic with respect to axial position with a period of one half the wavelength of the impressed resonant sound field.

This study also showed that when secondary flows were present, the average through-flow velocity, U, was small in comparison to the maximum time-periodic velocity, U_o. It also indicated that the pressure disturbance was small in comparison to the time-mean pressure. These observations, the analyses of Rayleigh and Westervelt, and the flow visualization study of Andrade formed the basis of the analysis which was presented in Chapter II.

It was originally anticipated that a study of the two-dimensional channel would produce the simplest experimental system. Consequently, the theoretical work was based upon the infinite parallel plate geometry. This geometry would also afford a comparison of Westervelt's solution with the special case of no through flow.

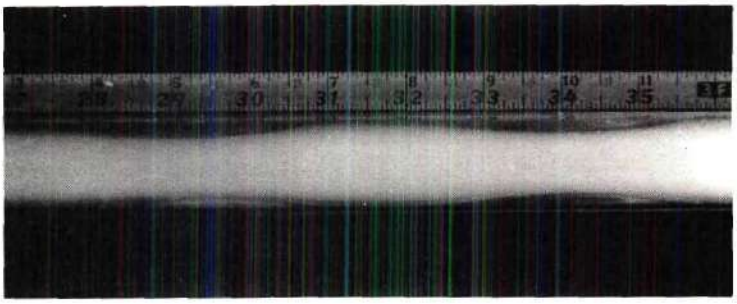

FLOW

(a) 1440 cps
$M \approx 1 \times 10^{-4}$

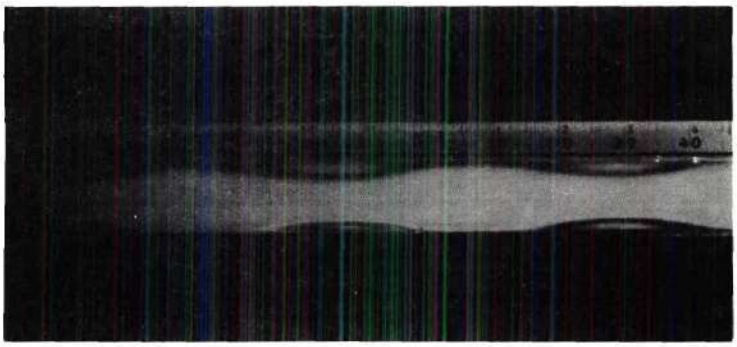

FLOW

(b) 1600 cps
$M \approx 1 \times 10^{-4}$

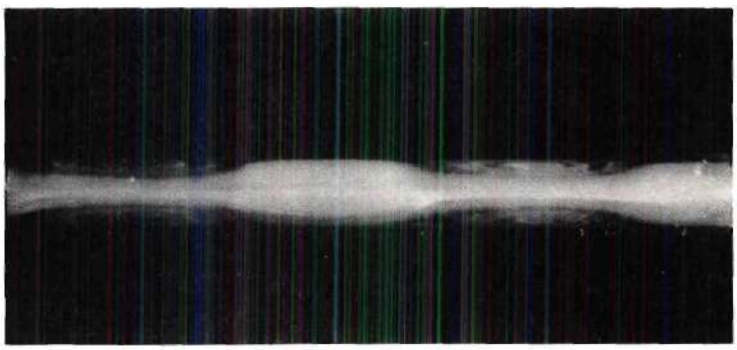

FLOW

(c) 1120 cps
$M \approx 0.5 \times 10^{-4}$

Figure 19. Qualitative Smoke Patterns from Preliminary Investigations for Circular Tube Flow.

A preliminary investigation of a rectangular duct verified the premise that standing vortices could also be produced in this flow. A typical vortex is shown in Figure 20. Unfortunately, this geometry from an experimental aspect has many disadvantages. Several of these are discussed below.

1. In order to improve a flow visualization apparatus from one which simply verifies the existence of standing vortices to one which will yield quantitative data, a great deal of care must be taken in the design to be certain that the actual flow is representative of the postulated channel flow. Since a side boundary layer is formed in a rectangular duct, the duct width to height ratio should be quite large so that the side boundary layer effect will be negligible.

2. In order to verify the analytical solution, the easiest parameter to measure is the size of the main vortices which should be solely a function of $U/(U_o M_o)$ or M/M_o^2. Accurate measurements from photographs require a duct height of at least 0.5 inch.

3. In order to produce the required acoustic field with a simple driver-horn system, the smallest horn outlet dimension should also be at least 0.5 inch. This in tern limits the minimum frequency which can be used without injuring the driver to about 1000 cps and a corresponding wavelength of approximately 14 inches for normal atmospheric air.

4. In order to have plane wave propagation, the largest duct dimension should be small in comparison to the wavelength.

If conditions 1 and 2 are satisfied then the duct should be at least 12 inches wide and, therefore, from condition 3 the duct width will be equal to, or greater than the wavelength. This is in direct contradiction

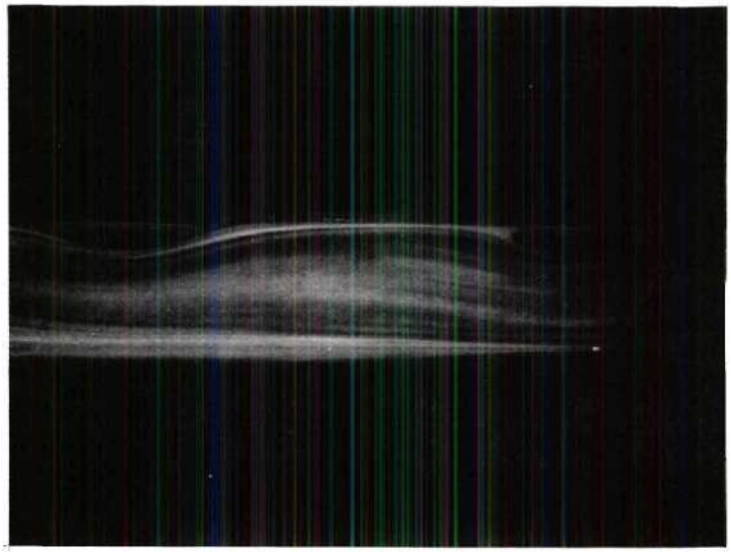

FLOW

FREQUENCY ≈ 1000 cps
MACH NUMBER ≈ 0.0001

Figure 20. Qualitative Smoke Patterns from Preliminary Investigations for Rectangular Tube Flow.

to condition 4. In order to overcome the above difficulties a new method of producing the sound field would have to be devised.

If the same factors are considered for a circular tube then it is found that no outstanding limitations exist other than relating the quantitative results for a tube to the analytical solution for a channel. Circular tube flow is axially symmetric (no extraneous side boundary layer effects) and the tube diameter can be made sufficiently small in comparison to the sound wavelength without sacrificing accuracy in the vortex measurements.

With the premise that the vortex size should be a function of the same parameter, M/M_o^2, for both circular tube flow and channel flow, it was decided to attempt to perfect the circular tube geometry in order to obtain quantitative flow visualization data.

Test Section

The test section, shown photographically in Figure 21, was composed of the following items:

Inlet Plenum Chamber. The inlet plenum chamber was a hollow-rectangular parallelepiped 15 inches wide, 12 inches long and 12 inches high. Five of the sides were constructed from 1/2 inch plywood and the sixth side was constructed from 1/2 inch plexiglass to permit observation of the fluid within the inlet plenum chamber.

The light beam or the sound pressure probe was admitted to the plenum chamber through changeable panels in the side directly opposite the tube entrance. These panels were sealed by compressing automotive weather stripping between the panel and the plenum with four bolts with wing nuts.

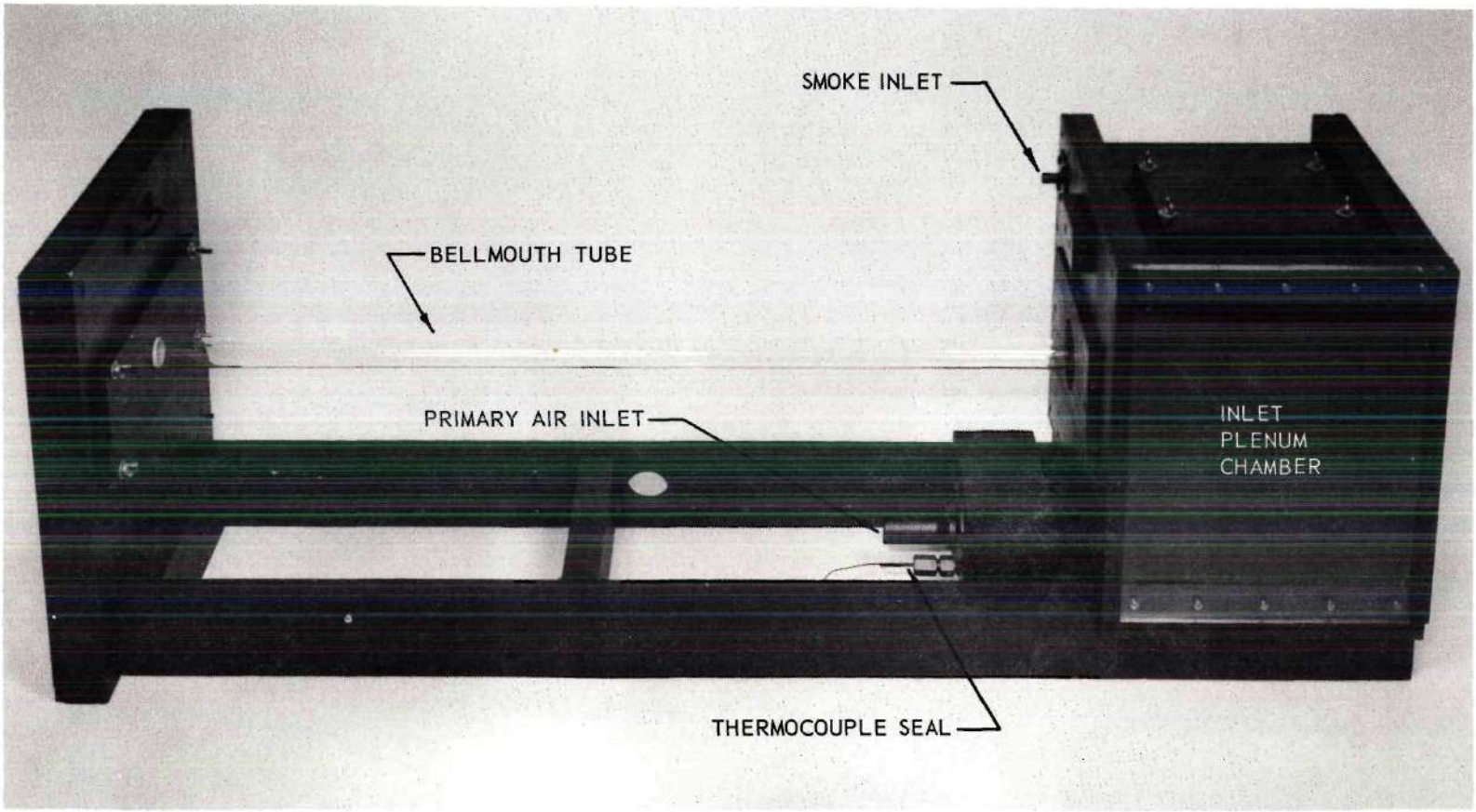

Figure 21. Photograph of the Circular Tube Test Section.

The flared end of the bellmouth tube was cemented to another panel which could be easily removed (the tube had to be removed for cleaning after one or two hours of operation). This panel was held in place with four bolts and wing nuts and the cracks were sealed from the inside with adhesive sealing tape. A 6-1/2 x 6-1/2 inch access panel was provided in the top side of the plenum to permit this sealing. An air-tight seal for this panel was achieved by compressing automotive weather stripping between the access panel and the top of the inlet plenum with four bolts and wing nuts.

The primary air was admitted to the inlet plenum chamber from a small calming chamber attached to its bottom surface. The air flow from this chamber was directed up and to the rear of the plenum by a 1/2 x 6 inch inclined duct which joined the two chambers. This provided sufficient residence time for the air to reach thermal equilibrium with the system and it also prevented appreciable distortion in the velocity profile at the tube inlet.

Smoke was admitted to the inlet plenum through a 1/2 inch tube near the top of the chamber.

The temperature of the fluid in the inlet plenum was measured with an iron-constantan thermocouple in conjunction with a Leeds and Northrup Cat. No. 8692 portable temperature potentiometer. The thermocouple was mounted in a Conax thermocouple gland seal fitting.

The inlet fluid (air-smoke mixture) temperature was constant to within the sensitivity of the potentiometer ($\pm$ 1/4° F) since the laboratory was air-conditioned and the thermal inertia of the air supply and test section was large enough to dampen the small oscillations in temperature that resulted from the cycling of the air-conditioning unit.

Bellmouth Tube. The air-smoke mixture passed directly from the inlet plenum chamber into a 1.094 inch I. D. bellmouth Pyrex glass tube that was 42 inches long. This length was chosen for the following reasons:

1. Pyrex glass tubing is supplied in 48 inch lengths. After one end of the tube was flared to form a bellmouth this length was reduced to approximately 45 inches.

2. The laboratory temperature was to be maintained between 72 and 80° F for personal comfort. This limited the range of the speed of sound, c_o.

3. For convenience, a fundamental frequency that was an integral multiple of five or ten should be chosen.

From equation 2.58, $\omega = 2\pi\, c_o/\lambda$, but the frequency, f, is related to the circular frequency, ω, by $\omega = 2\pi f$. Thus

$$\lambda = c_o/f \quad . \tag{3.1}$$

Morse (14) gives the following expression for the effective length of a small tube open at both ends:

$$L_e \cong L + 0.85\, D \tag{3.2}$$

where L is the actual length of the tube and D is the inside diameter of the tube. For an open-open tube the fundamental wavelength is twice the effective length of the tube. A trial and error solution of the foregoing equations resulted in a length of 42 inches, a fundamental frequency of 160 cps and an air inlet temperature of 75° F.

After flowing through the tube the air-smoke mixture was discharged into an exit plenum chamber and, subsequently, into the exhaust duct which

was vented to the atmosphere. In order to reduce the back pressure on the bellmouth tube and thereby reduce the possibility of leaks, a small centrifugal blower was installed in the exhaust duct. Enough secondary air was added to the exhaust flow to maintain the test section pressure slightly above that of the atmosphere.

Exit Plenum Chamber. The exit plenum chamber, a hollow thick walled rectangular parallelepiped that was 15 inches wide, 19-1/2 inches long and 15 inches high, served as the housing for the driver-horn assembly and as the receiver for the air-smoke mixture. It also provided an open tube acoustic boundary condition for the bellmouth tube. A hinged rear door was installed in this chamber to provide easy access to the driver and horn.

Light Source

Two light sources were used in this study; a 400 watt Ken-Rad Type H-25 mercury vapor lamp in conjunction with a Sola mercury lamp transformer and a Kemlite-Laboratories Model LTXM-4 150 watt-second line flashtube in conjunction with a Heiland Strobonar IV. The flow was illuminated by directing a light beam down the axis of the tube from its inlet end. Either two collimating slits were used to produce a light beam to illuminate a vertical plane of fluid through the axis of the tube or the beam was allowed to illuminate the entire flow field.

The mercury vapor lamp was used for continuous operation but the low intensity of light that it produced made it necessary to use time exposures of up to ten seconds. The flashtube unit permitted short duration exposures but since the time-mean flow was very steady the photographic data were the same for both light sources.

Although the plane beam of light produced superior streamline definition, several photographic experiments showed that sufficient detail of the main vortices to permit measurement of their size was obtained by illuminating the entire tube. Since the light intensity was appreciably greater when the entire tube was illuminated, this condition was used to obtain the quantitative data. The mercury vapor lamp system is shown photographically in Figure 22.

Air and Smoke Supply

Air Supply. Low pressure atmospheric air was supplied by a variable speed Roots-Connersville Type AF-22 rotary positive blower in conjunction with a Vickers 3/4 H.P. hydraulic transmission and a 1/4 H.P. electric motor. Air entered the blower through an inlet air filter, was compressed to a pressure of ten inches of water and was then discharged into a 3.2 cubic-foot surge tank. This tank was used to dampen the low frequency pressure pulsations that were produced by the positive displacement blower. The surge tank was maintained at a pressure of ten inches of water by a pressure relief valve situated between the blower and the tank. The blower speed was regulated to a value which produced a slow bleed of air through this valve.

The volumetric air flow from the surge tank was measured with an American Meter dry gas meter during the qualitative studies and with a Precision Scientific wet test meter during the quantitative studies. The flow rate was determined for both systems by measuring the time it took for at least ten complete revolutions of the gas meter dial with a Precision Scientific Time-It. The two air flow circuits that were used are shown schematically in Figure 23. The uncertainty in the flow rate is estimated to be less than ± 1 per cent.

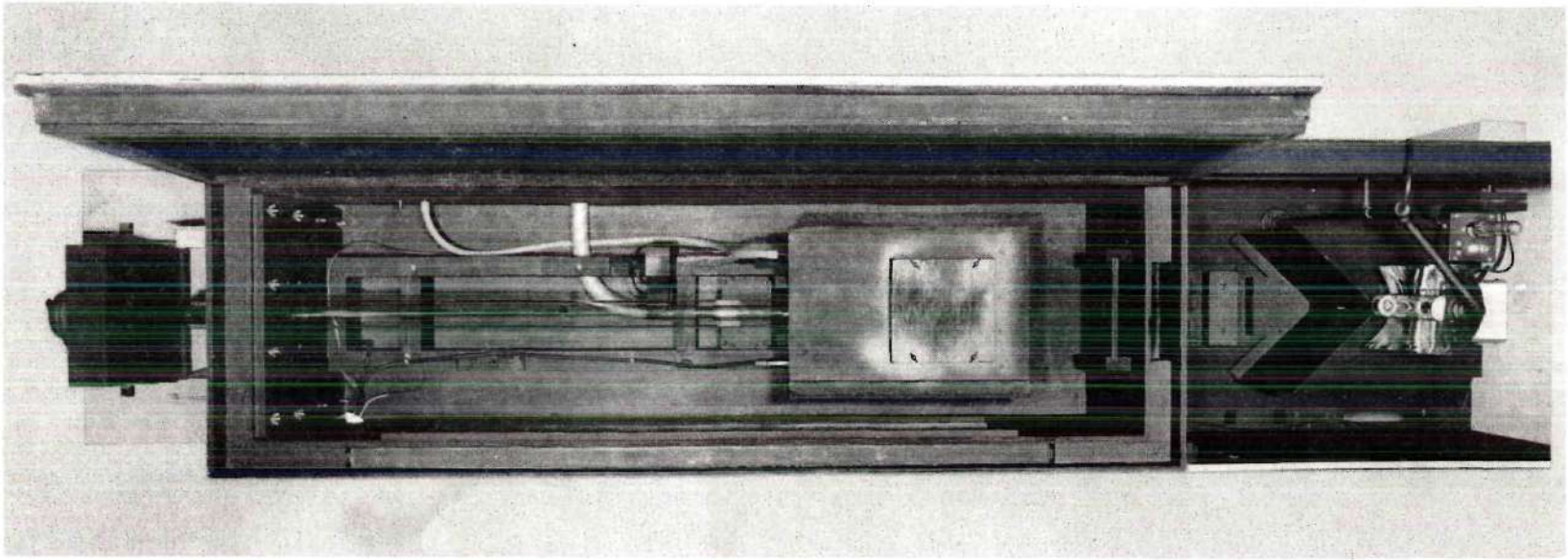

Figure 22. Top View of the Flow Visualization Equipment.

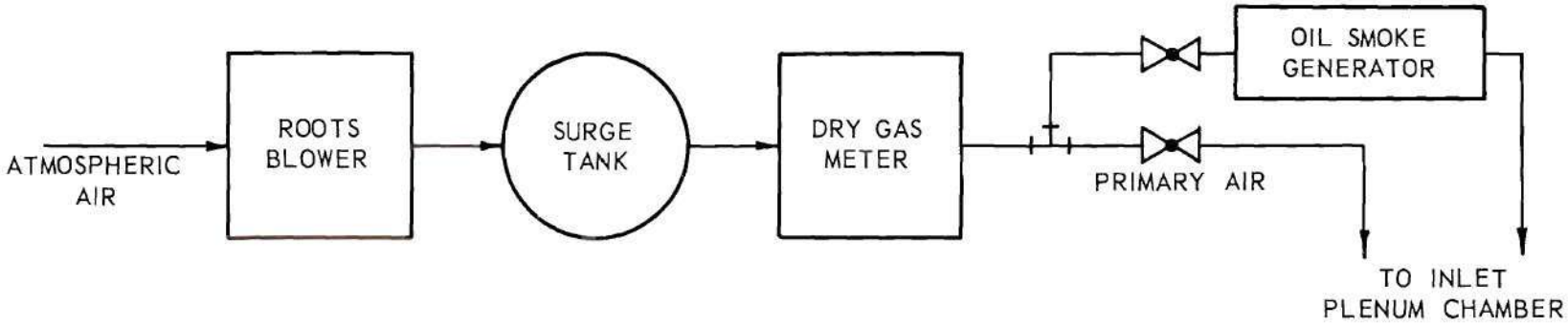

FLOW CIRCUIT FOR QUALITATIVE INVESTIGATIONS

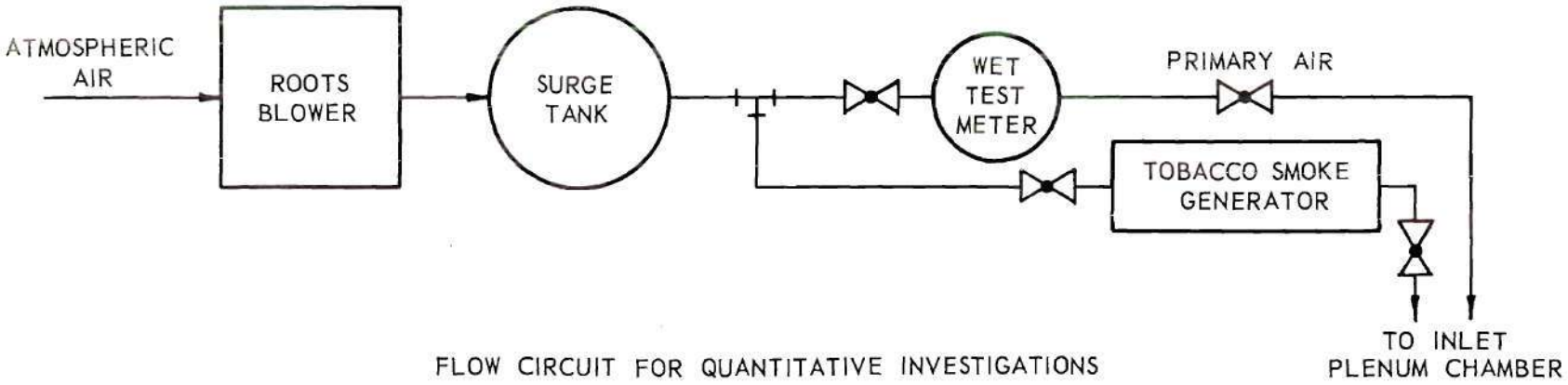

FLOW CIRCUIT FOR QUANTITATIVE INVESTIGATIONS

Figure 23. Flow Circuit Diagrams.

Smoke Supply. Several smoke generators were developed for the experimental studies. The first generator was similar to a very large tobacco bowl pipe. It was charged with approximately one fourth of a can of pipe tobacco and produced excellent smoke for about one hour. This system had to be cleaned after two hours of operation and this proved to be a very time consuming and distasteful task. In order to produce a clean continuous source of smoke an oil vaporizer was developed.

The oil vaporizer, shown photographically in Figure 24, consisted of an oil reservoir fitted with four fiberglass wicks which were heated to produce oil vapor by four spirally-wound nichrome resistance heaters. The heater temperature was controlled with a Superior Electric Powerstat by varying the A.C. voltage across the series-connected heaters. The wicks, the heaters, and the oil reservoir were enclosed in a sealed chamber which was held under a positive pressure by air from the air supply system. The air-smoke mixture left the generator through an exhaust tube located 1/2 inch from the heaters. Primary air was mixed with the air-smoke mixture from the oil vaporizer in the inlet plenum chamber. This system produced excellent qualitative data and it also permitted the very long runs which were necessary to perfect a satisfactory experimental technique. No qualitative difference between the streamline patterns produced by the tobacco smoke and the ones that were produced by the oil vapor could be observed. It was only after reliable quantitative data were taken that a noticeable difference occurred. (This point will be discussed further in Chapter IV.)

The tobacco smoke generator that was finally used to obtain the quantitative data is shown schematically in Figure 25. This generator, developed by Johnson (13) for his studies of Kindt's tubes, consisted of

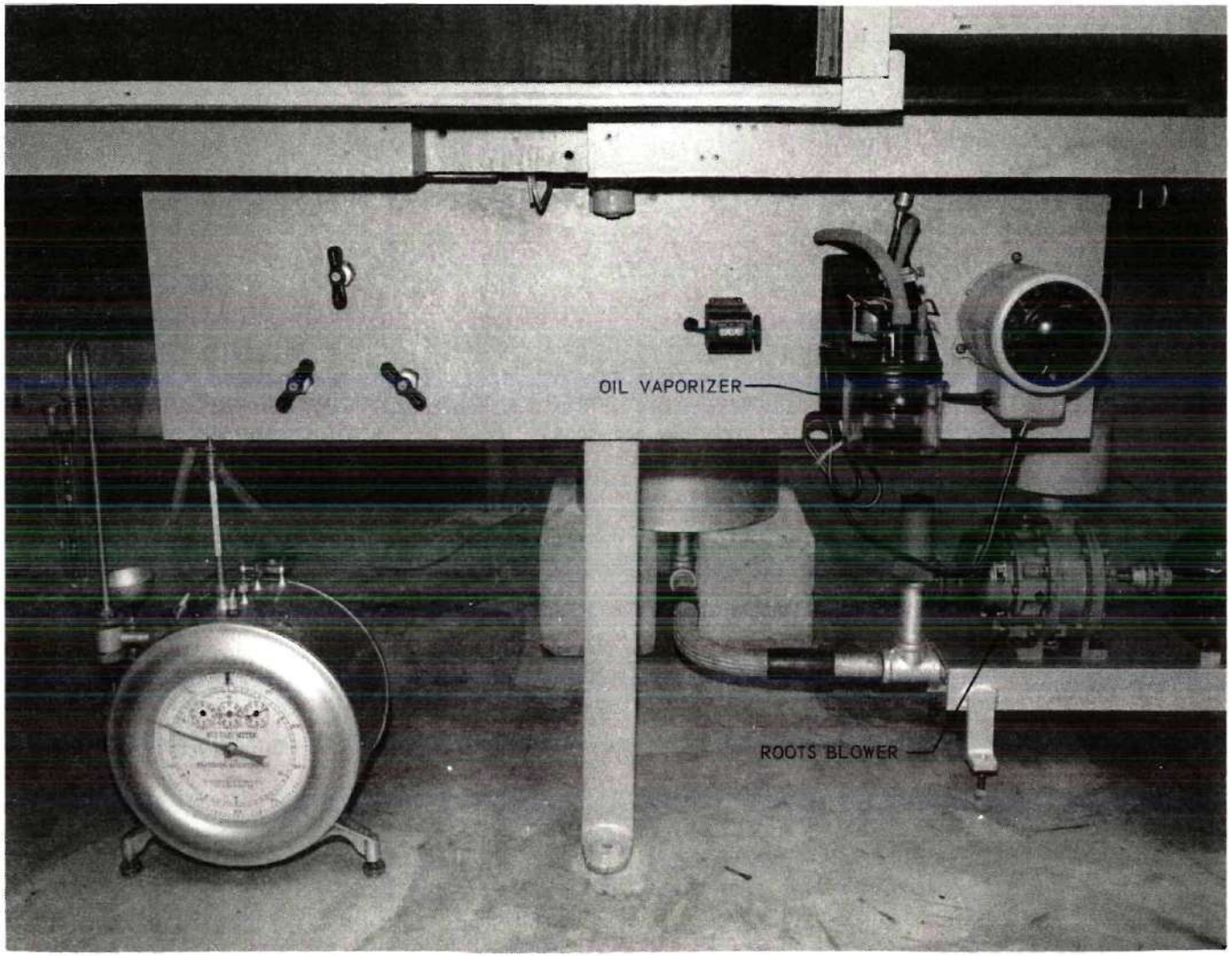

Figure 24. Oil Vaporizer System.

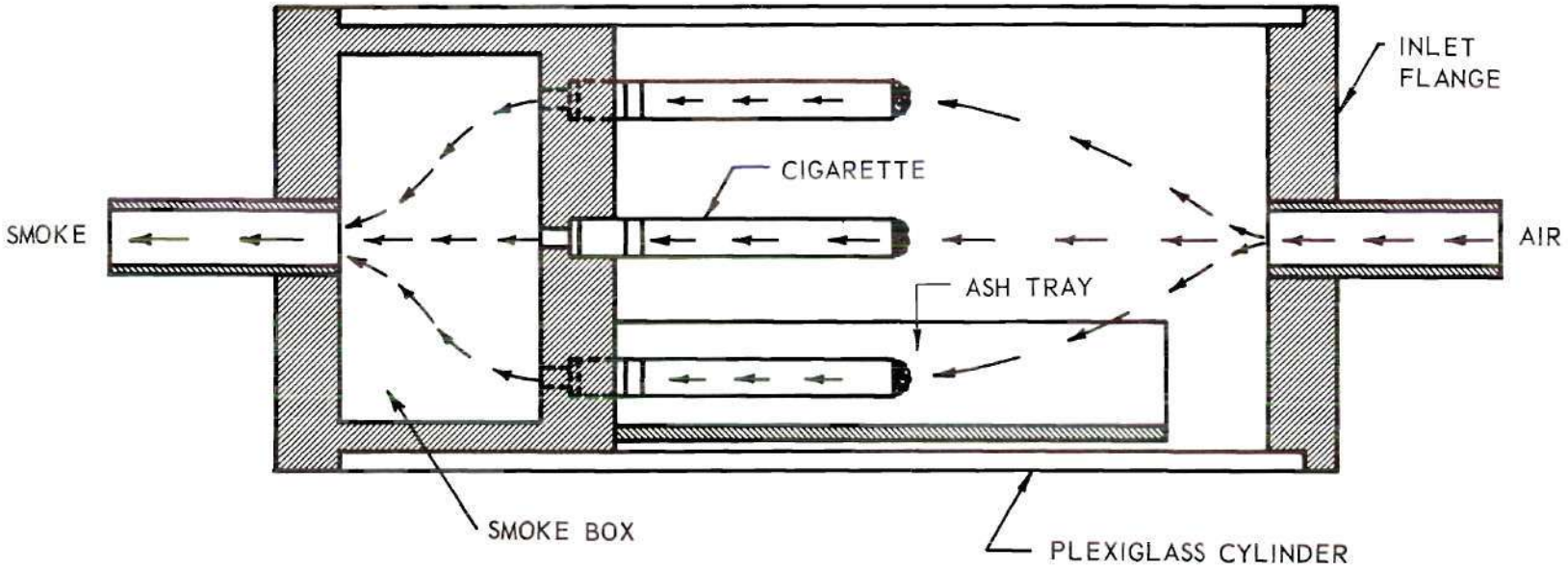

Figure 25. Tobacco Smoke Generator.

a 3 inch I. D. plexiglass cylinder closed at one end with an inlet flange fitted with a rubber tube fitting and at the other end with a smoke-box. This box was provided with receptacles for five filter tip cigaretts and an ash tray to protect the plexiglass cylinder. After lighting the cigarettes with a resistance heater, the inlet flange was clamped in place and the cylindrical chamber was then pressurized with fresh air from the surge tank. The air flow was regulated to produce a satisfactory burning rate. The cigarette smoke passed through the unburned tobacco and the filter; it entered the smoke-box, and was finally sent to the inlet plenum chamber without further filtration. The smoke produced by five cigarettes often lasted for as long as 30 minutes. This smoke was diluted in the inlet plenum chamber by the primary air stream and since the smoke was added periodically, the air-smoke mixture varied with time. This variation did not affect the streamline patterns, at least within the accuracy of the measurements that were made.

Tar from the tobacco smoke formed a deposit on the tube wall and made it necessary to clean the tube before each data run since these deposites caused additional secondary flows which distorted the desired flow patterns.

Sound Generating Equipment

The sound generating equipment is shown schematically in Figure 26 and photographically in Figure 27. A Hewlett-Packard Model 206A low distortion audio signal generator provided a source of continuously variable audio-frequency voltage at a total distortion level of less than 0.1 per cent. This signal was amplified by a Bogen Model CHA-75 amplifier. The amplifier output voltage, current, and power were measured with a John

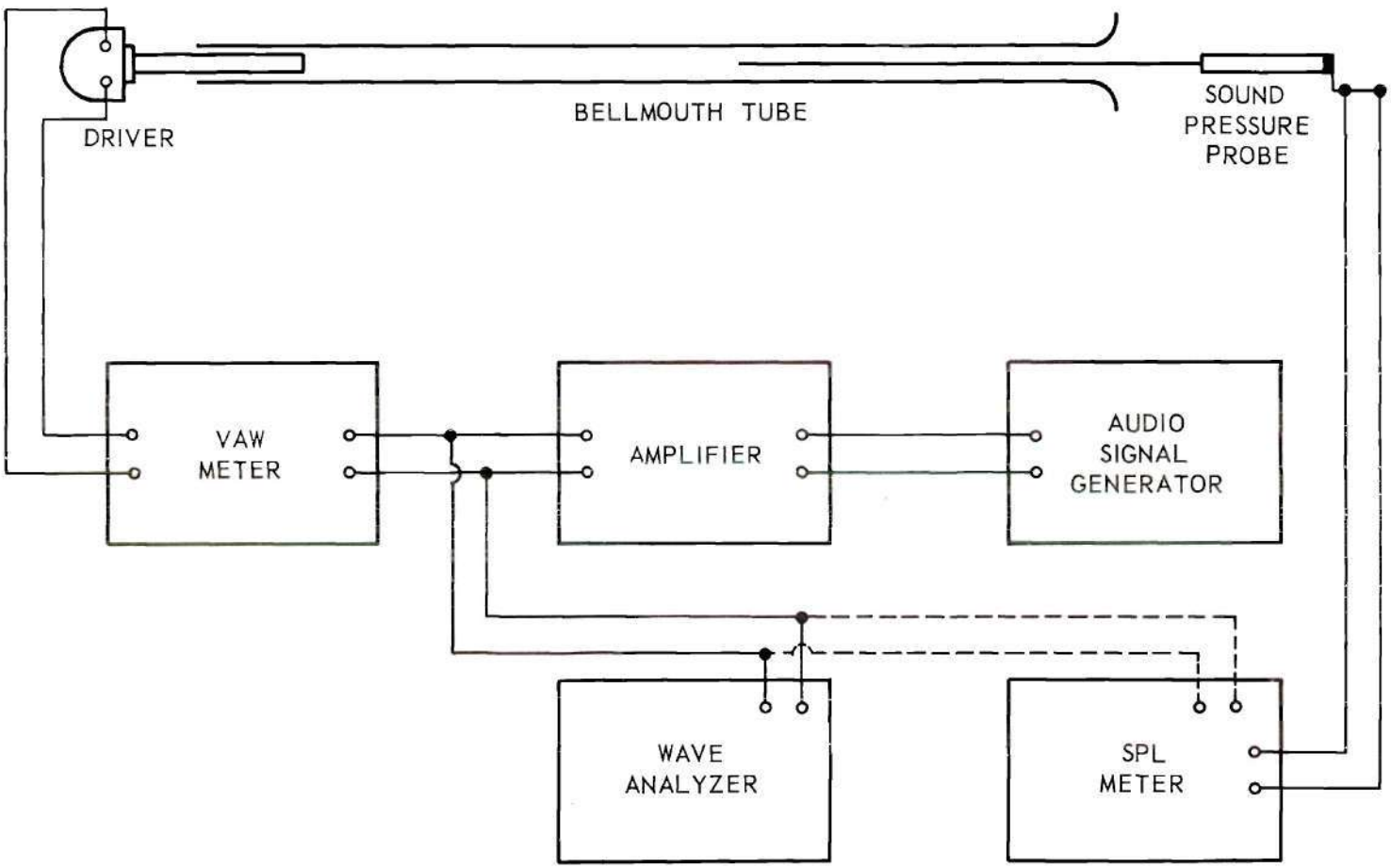

Figure 26. Schematic Diagram of the Sound Generating and Measuring Systems.

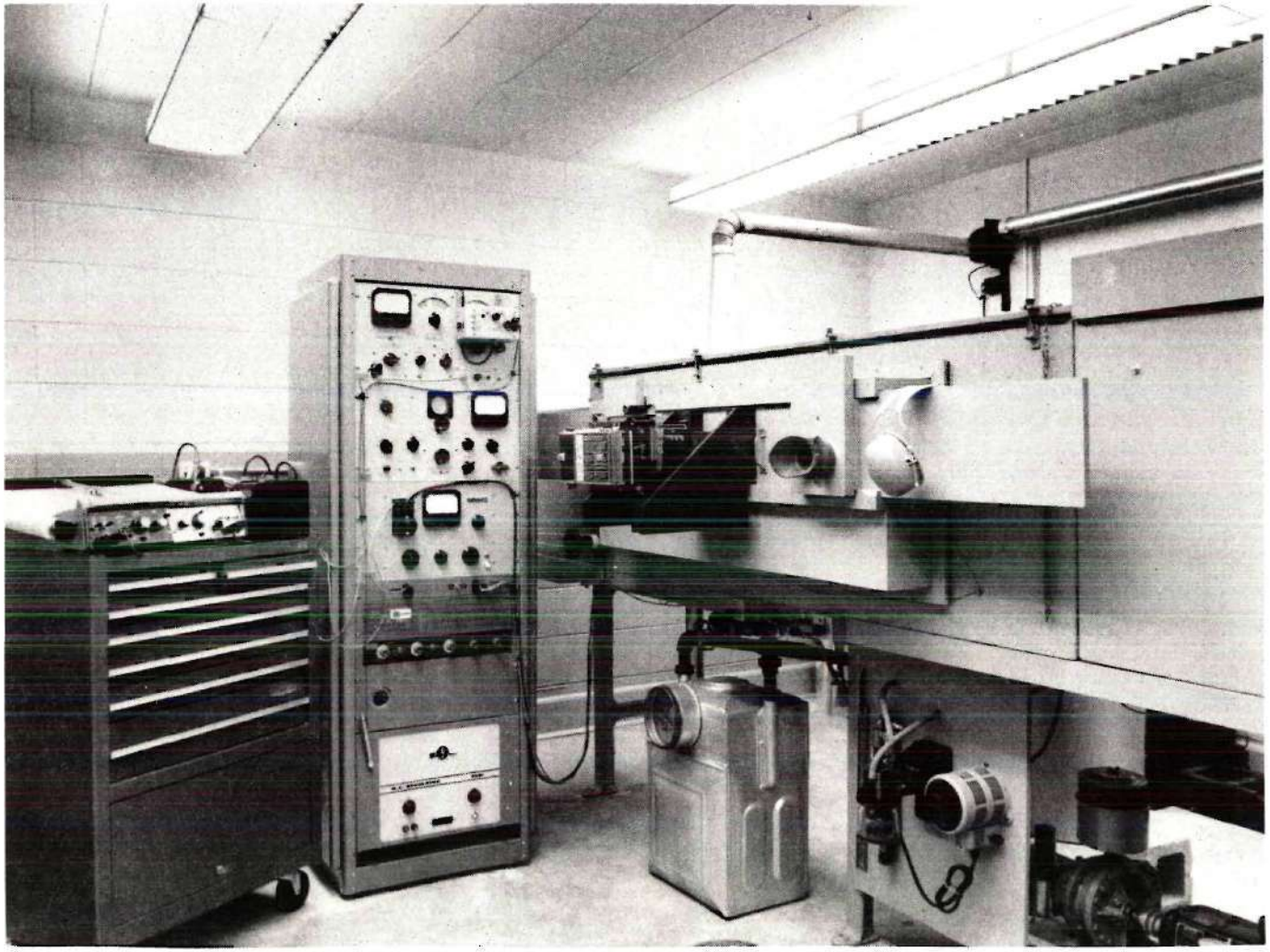

Figure 27. Photograph of the Flow Visualization Apparatus.

Fluke Model 102 "VAW" meter. The electrical to mechanical conversion was achieved with a University Model PA-HF speaker driver in conjunction with a one-inch O. D. by 12-1/2 inch long cylindrical horn. The speaker had a frequency response of 70 to 10,000 cps and a power rating of 25 watts when operated at a constant frequency.

In order to properly couple the driver-horn system to the resonant acoustic field in the tube, it was necessary to mount the driver-horn assembly on a sliding platform that could be moved in the axial direction by a hand wheel mounted on the exit plenum chamber. When the sound generating system was properly adjusted, wave analyses of the acoustic field showed that the distortion level was less than one per cent.

Sound Measuring Equipment

The sound measuring equipment included the following General Radio items:

Item	Type
Sound level meter	1551-A
Power supply	1262-A
High level microphone assembly	1551-P1H
20 db attenuator pad	1551-P11
Sound level calibrator	1552-B
Transistor oscillator	1307-A

In addition to the General Radio items listed above a Hewlett-Packard Model 302A wave analyzer in conjunction with a Hewlett-Packard Model 297A sweep drive and a Moseley Model 2D Autograf X-Y recorder were used to record and analyze the sound pressure in the test section.

In order to measure the axial distribution of the sound pressure in the test section, a pressure probe was made by mounting the high level microphone (Altec 21-BR-180 condenser microphone) in a special receptacle at one end of a six-foot long by 1/8-inch O. D. stainless steel tube. The tube was open at the other end. It was necessary to use this arrangement since the microphone could not be inserted directly into the 1.094-inch I. D. tube without appreciably changing the sound field.

The microphone end of the probe was supported by a small two-wheel carriage that ran on a 72-inch track. A ten-turn potentiometer and a dial cord were used to produce a linearly varying D.C. voltage that was proportional to the axial position of the probe. This voltage was used to excite the X-mode of the X-Y recorder. The output from either the microphone or the wave analyzer was used to excite the Y-mode. With this probe, shown photographically in Figure 28, the logarithm of the sound pressure was plotted versus axial position. A typical plot is shown in Figure 29.

Since the pressure probe was long, it was necessary to determine the probe attenuation as a function of frequency and intensity. This was achieved by producing a sound field in a two inch I. D. Pyrex glass tube and then by measuring the sound pressure level at a fixed axial position with the pressure probe and, subsequently, with the microphone alone. This process was carried out for each of the resonant frequencies that were used in the quantitative data runs. The attenuation was found to be virtually independent of intensity. The following table shows its dependence upon frequency:

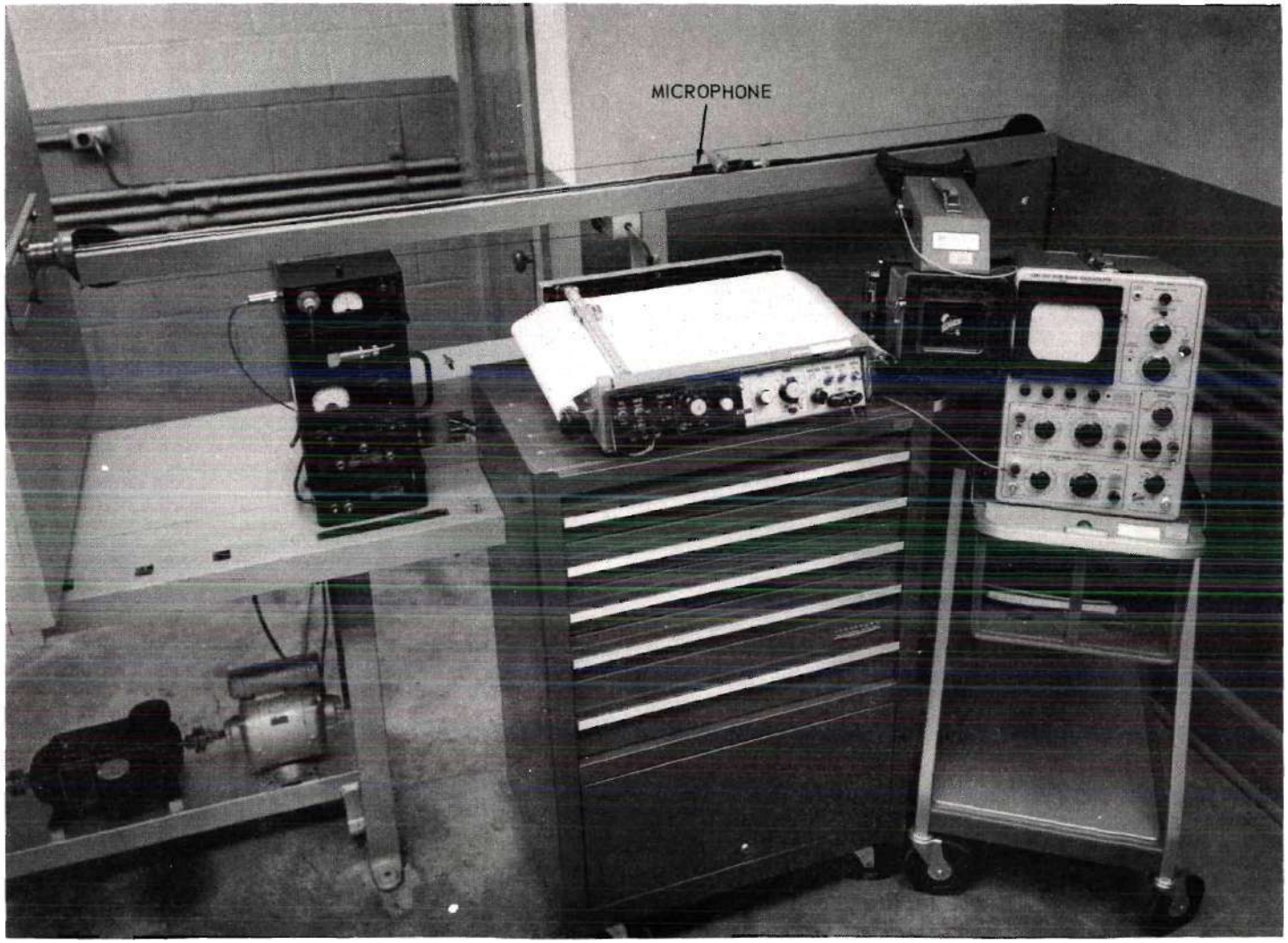

Figure 28. Photograph of the Sound-Pressure Probe.

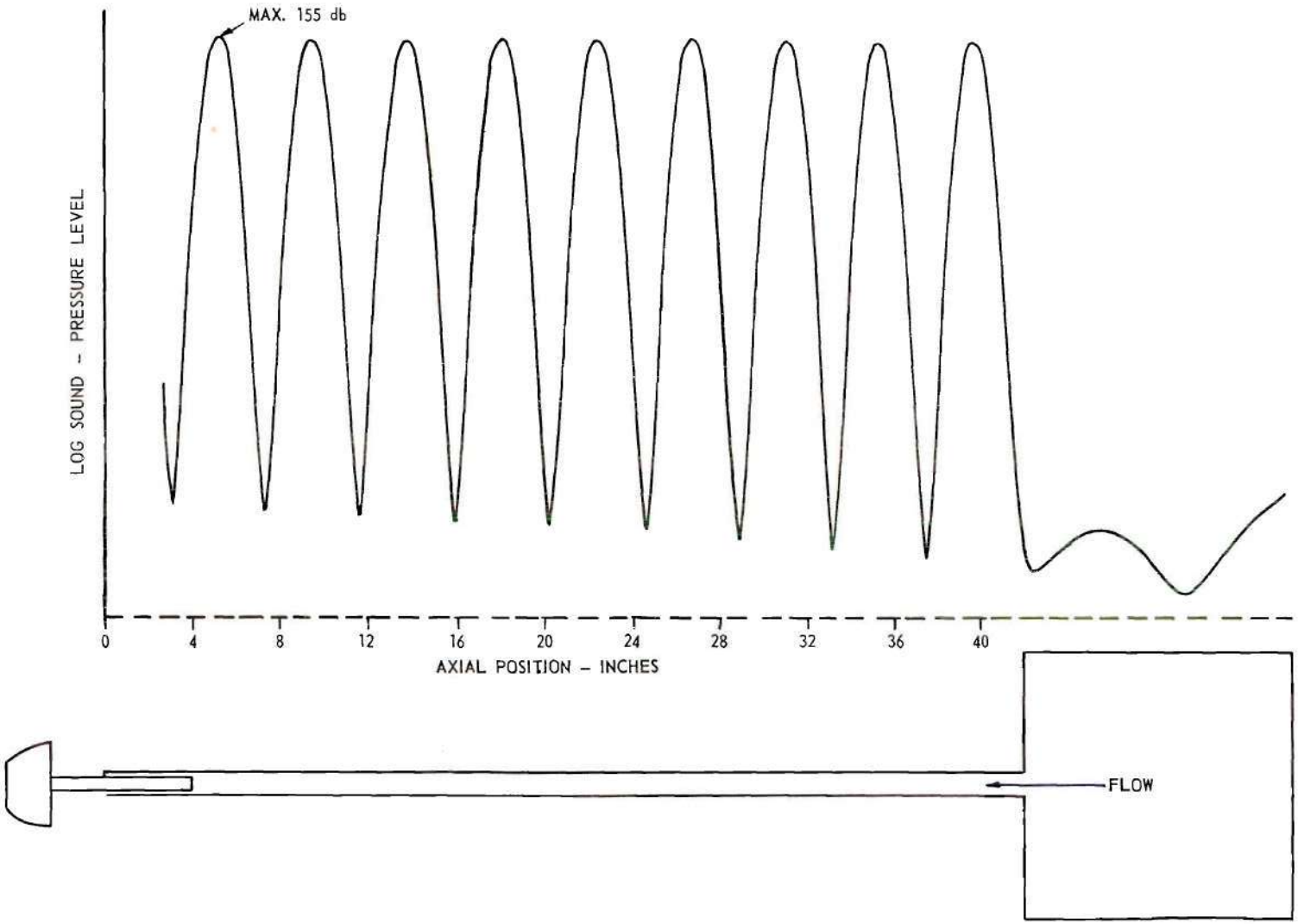

Figure 29. Typical Sound-Pressure Distribution (Frequency=1600 cps).

Table 1. Sound Probe Attenuation

Frequency (cps)	Attenuation (db)
800	24.4
960	26.5
1120	28.9
1280	30.1
1440	30.5

The condenser microphone was quite sensitive to humidity and, therefore, it was necessary to calibrate it before each run, with a General Radio Type 1552-B calibrator which produced a sound-pressure level of 121 ± 1 db (re 0.0002 μbar). The overall uncertainty in the sound-pressure probe measurements was estimated to be less than ± 1.5 db.

The sound-pressure level, SPL, measured relative to a pressure of 0.0002 microbar is defined (15) as

$$SPL \equiv 20 \log (P/0.0002) \text{ db} \tag{3.3}$$

where P is the r.m.s. pressure deviation due to the sound waves expressed in microbars. If the pressure and velocity are assumed to have the same relationship that they do in an inviscid perfect gas undergoing resonant acoustic vibrations

$$|p_1|_{max} = \sqrt{2}\ P_{max} = \rho_o c_o U_o \quad , \tag{3.4}$$

then the following expression can be obtained for the acoustic Mach number, M_o:

$$M_o \equiv \frac{U_o}{c_o} = 0.2 \cdot C_p \cdot 10^{[(SPL-180)/20]} \qquad (3.5)$$

where C_p is the ratio of standard atmospheric pressure to the static pressure in the tube. It is of interest to note that an uncertainty of ± 1.5 db in the SPL results in an uncertainty of approximately ± 17 per cent in M_o. If this is combined with the uncertainty in the flow rate measurements, then the uncertainty in the parameter M_o^2/M is approximately ± 35 per cent.

A Sorensen Model 2501 A.C. line voltage regulator was used to supply 117-volt A.C. power to all of the electronic equipment.

Photographic Equipment

The photographic equipment consisted of a Graflex 4 x 5 inch Speed Graphic camera with a Schneider Xenctar 1:2, 8/150 lens and a Polaroid Land Camera back. Polaroid Type 47 film (3000 speed) was used exclusively. Due to the low intensity of light produced by the mercury vapor lamp, it was necessary to use film exposures of five to ten seconds.

In order to obtain photographic data from various regions along the tube axis, the camera was mounted on a sliding frame (see Figure 27) which permitted axial movement of the camera parallel to the tube axis.

A strip of 10 x 10 to the 1/2 inch graph paper was cemented to a wooden strip and this strip was inserted in the tube such that the graph paper was in a vertical plane through the tube axis. Photographs of this grid showed that the tube produced no measurable distortion; at least not to the accuracy of the measurements that were used to determine the main vortex size.

Experimental Procedure

The experimental procedure that was used to obtain the quantitative data consisted of the following steps:

1. The power (117 volts, 60 cycle A.C. regulated to within ± 0.01 per cent) to the electronic equipment was turned on and a warm-up period of at least three hours was provided.

2. While the electronic equipment was stabilizing, the mercury vapor lamp, the air supply blower, and the exhaust duct blower were turned on. These items stabilized in approximately 30 minutes. The bellmouth tube was removed from the test section; it was washed and dried and then it was reinstalled in the test section. The tobacco smoke generator was also cleaned and charged during this period of time.

3. The primary air flow was adjusted to produce the desired through-flow Mach number, M. For the tube which was used the expression which related the volumetric flow rate to the through-flow Mach number is

$$M = 0.135\ Q \tag{3.6}$$

where Q is volumetric flow rate expressed in cubic feet per second.

4. One of the five resonant frequencies that were used in these investigations was set on the audio signal generator.

5. The amplifier gain was increased until audible sound was emitted by the speaker system.

6. The sound-pressure probe was inserted in the tube to the axial position where the first pressure loop occurred ($x = \lambda/4$). The amplifier gain was then increased to produce the desired acoustic Mach number, M_o. M_o was related to the sound-pressure level in the following fashion:

$$M_o = 0.2 \cdot C_p \cdot 10^{[(SPL-180)/20]} \quad . \qquad (3.5)$$

7. The axial position of the driver-horn assembly was then adjusted until the sound-pressure level, SPL, became a maximum. This adjustment also corresponded to either maximizing the voltage or to minimizing the current or power to the speaker-driver while the amplifier gain was held constant. Due to the sensitivity of the "VAW" meter, it was possible to accurately position the driver-horn assembly without using the sound-pressure probe.

Minimizing the power was the most sensitive indication of position and, therefore, this method was used exclusively.

8. A fine adjustment in the signal frequency was next made to further maximize the SPL or as in the last step, minimize the power to the speaker-driver.

The tube was resonant when for a set value of the amplifier gain the SPL could not be increased by either adjusting the axial position of the driver-horn assembly or by adjusting the signal frequency. The resonant state was also characterized by the fact that for a set value of the amplifier gain the power supplied to the speaker-driver could not be decreased by adjusting either of the above quantities and, therefore, a true resonant state could be obtained without using the sound-pressure probe. This permitted frequent checks for resonance even after the sound-pressure probe was removed from the tube.

9. The five cigarettes were lighted with a resistance heater; the air supply to the smoke generator was opened; the inlet flange of the generator was clamped in place; the air supply flow rate was adjusted such

that the cigarettes burned slowly; the tobacco smoke was blown into the inlet plenum chamber until the cigarettes burned out; the smoke-generator valves were then closed.

10. The amplifier gain was again adjusted to produce the desired value of M_o. The system was then checked for resonance and, if necessary, steps 7, 8 and 10 were repeated until the tube was resonant and the desired value of M_o was obtained.

11. The maximum value of the sound-pressure level in the tube was recorded and then the probe was removed from the tube.

12. A time period of from 10 to 15 minutes was allowed to be certain that the system was in a steady-state condition.

13. Photographs of the flow were taken at two or three different axial positions. This usually resulted in photographs of four or five pairs of "main" vortices.

14. The data that were taken during the time-interval between when the first and the last photographs were taken are: frequency (cps), power supplied to the driver (watts), volumetric flow rate of the primary air (ft^3/sec), inlet plenum chamber temperature (^oF), the wet test meter and inlet plenum chamber pressures (inches of water), and the barometric pressure (inches of mercury).

15. At the conclusion of the run the sound-pressure probe was again inserted in the tube to the axial position of the first sound-pressure loop and the maximum SPL in the tube was again recorded. If this value differed by more than $\pm$ 0.2 db from the previously recorded value of SPL, then the run was discarded.

16. The main-vortex "size" was determined by measuring the lengths $\bar{A}$ and $\bar{B}$ which are shown in Figure 30.

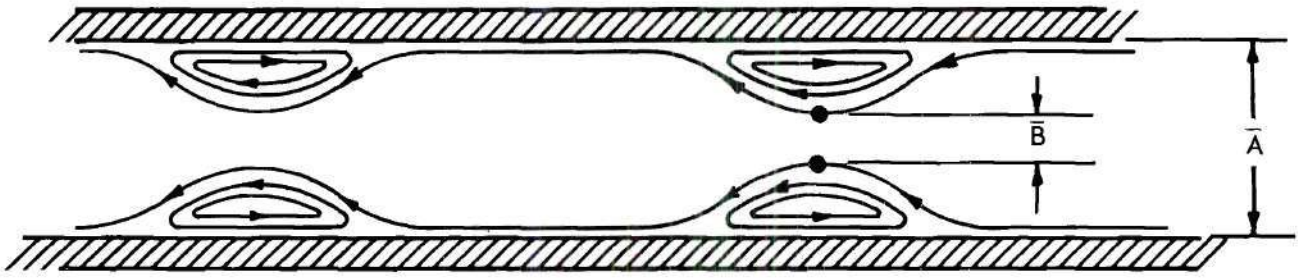

Figure 30. Schematic Diagram of Two Pairs of Main Vortices.

The main-vortex "size" is given by

$$\gamma_m = 1 - \bar{B}/\bar{A} \tag{3.7}$$

For a given lens and tube, the value of $\bar{A}$ was constant and, therefore, it was only necessary to measure $\bar{B}$. This measurement was made with a divider and scale (100 divisions per inch) and the value of $\bar{B}$ was taken as the arithematic mean of the values of $\bar{B}$ for each pair of main vortices that were photographed.

The uncertainty in the measurement of $\bar{A}$ was approximately ± 0.002 inch and that of $\bar{B}$ was approximately ± 0.005 inch. Thus, for a value of $\gamma_m = 0.1$ the uncertainty was ± 20 per cent whereas for a value of $\gamma_m = 0.5$ the uncertainty was only ± 3.5 per cent.

Discussion of Results

The results of the quantitative studies are shown graphically in Figure 31. The crosshatched region represents the uncertainty in the sound pressure level measurements (± 1.5 db) which is reflected in a corresponding uncertainty in the value of M/M_o^2. The uncertainty in the

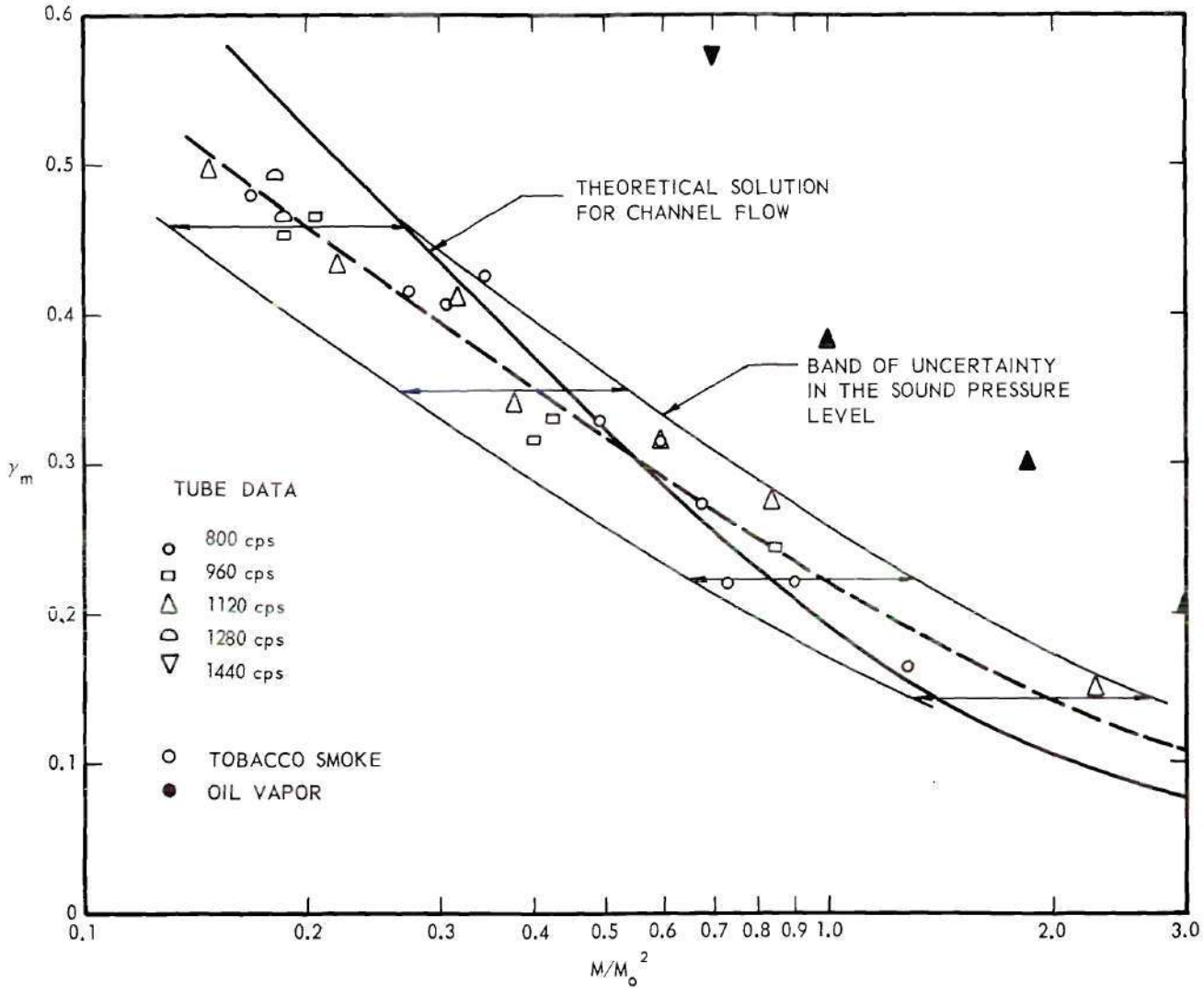

Figure 31. Comparison of Experimental γ_m for a Tube with Theoretical γ_m for a Channel.

vortex size measurements is well within this region. The dashed curve represents the general trend of the tube data and based on a given value of M/M_o^2 the scatter about this curve is less than ± 16 per cent.

The unshaded data points were obtained with tobacco smoke whereas the shaded data points were obtained with oil vapor. There is a definite quantitative difference between the streamline patterns that were produced by these tracers. This difference is attributed to the fact that the oil vapor particles were considerably larger than the tobacco smoke particles. For a given value of M/M_o^2 the vortex size was larger for the oil vapor and air mixture than it was for the tobacco smoke and air mixture. If the particle size of the tracer is extrapolated to "zero" then the true curve should lie below the present curve for tobacco smoke.

The most remarkable result of this study is the relatively close agreement of the experimental data with the theoretical vortex size for a channel. However, the slopes of the curves are different and there is a definite indication that it takes a stronger sound field to produce a given size vortex in a tube than it does in a channel.

CHAPTER IV

DISCUSSION OF RESULTS

The results which directly pertained to the effect of a resonant acoustic field upon laminar channel flow have already been presented in Chapters II and III. The discussion which follows will be concerned with a qualitative explanation of the local heat transfer effects that were discovered by Jackson, et al.

The streamline pattern shown in Figure 16 will now be closely examined in an attempt to qualitatively explain the variation in the local heat transfer coefficient that is shown in Figure 6. (Figures 6 and 16 are repeated on the following pages for convenience.) It is assumed that the channel walls are isothermal, that there is a thermal entrance at $x/\lambda = 0$ and that thereafter the walls are at a higher temperature than the mixed mean temperature of the fluid at any position x/λ.

Consider a particle of fluid X which starts at point A and then moves along its streamline in the positive x-direction. As x/λ increases the particle moves closer to the wall and since it is cooler than the wall there will be heat transfer to the particle and its temperature will increase. After passing $x/\lambda = 1/8$ the particle moves slightly away from the wall but its temperature continues to increase until it reaches $x/\lambda = 1/4$. At this point it diverges from the wall and moves along outside the main vortex parallel to another particle Y that starts at point B.

As the two particles move out into the main stream along their respective streamlines they significantly steepen the temperature gradient

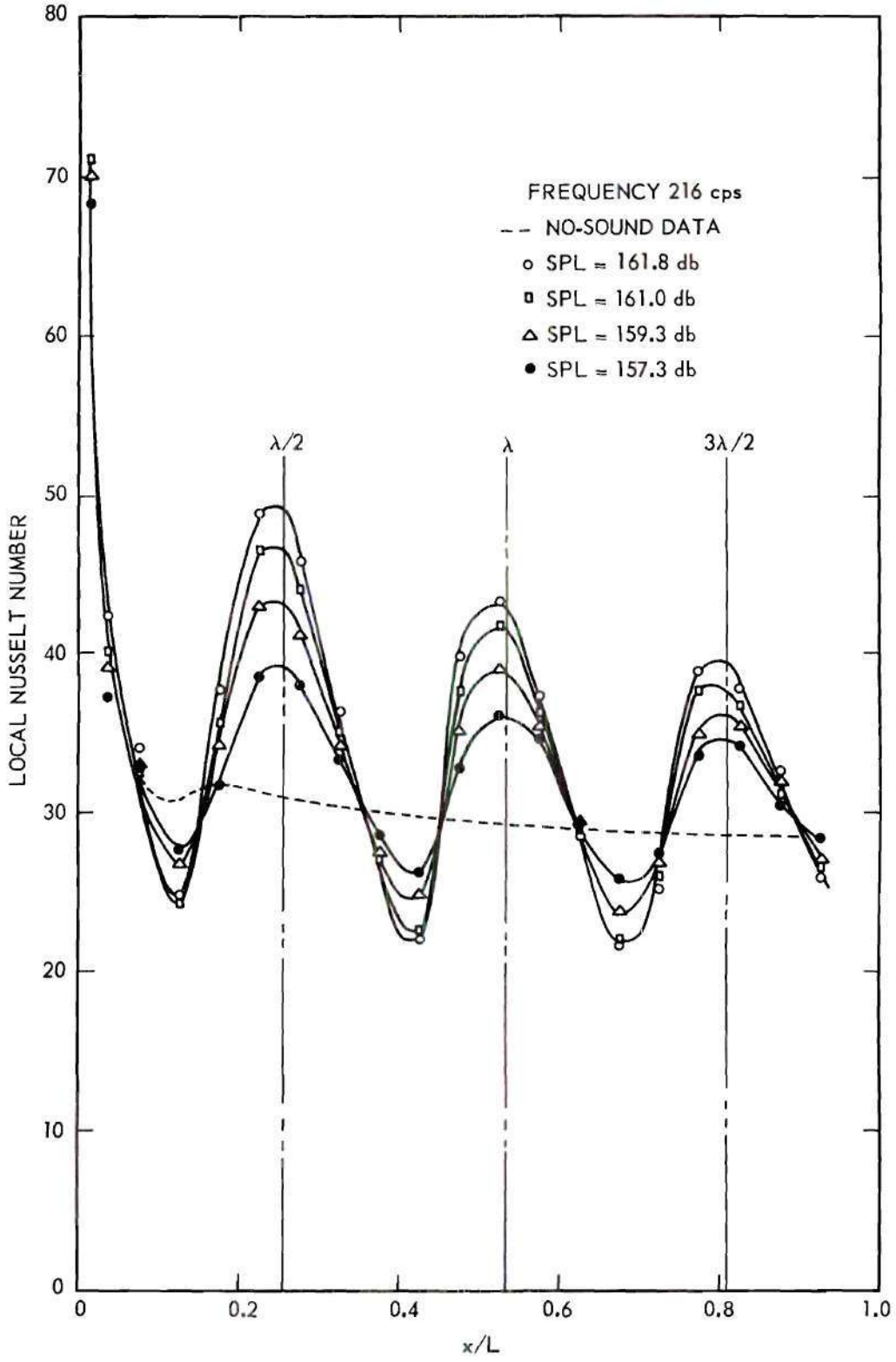

Figure 6. Local Nusselt Numbers Versus x/L for Various Sound-Pressure Levels, Reynolds Number ≈ 11,600.

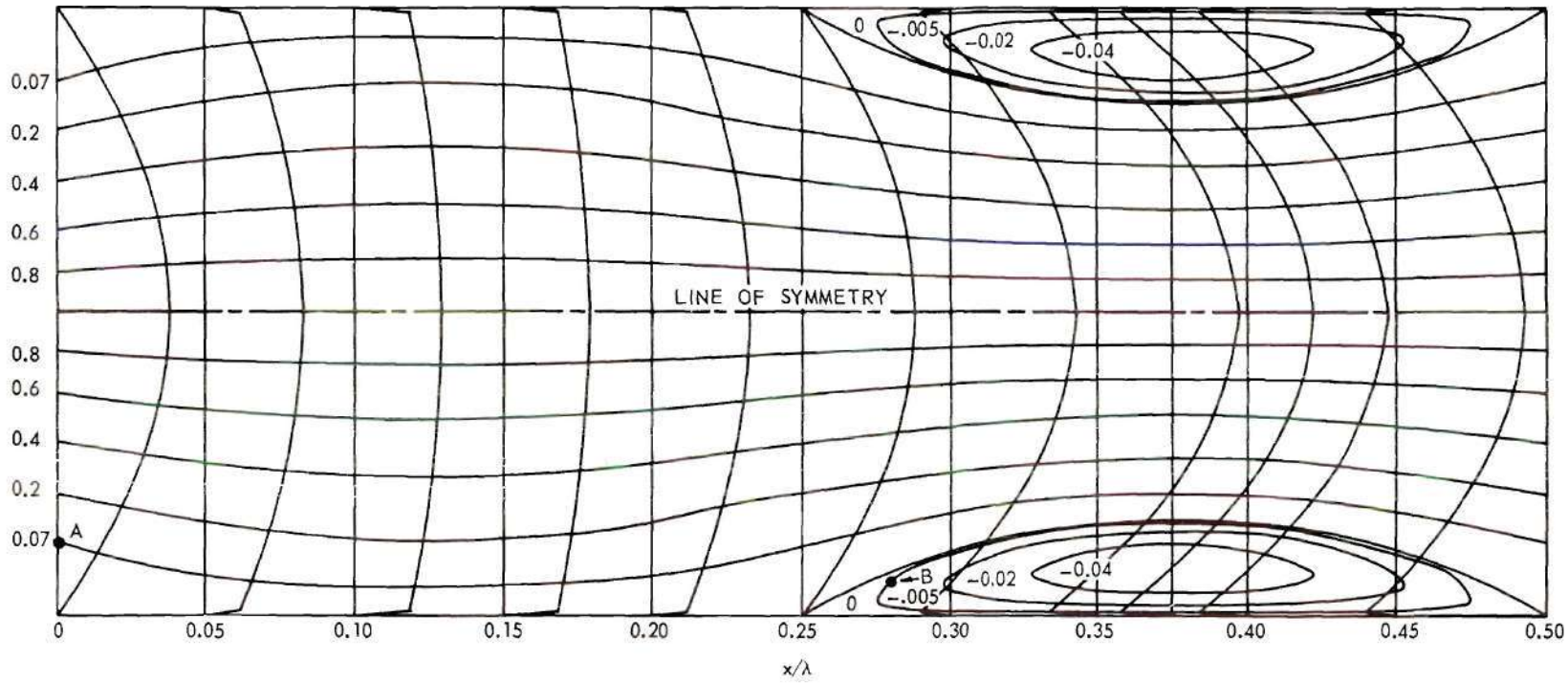

Figure 16. Time-Mean Stream Function for $M/M_0^2 = 1/2$.

in this region. This steepening produces heat transfer from particle X to the adjacent main stream and, therefore, as it travels from $x/\lambda = 1/4$ to $x/\lambda = 1/2$, its temperature decreases. At $x/\lambda = 1/2$ particle X starts the process over again but it is at a higher temperature than it was at point A. Particle Y, however, "impinges" upon the wall near $x/\lambda = 1/2$ and then moves back toward point B. It is trapped in this loop.

With this description of what happens to the temperature of two typical particles of fluid, one flowing just outside of the main vortices and the other one flowing just inside one of the main vortices, a qualitative analysis of the local heat transfer rate can now be given. The analysis will begin with particle X at point A. Coupled with X's movement in the positive x-direction will be a wallward translation thereby bringing cool fluid near to the wall and subsequently increasing the heat transfer rate in this region. A wallward translation of cool fluid is also occurring within the main vortices near the positions $x/\lambda = 0, 1/2, 1, 3/2,$ etc., that is, near the velocity loops. This process is similar to a cool jet impinging on a heated plate and, therefore, the local heat transfer rate should be quite large in these regions. The maximum values of the local rate should occur slightly before the velocity loops since the streamline impingement is sharper in this region. Jackson's data which are presented graphically in Figure 6 show this very clearly.

As particle X moves toward $x/\lambda = 1/2$ its temperature increases and it diverges from the wall after passing $x/\lambda = 1/8$. This should result in a decrease in the local heat transfer rate from its maximum value which occurs near the velocity loop all the way to the velocity node at $x/\lambda \approx 1/4$. The same argument is applicable to particle Y as it moves from the loop

($x/\lambda \approx 1/2$) toward the node at $x/\lambda = 1/4$. The minimum heat transfer rate should occur slightly before $x/\lambda = 1/4$ since the streamline divergence from the wall is greater in this region. This is also verified by Jackson's tube data.

Another interesting outgrowth of this study is the correlation of the threshold data of Eastwood. Eastwood measured the local heat transfer rate for forced convection in a horizontal isothermal tube with an impressed resonant acoustic field. He defined the sound threshold level to be the sound-pressure level below which no noticeable change in the local heat transfer rate occurred due to sound. If this is interpreted in terms of the flow field which existed, then it should follow that a certain magnitude of disturbance in the flow is necessary to produce an observable change in the heat transfer characteristics of the tube. From the present theoretical analysis the magnitude of this disturbance (evidenced by vortex size) should be characterized by the parameter M/M_o^2. Eastwood's threshold level data are given below in tabular form.

Table 2. Eastwood's Threshold Level Data

Re	M	SPL	M_o	M/M_o^2
2100	0.001015	151.5	0.0075	18.1
11600	0.005609	153.5	0.00942	63.2
16000	0.007736	155.0	0.01121	61.4
33000	0.01596	158.0	0.01582	63.8

From these data it is clear that the sound threshold level is given by $M/M_o^2 \approx 63$. The one level that does not fit this correlation can be

easily explained. Heat transfer tests without sound (1) on the apparatus that was used by Eastwood showed that combined free and forced convection exists when the Reynolds number is less than approximately 10,000 and, therefore, the parameter M/M_o^2 does not sufficiently describe the secondary flow field in this Reynolds number region.

CHAPTER V

CONCLUSIONS AND RECOMMENDATIONS

An analytical and experimental investigation of the effect of a resonant acoustic field has been made. The analytical study treated flow in an infinite channel whereas the experimental study considered flow in a circular tube. The conclusions from these investigations are

1. A resonant acoustic field will produce steady secondary flow in a channel or a circular tube with or without through flow.

2. The "size" of the standing vortices which are formed in the case of through flow is, to a first approximation, solely a function of the parameter M/M_o^2.

3. The effect of sound on the local heat transfer rate for a horizontal isothermal tube as obtained by Jackson is qualitatively explained in terms of the flow field which was observed experimentally and predicted analytically.

4. The sound threshold levels obtained by Eastwood (the sound levels below which a resonant acoustic field does not locally affect the heat transfer rate) correspond to the condition for which $M/M_o^2 \approx 63$.

The following items are recommended as a logical extension of the work which has been presented:

1. Using an order of magnitude analysis similar to the one presented here, the governing equations for laminar flow in a circular tube should be obtained and solved. A quantitative check of this solution

should then be made by comparing the analytically determined vortex size with the one which was experimentally determined here.

2. The energy equation should be solved for the channel and the circular tube geometries with a thermal entrance at a position where the velocity field is fully developed.

3. An experimental apparatus should be constructed similar to the one used by Jackson but with an entrance length sufficiently long to produce fully-developed flow at the thermal entrance. The heat transfer rates should be determined with and without a resonant acoustic field and they should then be compared with the analytically predicted ones (this requires the results of the previous recommendation).

4. Flow visualization studies should be continued to determine the effects of: (i) high intensity sound, (ii) off-resonance, and (iii) free convection on the flow field.

APPENDICES

APPENDIX A

ONE-DIMENSIONAL ACOUSTIC WAVE EQUATION

In order to present a complete analysis of the problem under consideration, the one-dimensional acoustic wave equation will be derived. The derivation of this equation is presented in several very good references (14), (16) and (17); however, the derivation which is presented here emphasizes the order of magnitude assumptions which are necessary to obtain the wave equation. The order of magnitude analysis will be the same as the one which is used in Appendix B to obtain the governing equations for the case of viscous, compressible, channel flow under the influence of a resonant acoustic field.

Derivation of the Wave Equation

The wave equation for a stagnant, inviscid, ideal gas will be derived from the following set of governing equations:

Continuity

$$\frac{\partial \rho}{\partial t} + \frac{\partial}{\partial x}(\rho u) = 0 \qquad (A.1)$$

Momentum

$$\rho \frac{\partial u}{\partial t} + \rho u \frac{\partial u}{\partial x} + \frac{\partial p}{\partial x} = 0 \qquad (A.2)$$

Equation of State

$$p = \rho RT , \quad c_p = \text{constant} \tag{A.3}$$

Second Law

$$s = \text{constant} \tag{A.4}$$

Acoustic waves by their definition produce only small deviations in properties from their values in the undisturbed or time-mean state. For this reason the density, pressure, and velocity of the fluid will be expressed as the sum of the value of the time-mean property and the deviation of the property due to the acoustic wave, i.e.

$$\rho = \bar{\rho} + \rho_1 , \tag{A.5}$$

$$p = \bar{p} + p_1 , \tag{A.6}$$

and

$$u = \bar{u} + u_1 \tag{A.7}$$

where $\bar{\rho}$, $\bar{p}$ and $\bar{u}$ are the time-mean values of the density, pressure, and velocity, respectively, and ρ_1, p_1, and u_1 represent the respective time-dependent deviations from these values. For the case of a "stagnant" gas, $\bar{u}$ is zero and $\bar{\rho}$ and $\bar{p}$ are constant and will be denoted hereafter as ρ_o and p_o, respectively. The one-dimensional wave equation will now be obtained by the following steps:

Step 1. Solve the continuity equation for $\frac{\partial \rho}{\partial t}$ and then determine $\frac{\partial^2 \rho}{\partial t \partial x}$. This yields

$$\frac{\partial^2 \rho}{\partial t \partial x} = -\frac{\partial^2}{\partial x^2}(\rho u) \quad . \tag{A.8}$$

Step 2. Since the flow is assumed to be isentropic, the pressure is solely a function of density and, therefore,

$$\frac{\partial p}{\partial x} = \frac{\partial p}{\partial \rho}\frac{\partial \rho}{\partial x} = c^2 \frac{\partial \rho}{\partial x} \tag{A.9}$$

or

$$\frac{\partial^2 \rho}{\partial t \partial x} = c^2 \frac{\partial^2 \rho}{\partial t \partial x} + \frac{\partial \rho}{\partial x}\frac{\partial c^2}{\partial t} \tag{A.10}$$

since by definition

$$c^2 = \left(\frac{\partial p}{\partial \rho}\right)_s \quad . \tag{A.11}$$

For an isentropic flow $\left(\frac{\partial p}{\partial \rho}\right)_s = \frac{dp}{d\rho}$ and if $\frac{dp}{d\rho}$ is expressed in Taylor series about the time-mean state, then equation A.11 becomes

$$c^2 = \frac{dp}{d\rho} = \left[\frac{dp}{d\rho}\right]_o + \left[\frac{d^2 p}{d\rho^2}\right]_o (\rho - \rho_o) + \cdots \quad . \tag{A.12}$$

Also, for an isentropic process in an ideal gas $p = p_o \rho_o^{-k} \rho^k$ and, therefore,

$$\left[\frac{dp}{d\rho}\right]_o = k\, p_o\, \rho_o^{-k}\, \rho_o^{k-1} = c_o^2 \quad , \tag{A.13}$$

$$\left[\frac{d^2 p}{d\rho^2}\right]_o = k(k-1)\, p_o\, \rho_o^{-k}\, \rho_o^{k-2} = (k-1)\, c_o^2/\rho_o \tag{A.14}$$

and finally

$$c^2 = c_o^2 \left[1 + (k-1)\, \rho_1/\rho_o + \cdots\right] \quad . \tag{A.15}$$

The higher order terms in ρ_1/ρ_o will be omitted in the analysis which follows.

Step 3. Combine equations A.8, A.10 and A.15 to obtain the following approximate expression:

$$\frac{\partial^2 p}{\partial t \partial x} = - c^2 \frac{\partial^2}{\partial x^2} (\rho u) + \frac{c_o^2 (k-1)}{\rho_o} \frac{\partial \rho}{\partial x} \frac{\partial \rho_1}{\partial t} \tag{A.16}$$

Step 4. Solve the momentum equation for $\frac{\partial p}{\partial x}$ and then determine $\frac{\partial^2 p}{\partial t \partial x}$. This yields

$$\frac{\partial^2 p}{\partial t \partial x} = - \frac{\partial}{\partial t} \left(\rho \frac{\partial u}{\partial t}\right) - \frac{\partial}{\partial t} \left(\rho u \frac{\partial u}{\partial x}\right) \tag{A.17}$$

Step 5. Combine equations A.16 and A.17 to obtain

$$\frac{\partial^2 u}{\partial t^2} - c^2 \frac{\partial^2 u}{\partial x^2} = \frac{c^2 u}{\rho} \frac{\partial^2 \rho}{\partial x^2} - \frac{c_o^2 (k-1)}{\rho\, \rho_o} \frac{\partial \rho}{\partial x} \frac{\partial \rho_1}{\partial t} - \frac{1}{\rho} \frac{\partial \rho}{\partial t} \frac{\partial u}{\partial t} - \frac{1}{\rho} \frac{\partial}{\partial t} \left(\rho u \frac{\partial u}{\partial x}\right) \tag{A.18}$$

The left side of equation A.18 is the desired wave equation and, therefore, it must be shown that the right side of the equation is approximately zero.

Step 6. An order of magnitude analysis will now be used to determine the relative magnitude of the terms in equation A.18. It is first necessary to define the following dimensionless variables which have an order of magnitude of one:

$$\rho = \rho_o \rho' = \rho_o + \rho_1 \tag{A.19a}$$

$$p = p_o p' = p_o + p_1 \tag{A.19b}$$

$$u = U_o u' = u_1$$

where the prime superscript denotes a dimensionless property. The characteristic velocity, U_o, represents the maximum positive value of u_1. Since acoustic waves are being considered, the following orders of magnitude are assumed:

$$\theta(\rho_o', p_o', u_1') = 1 \tag{A.20a}$$

$$\theta(\rho_1', p_1') = \delta \text{ , where } \delta \ll 1 \tag{A.20b}$$

$$\theta(U_o/c) = \delta$$

Dimensionless length and time must now be chosen such that derivatives with respect to them are of the order of magnitude of one. For the periodic sound waves which will be considered later in this analysis the characteristic values of length and time will be taken as $\lambda/2$ and $\lambda/(2c)$, respectively. Thus

$$x = x' \lambda/2 \tag{A.21a}$$

$$t = t' \lambda/(2c_o) = t' \pi/\omega \tag{A.21b}$$

and

$$\theta\left(\frac{\partial}{\partial x'}, \frac{\partial}{\partial t'}\right) = 1 \tag{A.22}$$

where λ is the wavelength of the sound wave. Under these assumptions equation A.18 in dimensionless form is

$$\underset{1}{\frac{\partial^2 u_1'}{\partial t'^2}} - \underset{1}{\frac{\partial^2 u_1'}{\partial x'^2}} = \underset{1/1}{\frac{u_1'}{\rho'}} \underset{\delta}{\frac{\partial^2 \rho_1'}{\partial x'^2}} - \underset{1/\delta}{\frac{(k-1)}{M_o}} \underset{1}{\left[\frac{c_o}{c}\right]^2} \underset{1}{\frac{1}{\rho'}} \underset{\delta}{\frac{\partial \rho_1'}{\partial x'}} \underset{\delta}{\frac{\partial \rho_1'}{\partial t'}} \qquad \text{(A.23)}$$

$$- \underset{1}{\frac{1}{\rho'}} \underset{\delta}{\frac{\partial \rho_1'}{\partial t'}} \underset{1}{\frac{\partial u_1'}{\partial t'}} - \underset{\delta}{M_o} \underset{1}{\frac{1}{\rho'}} \frac{\partial}{\partial t'} \left[\underset{1}{\rho'} \underset{1}{u_1'} \underset{1}{\frac{\partial u_1'}{\partial x'}}\right]$$

The term $\left[\frac{c_o}{c}\right]^2$ is of the order one since

$$\left[\frac{c_o}{c}\right]^2 = \left[\frac{p_o}{p}\right] \left[\frac{\rho}{\rho_o}\right] = \frac{\rho'}{p'} \quad .$$

If only the terms which are of the order of magnitude of one are retained, then the one-dimensional acoustic wave equation in dimensional form is

$$\frac{\partial^2 u_1}{\partial t^2} = c_o^2 \frac{\partial^2 u_1}{\partial x^2} \quad . \qquad \text{(A.24)}$$

The momentum equation in dimensionless form is

$$\underset{1}{\rho'} \underset{1}{\frac{\partial u_1'}{\partial t'}} + \underset{\delta}{M_o} \underset{1}{\rho'} \underset{1}{u_1'} \underset{1}{\frac{\partial u_1'}{\partial x'}} + \underset{1/\delta}{\frac{1}{M_o}} \underset{\delta}{\frac{\partial p_1'}{\partial x'}} = 0 \quad . \qquad \text{(A.25)}$$

If only the terms in equation A.25 which are of the order one are retained, then the momentum equation in dimensional form is approximately given by

$$\rho_o \frac{\partial u_1}{\partial t} + \frac{\partial p_1}{\partial x} = 0 \quad . \qquad \text{(A.26)}$$

The continuity equation in dimensionless form is

$$\frac{\partial \rho_1'}{\partial t'} + M_o \frac{\partial}{\partial x'} [(\rho_o' + \rho_1')(u_1')] = 0 \quad . \qquad (A.27)$$

Again, if only the terms which are of the order δ are retained, then the continuity equation in dimensional form is

$$\frac{\partial \rho_1}{\partial t} + \rho_o \frac{\partial u_1}{\partial x} = 0 \quad . \qquad (A.28)$$

APPENDIX B

ORDER OF MAGNITUDE ANALYSIS

The following is a summary of the order of magnitude analysis which was used to linearize the continuity and momentum equations. This analysis embodies the assumptions that the density, pressure and velocity may each be represented as the sum of a time-mean component and a periodic component and that the viscosity is constant.

The first step in this analysis is to choose characteristic values of the properties x, y, t, u, v, p, ρ and μ, such that the order of magnitude of a dimensionless property formed by dividing the property by its characteristic value is one. In addition, the characteristic values of length and time should be chosen such that derivatives with respect to these quantities are of the order one. The values which were picked for this analysis are $\lambda/2$, δ_{ac}, π/ω, $\bar{U}$ and U_o, $\bar{V}$ and V_o, p_o and $\rho_o c_o U_o$, ρ_o and $\rho_o M_o$, and μ_o, respectively. Thus, the dimensionless properties, denoted by a prime superscript, are

$$x = \lambda/2\ x' \tag{B.1}$$

$$y = \delta_{ac}\ y' \tag{B.2}$$

$$t = \pi/\omega\ t' \quad \text{or} \quad \lambda/c_o\ t' \tag{B.3}$$

$$\bar{u} = \bar{U}\ \bar{u}' \tag{B.4}$$

$$u_1 = U_o\ u_1' \tag{B.5}$$

$$\bar{v} = \bar{V}\ \bar{v}' \tag{B.6}$$

$$v_1 = V_o \, v_1' \tag{B.7}$$

$$\bar{p} = p_o \, \bar{p}' \tag{B.8}$$

$$p_1 = \rho_o c_o U_o p_1' \tag{B.9}$$

$$\bar{\rho} = \rho_o \, \bar{\rho}' \tag{B.10}$$

$$\rho_1 = \rho_o M_o \rho_1' \tag{B.11}$$

$$\mu = \mu_o \, \mu' \tag{B.12}$$

A justification of the characteristic values will now be given.

$\lambda/2$. It is anticipated that the flow field under consideration will be duplicated in half wavelength sections. This supposition is in agreement with the analytical analyses of Rayleigh (5) and Westervelt (7) and with the experimental program which was conducted in conjunction with the theoretical analysis that is being presented here. Due to the presence of a resonant acoustic field the x-component of the periodic velocity will also be periodic in position x with a period of λ (see Appendix A). Thus the derivatives of periodic velocity with respect to x' will be of order one. It is assumed that the derivatives of the time-mean velocity with respect to x' will also be of order one.

δ_{ac}. The characteristic length, δ_{ac}, is referred to in the literature as the A.C. boundary layer thickness and is given by the expression, $\delta_{ac} \equiv \sqrt{2\nu_o/\omega}$, where ν_o is the kinematic viscosity and ω is the circular frequency of the resonant acoustic field. Periodic flow fields all have large changes in velocity in the direction normal to the wall. These changes, for the most part, are restricted to a thin layer of fluid near the wall which is referred to as the A.C. boundary layer. Thus, by using

δ_{ac} as the y-characteristic length the derivatives of the dimensionless velocity with respect to y' should be of order one.

π/ω. The characteristic time, π/ω or its equivalent $\lambda/2c$, is chosen since the circular frequency of the periodic components of density, pressure, and velocity is ω (see Appendix A). Thus an order of magnitude change of one in time t' results in an order of magnitude change of one in the components ρ_1', p_1', u_1' and v_1'.

$\bar{U}$. The characteristic velocity, $\bar{U}$, is associated with the time-mean flow field. Its relation to the periodic flow field is to be determined.

U_o. The characteristic velocity, U_o, is taken as the maximum amplitude of the x-component of the periodic velocity, u_1. It is assumed to be equal to the maximum amplitude of the periodic velocity for an inviscid fluid undergoing resonant acoustic vibrations (see Appendix A, equation A.37).

$\bar{V}$. The characteristic velocity, $\bar{V}$, is associated with the y-component of the time-mean velocity. Its relation to $\bar{U}$ will be determined by an order of magnitude analysis of the time-mean continuity equation.

V_o. The characteristic velocity, V_o, is associated with the y-component of the periodic velocity. Its relation to U_o will also be determined by an order analysis of the continuity equation.

p_o. The characteristic pressure, p_o, is taken as the time-mean component of pressure at the position $x = 0$, $y = a$. For the through-flow rates to be considered, the pressure will not deviate appreciably from p_o.

$\rho_o c_o U_o$. The characteristic pressure, $\rho_o c_o U_o$, is picked since this represents the maximum amplitude of the periodic component of pressure for

an inviscid fluid undergoing resonant acoustic vibrations and for which the maximum amplitude of velocity is U_o (see equation A.38).

ρ_o. The characteristic density, ρ_o, is taken as the time-mean density at the position $x = 0$, $y = a$. It is assumed that the time-mean density of the fluid is constant and equal to ρ_o throughout the flow field.

$\rho_o M_o$. The characteristic density, $\rho_o M_o$, is picked since the maximum amplitude of the periodic component of density for an inviscid fluid undergoing resonant acoustic vibrations and for a maximum amplitude of velocity, U_o, is $\rho_o M_o$ (see equation A.39).

μ_o. The characteristic viscosity, μ_o, is taken as the viscosity of the fluid. Since the viscosity has been assumed to be constant, μ' will be identically one.

Continuity Equation

The continuity equation will now be analyzed in light of the foregoing variable changes and the following assumptions concerning the orders of magnitude of various quantities:

$$\theta\left(\frac{\partial}{\partial x'}, \frac{\partial}{\partial y'}, \frac{\partial}{\partial t'}, \bar{u}', u_1', \bar{v}', v_1', \bar{p}', p_1', \bar{\rho}', \rho_1', \mu'\right) = 1 \qquad \text{(B.13)}$$

$$\theta\left(2\,\delta_{ac}/\lambda,\ U_o/c_o,\ \bar{U}/U_o\right) = \delta \qquad \text{(B.14)}$$

The three assumptions listed in equation B.14 require justification.

The first term, $2\,\delta_{ac}/\lambda = \sqrt{4\,\nu_o/\pi\lambda c_o}$, is very small for a gas at normal pressures and temperatures and for "long" wavelengths. As an example, air at one atmosphere of pressure and a temperature of 522° R will be considered. For a wavelength of one foot, $\delta = 2.13 \times 10^{-4} \ll 1$.

Acoustic waves, by their definition, are very small deviations in property values from their time-mean values; thus, the second term $U_o/c_o \ll 1$ and will be assumed to be of the order of δ.

The third term, $\bar{U}/U_o$, is assumed to be small in comparison to one in order that the momentum equation can be linearized. The importance of this assumption can be seen by a careful analysis of equations B.21 and B.22.

In dimensionless form the continuity equation becomes

$$\frac{2\,U_o\rho_o}{\lambda}\left\{\underset{1/\delta}{\frac{1}{M_o}}\ \underset{\delta}{\frac{\partial}{\partial t'}}\ (M_o\rho_1') + \underset{1\quad\delta\quad\delta\quad 1}{\frac{\partial}{\partial x'}\left[(\bar{\rho}' + M_o\rho_1')\left(\frac{\bar{U}}{U_o}\,\bar{u}' + u_1'\right)\right]}\right. \tag{B.15}$$

$$\left. + \underset{1/\delta\quad 1\quad\delta}{\frac{\lambda}{2\,\delta_{ac}}\ \frac{\partial}{\partial y'}\left[(\bar{\rho}' + M_o\rho_1')\left(\frac{\bar{V}}{U_o}\,\bar{v}' + \frac{V_o}{U_o}\,v_1'\right)\right]}\right\} = 0$$

The time average of equation B.15 is

$$\underset{\delta}{\frac{\partial}{\partial x'}\left[\frac{\bar{U}}{U_o}\,\bar{\rho}'\bar{u}'\right]} + \underset{\delta}{M_o\,\overline{\rho_1'u_1'}} + \underset{\delta}{\frac{\lambda}{2\,\delta_{ac}}\ \frac{\partial}{\partial y'}\left[\frac{\bar{V}}{U_o}\,\bar{\rho}'\bar{v}'\right]} + \underset{\delta}{M_o\,\frac{V_o}{U_o}\,\overline{\rho_1'v_1'}} = 0 \tag{B.16}$$

Inspection of equations B.15 and B.16 indicates that the orders of magnitude of $\bar{V}/U_o$ and V_o/U_o are

$$\theta(\bar{V}/U_o) = \delta^2 \tag{B.17}$$

and

$$\theta(V_o/U_o) = \delta \tag{B.18}$$

The time-dependent continuity equation is obtained by retaining only the terms in equation B.15 which are of order one. This gives the following equation in dimensional form:

$$\frac{\partial \rho_1}{\partial t} + \rho_o \left\{ \frac{\partial u_1}{\partial x} + \frac{\partial v_1}{\partial y} \right\} = 0 \qquad \text{(B.19)}$$

The time-mean continuity equation is given by equation B.16. In terms of dimensional quantities, it becomes

$$\frac{\partial \bar{u}}{\partial x} + \frac{\partial \bar{v}}{\partial y} = - \frac{1}{\rho_o} \left\{ \frac{\partial}{\partial x} \left(\overline{\rho_1 u_1} \right) + \frac{\partial}{\partial y} \left(\overline{\rho_1 v_1} \right) \right\} \qquad \text{(B.20)}$$

Momentum Equation

The momentum equations, equations 2.2 and 2.3, will now be analyzed using the foregoing variable changes and the assumed orders of magnitude. In dimensionless form they are

$$\underset{1}{\left[\bar{\rho}' + \underset{\delta}{M_o \rho_1'} \right]} \underset{1/\delta}{\left[\frac{1}{M_o} \frac{\partial u_1'}{\partial t'} + \left(\underset{\delta}{\frac{\bar{U}}{U_o}} \bar{u}' + \underset{1}{u_1'} \right) \underset{\delta}{\frac{\partial}{\partial x'}} \left(\underset{\delta}{\frac{\bar{U}}{U_o}} \bar{u}' + \underset{1}{u_1'} \right) \right.} \qquad \text{(B.21)}$$

$$\left. + \underset{1/\delta}{\frac{\lambda}{2 \delta_{ac}}} \left(\underset{\delta^2}{\frac{\bar{V}}{U_o}} \bar{v}' + \underset{\delta}{\frac{V_o}{U_o}} v_1' \right) \underset{\delta}{\frac{\partial}{\partial y'}} \left(\underset{\delta}{\frac{\bar{U}}{U_o}} \bar{u}' + \underset{1}{u_1'} \right) \right] = \underset{1/\delta^2 \ \delta^2}{- \frac{p_o}{\rho_o U_o^2} \frac{\partial \bar{p}'}{\partial x'}}$$

$$\underset{1/\delta}{- \frac{1}{M_o} \frac{\partial p_1'}{\partial x'}} + \underset{1}{\frac{1}{\frac{U_o \lambda}{2 \nu_o}}} \left\{ \underset{\delta}{\frac{\partial}{\partial x'}} \left[\underset{1}{\mu'} \left\{ 2 \underset{\delta}{\frac{\partial}{\partial x'}} \left(\underset{\delta}{\frac{\bar{U}}{U_o}} \bar{u}' + \underset{1}{u_1'} \right) \right. \right. \right.$$

$$- \frac{2}{3}\left[\frac{\partial}{\partial x'}\left(\frac{\bar{U}}{U_o}\bar{u}' + u_1'\right) + \frac{\lambda}{2\,\delta_{ac}}\frac{\partial}{\partial y'}\left(\frac{\bar{V}}{U_o}\bar{v}' + \frac{V_o}{U_o}v_1'\right)\right]\right]$$

$$\delta \qquad 1 \qquad 1/\delta \qquad \delta^2 \qquad \delta$$

$$+ \frac{\lambda}{2\,\delta_{ac}}\frac{\partial}{\partial y'}\left[\mu'\left\{\frac{\lambda}{2\,\delta_{ac}}\frac{\partial}{\partial y'}\left(\frac{\bar{U}}{U_o}\bar{u}' + u_1'\right) + \frac{\partial}{\partial x'}\left(\frac{\bar{V}}{U_o}\bar{v}' + \frac{V_o}{U_o}v_1'\right)\right\}\right]\Bigg\}$$

$$1/\delta \qquad 1 \qquad 1/\delta \qquad \delta \qquad 1 \qquad \delta^2 \qquad \delta$$

and

$$\left[\bar{\rho}' + M_o\rho_1'\right]\left[\frac{1}{M_o}\frac{V_o}{U_o}\frac{\partial v_1'}{\partial t'} + \left(\frac{\bar{U}}{U_o}\bar{u}' + u_1'\right)\frac{\partial}{\partial x'}\left(\frac{\bar{V}}{U_o}\bar{v}' + \frac{V_o}{U_o}v_1'\right)\right. \qquad \text{(B.22)}$$

$$1 \quad \delta \qquad 1/\delta \quad \delta \qquad \delta \qquad 1 \qquad \delta^2 \qquad \delta$$

$$\left. + \frac{\lambda}{2\,\delta_{ac}}\left(\frac{\bar{V}}{U_o}\bar{v}' + \frac{V_o}{U_o}v_1'\right)\frac{\partial}{\partial y'}\left(\frac{\bar{V}}{U_o}\bar{v}' + \frac{V_o}{U_o}v_1'\right)\right] = -\frac{\lambda}{2\,\delta_{ac}}\frac{p_o}{\rho_o U_o{}^2}\frac{\partial \bar{p}'}{\partial y'}$$

$$1/\delta \quad \delta^2 \qquad \delta \qquad \delta^2 \qquad \delta \qquad 1/\delta \quad 1/\delta^2 \quad \delta^4$$

$$- \frac{\lambda}{2\,\delta_{ac}}\frac{1}{M_o}\frac{\partial p_1'}{\partial y'} + \frac{1}{\frac{U_o\,\lambda}{2\,\nu_o}}\left\{\frac{\lambda}{2\,\delta_{ac}}\frac{\partial}{\partial y'}\left[\mu'\left\{2\,\frac{\lambda}{2\,\delta_{ac}}\frac{\partial}{\partial y'}\left(\frac{\bar{V}}{U_o}\bar{v}' + \frac{V_o}{U_o}v_1'\right)\right.\right.\right.$$

$$1/\delta \quad 1/\delta \quad \delta^2 \qquad \delta \qquad 1/\delta \qquad 1 \qquad 1/\delta \qquad \delta^2 \qquad \delta$$

$$\left.\left.\left. - \frac{2}{3}\left[\frac{\partial}{\partial x'}\left(\frac{\bar{U}}{U_o}\bar{u}' + u_1'\right) + \frac{\lambda}{2\,\delta_{ac}}\frac{\partial}{\partial y'}\left(\frac{\bar{V}}{U_o}\bar{v}' + \frac{V_o}{U_o}v_1'\right)\right]\right\}\right]$$

$$\delta \qquad 1 \qquad 1/\delta \qquad \delta^2 \qquad \delta$$

$$+ \frac{\partial}{\partial x'}\left[\mu'\left\{\frac{\lambda}{2\,\delta_{ac}}\frac{\partial}{\partial y'}\left(\frac{\bar{U}}{U_o}\bar{u}' + u_1'\right) + \frac{\partial}{\partial x'}\left(\frac{\bar{V}}{U_o}\bar{v}' + \frac{V_o}{U_o}v_1'\right)\right\}\right]\Bigg\}$$

$$1 \qquad 1/\delta \qquad \delta \qquad 1 \qquad \delta^2 \qquad \delta$$

Consideration must now be given to the orders of magnitude of the quantities $\frac{p_o}{\rho_o U_o{}^2}$, $\frac{U_o\,\lambda}{2\,\nu_o}$, $\frac{\partial \bar{p}'}{\partial x'}$, $\frac{\partial \bar{p}'}{\partial y'}$ and $\frac{\partial p_1'}{\partial y'}$.

$\frac{p_o}{\rho_o U_o^2}$. The fluid under consideration is assumed to be a perfect gas and, therefore, the speed of sound squared is given by $c_o^2 = k \frac{p_o}{\rho_o}$. Thus $\frac{p_o}{\rho_o U_o^2}$ may be expressed as $\frac{p_o}{\rho_o U_o^2} = \frac{1}{k M_o^2}$ and finally, the order of magnitude is $1/\delta^2$, i.e. $\theta(\frac{p_o}{\rho_o U_o^2}) = 1/\delta^2$.

$\frac{U_o \lambda}{2 \nu_o}$. The A.C. boundary layer is a region in which the inertial and the viscous forces are of the same order of magnitude. If the terms in the x-momentum equation involving periodic quantities are investigated, then it is noted that the largest inertial term, $\frac{1}{M_o} \bar{\rho}' \frac{\partial u_1'}{\partial t'}$, is of the order $1/\delta$. Thus the largest viscous term, $\frac{1}{\frac{U_o \lambda}{2 \nu_o}} \frac{\lambda^2}{4 \delta_{ac}^2} \mu' \frac{\partial^2 u_1'}{\partial y'^2}$, must also be of the order $1/\delta$. Since $\mu' \frac{\partial^2 u_1'}{\partial y'^2}$ and $\bar{\rho} \frac{\partial u_1'}{\partial t'}$ are of the order one, the quantity $\frac{1}{\frac{U_o \lambda}{2 \mu_o}} \frac{\lambda^2}{4 \delta_{ac}^2}$ must be of the order of magnitude of $\frac{1}{M_o}$. It has been previously assumed that the order of magnitude of both M_o and $\frac{2 \delta_{ac}}{\lambda}$ are δ . Therefore, $\frac{U_o \lambda}{2 \nu_o}$ is of the order $1/\delta$.

The A.C. boundary layer thickness can also be estimated from the foregoing expressions as follows:

$$\frac{1}{M_o} = \frac{c}{U_o} \approx \frac{2 \nu_o}{U_o \lambda} \frac{\lambda^2}{4 \delta_{ac}^2}$$

or

$$\delta_{ac} \approx \sqrt{\frac{\nu_o \lambda}{2 c}}$$

but for a resonant acoustic field

$$\lambda/c = 2\pi/\omega$$

and, therefore,

$$\delta_{ac} \approx \sqrt{\pi\nu_o/\omega} \quad .$$

In order to conform with the form of δ_{ac} which is normally found in the literature, it will be defined as $\delta_{ac} \equiv \sqrt{2\nu_o/\omega}$.

$\frac{\partial \bar{p}'}{\partial x'}$. If the time average of the x-momentum equation is taken, then the order of magnitude of the largest term is one. This implies that the term

$$\frac{p_o}{\rho_o U_o^2} \frac{\partial \bar{p}'}{\partial x'}$$

must also be of the order one, or

$$\theta\left[\frac{\partial \bar{p}'}{\partial x'}\right] = \theta\left[\frac{\rho_o U_o^2}{p_o}\right] = \delta^2 \quad .$$

$\frac{\partial \bar{p}'}{\partial y'}$. If the time average of the y-momentum equation is taken, then the order of magnitude of the largest term is δ. This implies the term

$$\frac{\lambda}{2\delta_{ac}} \frac{p_o}{\rho_o U_o^2} \frac{\partial \bar{p}'}{\partial y'}$$

must also be of order δ, or

$$\theta\left[\frac{\partial \bar{p}'}{\partial y'}\right] = \theta\left[\frac{\lambda}{2\,\delta_{ac}} \frac{p_o}{\rho_o U_o^2}\right] \cdot \delta = \delta^4 \quad .$$

$\frac{\partial p_1'}{\partial y'}$. The order of magnitude of the term

$$\frac{\lambda}{2\,\delta_{ac}} \frac{1}{M_o} \frac{\partial p_1'}{\partial y'}$$

must be equal to one since this is the order of the largest time-dependent term in the y-momentum equation. This implies that

$$\theta\left[\frac{\partial p_1'}{\partial y'}\right] = \theta\left[\frac{2\,\delta_{ac}}{\lambda} M_o\right] = \delta^2 \quad .$$

Since $\frac{\partial p_1'}{\partial y'}$ is very much less than $\frac{\partial p_1'}{\partial x'}$, the periodic component of pressure, p_1, will be assumed to be solely a function of position x and time t.

Time-Dependent Equations

The reduced forms of the momentum equations are obtained by retaining only the terms which are of the order of magnitude $1/\delta$. The following dimensional equations are the result of this operation:

$$\frac{\partial u_1}{\partial t} + \frac{1}{\rho_o} \frac{\partial p_1}{\partial x} = \nu_o \frac{\partial^2 u_1}{\partial y^2} \qquad \text{(B.23)}$$

$$\frac{\partial p_1}{\partial y} = 0 \qquad \text{(B.24)}$$

The full set of governing equations for the time-dependent velocity components consists of equations B.23 and B.24 above and the continuity equation, equation B.19, which is

$$\frac{\partial \rho_1}{\partial t} + \rho_o \left\{ \frac{\partial u_1}{\partial x} + \frac{\partial v_1}{\partial y} \right\} = 0 \qquad \text{(B.19)}$$

Time-Mean Equations

The time-mean momentum equations can be obtained from equations B.21 and B.22 by first taking the time average of these equations and then retaining only the terms which are of order one. This operation results in an equation which involves the partial derivative of the time-mean pressure with respect to x'. Since an expression for the time-mean pressure is unknown, it is necessary to eliminate the pressure terms in the momentum equation. This can be done by

1. Noting that $\frac{\partial p'}{\partial x' \partial y'} = \frac{\partial p'}{\partial y' \partial x'}$
2. Performing the following mathematical operations:

$$\frac{\lambda}{2\,\delta_{ac}} \frac{\partial}{\partial y'} \{\text{Equation B.21}\} - \frac{\partial}{\partial x'} \{\text{Equation B.22}\} \quad . \qquad \text{(B.25)}$$

Equation B.25 is independent of periodic and time-mean pressure terms.

The time-mean equation of motion is obtained first by taking the time average of equation B.25 and then by retaining only the terms which are of order $1/\delta$. The result of these operations in dimensional form is

$$\nu_o \frac{\partial^3 \bar{u}}{\partial y^3} = \frac{1}{\rho_o} \frac{\partial}{\partial y} \left[\overline{\rho_1 \frac{\partial u_1}{\partial t} + \bar{\rho} \left(u_1 \frac{\partial u_1}{\partial x} + v_1 \frac{\partial u_1}{\partial y} \right)} \right] \qquad \text{(B.26)}$$

The bar over the right hand side of equation B.26 represents the time average of the quantities within the brackets. The full set of governing equations for the time-mean velocity components is given by equation B.26 above in conjunction with the time-mean continuity equation

given below.

$$\frac{\partial \bar{u}}{\partial x} + \frac{\partial \bar{v}}{\partial y} = -\frac{1}{\rho_o}\left\{\frac{\partial}{\partial x}\left(\overline{\rho_1 u_1}\right) + \frac{\partial}{\partial y}\left(\overline{\rho_1 v_1}\right)\right\} \qquad \text{(B.20)}$$

APPENDIX C

SECOND APPROXIMATION TO THE TIME-DEPENDENT VELOCITIES

In Appendix B the governing equations for the time-dependent velocities were obtained by retaining only the terms in the dimensionless continuity and momentum equations which were of the highest order of magnitude. A method for determining the governing equations for the time-dependent velocities to a second approximation will now be given.

Governing Equations

Continuity Equation

The continuity equation is obtained by retaining the periodic terms in equation B.15 which are of the order of magnitude of δ or larger. This yields the following dimensional equation:

$$\frac{\partial \rho_1}{\partial t} + \rho_o \left\{\frac{\partial u_1}{\partial x} + \frac{\partial v_1}{\partial y}\right\} + \frac{\partial (\rho_1 u_1)}{\partial x} + \frac{\partial (\rho_1 v_1)}{\partial y} = 0 \qquad \text{(C.1)}$$

Momentum Equation

The momentum equations which govern the behavior of the time-dependent velocities are obtained by retaining only those terms in equations B.21 and B.22 which are of the order of magnitude of one or larger. This yields the following dimensional equations:

$$\frac{\partial u_1}{\partial t} + \left\{u_1 \frac{\partial u_1}{\partial x} + v_1 \frac{\partial u_1}{\partial y}\right\} = -\frac{1}{\rho_o} \frac{\partial \rho_1}{\partial x} + \nu_o \frac{\partial^2 u_1}{\partial y^2} \qquad \text{(C.2)}$$

and

$$\frac{\partial p_1}{\partial y} = 0 \quad . \tag{C.3}$$

If the equations above are compared with equations B.23 and B.24, then it is seen that two nonlinear terms, namely $u_1 \frac{\partial u_1}{\partial x}$ and $v_1 \frac{\partial u_1}{\partial y}$, have been added to the x-momentum equation.

Method of Solution

The following is an outline of a method which may be used to solve the time-dependent equations.

Step 1. Express the time-dependent components of density and pressure in Fourier series as follows:

$$\rho_1(x,y,t) = \text{REAL}\left[\sum_{n=1}^{\infty} \rho_{1n}(x,y)\, \exp(-in\omega t)\right] \tag{C.4}$$

and

$$p_1(x,y,t) = \text{REAL}\left[\sum_{n=1}^{\infty} p_{1n}(x,y)\, \exp(-in\omega t)\right] \quad . \tag{C.5}$$

Step 2. Express the time-dependent components of velocity in Fourier series as follows:

$$u_1(x,y,t) = \text{REAL}\left[\sum_{n=1}^{\infty} u_{1n}(x,y)\, \exp(-in\omega t)\right] \tag{C.6}$$

and

$$v_1(x,y,t) = \text{REAL}\left[\sum_{n=1}^{\infty} v_{1n}(x,y)\, \exp(-in\omega t)\right] \quad . \tag{C.7}$$

Step 3. The foregoing expressions for density, pressure and velocity are now substituted into equations C.1, C.2 and C.3 and then the factors of $\exp(-in\omega t)$, for $n = 1,2,3,\cdots$, are equated to zero. This results in the following set of linear partial differential equations:

Factors of $\exp(-i\omega t)$

$$\frac{\partial u_{11}}{\partial x} + \frac{\partial v_{11}}{\partial y} = \frac{i\omega}{\rho_o} \rho_{11} \tag{C.8}$$

$$\nu_o \frac{\partial^2 u_{11}}{\partial y^2} = - i \omega u_{11} + \frac{1}{\rho_o} \frac{\partial p_{11}}{\partial x} \tag{C.9}$$

$$\frac{\partial p_{11}}{\partial y} = 0 \tag{C.10}$$

Factors of $\exp(-i2\omega t)$

$$\frac{\partial u_{12}}{\partial x} + \frac{\partial v_{12}}{\partial y} + \frac{\partial}{\partial x} \left(\frac{\rho_{11}}{\rho_o} u_{11}\right) + \frac{\partial}{\partial y} \left(\frac{\rho_{11}}{\rho_o} v_{11}\right) = \frac{i2\omega}{\rho_o} \rho_{12} \tag{C.11}$$

$$\nu_o \frac{\partial^2 u_{12}}{\partial y^2} = - i2\omega u_{12} + \frac{1}{\rho_o} \frac{\partial p_{12}}{\partial x} + u_{11} \frac{\partial u_{11}}{\partial x} + v_{11} \frac{\partial u_{11}}{\partial y} \tag{C.12}$$

$$\frac{\partial p_{12}}{\partial y} = 0 \tag{C.13}$$

Etc.

In order to solve the foregoing set of equations the time-dependent components of density and pressure must be known. It is of interest to note in equation C.12 that even if a single frequency pressure disturbance ($p_{1n} = 0,\ n > 1$) is used the nonlinearity of the momentum equation produces higher harmonic components of velocity.

Solution for $u_1(x,y,t)$

A solution for $u_1(x,y,t)$ to a second approximation will now be given for two reasons; first to demonstrate the method of solution and second to show that for the periodic component of pressure which was chosen in Chapter II, the time-dependent velocity, to a first approximation as given in Chapter II, sufficiently represents the time-dependent velocity.

As in Chapter II, the components of density and pressure will be taken as

$$p_1(x,t) = \text{REAL}\left[- i\, \rho_o\, c\, U_o \sin(\omega x/c) \exp(-i\omega t)\right] \qquad (C.14)$$

$$\rho_1(x,t) = \text{REAL}\left[- i\, \rho_o M_o \sin(\omega x/c) \exp(-i\omega t)\right] \qquad (C.15)$$

These equations yield

$$p_{11} = - i\, \rho_o\, c\, U_o \sin(\omega x/c) \qquad (C.16a)$$

$$p_{1n} = 0 \quad \text{for} \quad 1 < n \qquad (C.16b)$$

and

$$\rho_{11} = - i\, \rho_o M_o \sin(\omega x/c) \qquad (C.17a)$$

$$\rho_{1n} = 0 \quad \text{for} \quad 1 < n \qquad (C.17b)$$

The time-dependent components of velocity to a second approximation are assumed to be

$$u_1(x,y,t) = \text{REAL}\left[u_{11}(x,y) \exp(-i\omega t) + u_{12}(x,y) \exp(-i2\omega t)\right] \qquad (C.18)$$

$$v_1(x,y,t) = \text{REAL}\left[v_{11}(x,y) \exp(-i\omega t) + v_{12}(x,y) \exp(-i2\omega t)\right] \qquad (C.19)$$

Solution for $u_{11}(x,y)$ and $v_{11}(x,y)$. The functions $u_{11}(x,y)$ and $v_{11}(x,y)$ are determined by the assumed form of $p_1(x,t)$ and $\rho_1(x,t)$ and equations C.8 and C.9. These equations are the same as the ones which were used in Chapter II to determine the functions $u_{11}(x,y)$, $v_{11}(x,y)$ and, therefore, the solutions for $u_{11}(x,y)$ and $v_{11}(x,y)$ are given by

$$u_{11}(x,y) = - U_o \cos(\omega x/c) \left[1 - \exp\{-(1-i)\, y'\}\right] \tag{C.20}$$

and

$$v_{11}(x,y) = \frac{1}{2} \omega \delta_{ac} M_c (1+i) \sin(\omega x/c) \left[1 - \exp\{-1\cdot(1-i)\, y'\}\right] \tag{C.21}$$

In obtaining the foregoing equations the following boundary conditions were applied:

$$\text{for } y = 0 \text{ and all } t: \quad u_1 = 0\,, \quad v_1 = 0 \tag{C.22}$$

$$\text{for } y = a \text{ and all } t: \quad \frac{\partial u_1}{\partial y} = 0 \tag{C.23}$$

An inspection of equations C.18 and C.19 indicates that the boundary conditions can be written as follows:

$$\text{for } y = 0 \text{ and all } t: \quad \text{REAL}\left[u_{11} \exp(-i\omega t)\right] = 0 \tag{C.24}$$

$$\text{REAL}\left[u_{12} \exp(-i2\omega t)\right] = 0$$

$$\text{REAL}\left[v_{11} \exp(-i\omega t)\right] = 0$$

$$\text{REAL}\left[v_{12} \exp(-i2\omega t)\right] = 0$$

$$\text{for } y = a \text{ and all } t: \quad \text{REAL}\left[\frac{\partial u_{11}}{\partial y} \exp(-i\omega t)\right] = 0 \tag{C.25}$$

$$\text{REAL}\left[\frac{\partial u_{12}}{\partial y} \exp(-i2\omega t)\right] = 0$$

Therefore, the solution for $u_1(x,y,t)$ to a second approximation will be the solution given in Chapter II plus the additional component REAL $[u_{12}(x,y) \cdot \exp(-i2\omega t)]$.

Solution for $u_{12}(x,y)$. The function $u_{12}(x,y)$ can now be determined from equation C.12 as follows:

Equation C.12 will first be rewritten as

$$\nu_o \frac{\partial^2 u_{12}}{\partial y^2} + i2\omega\, u_{12} = u_{11} \frac{\partial u_{11}}{\partial x} + v_{11} \frac{\partial u_{11}}{\partial y} \qquad (C.26)$$

since $p_{12} = 0$.

If the expressions for $u_{11}(x,y)$ and $v_{11}(x,y)$ are substituted into equation C.26 and the definition of δ_{ac} is introduced, then equation C.26 becomes

$$\frac{\partial^2 u_{12}}{\partial y'^2} + 4\, i\, u_{12} = U_o M_o \sin(2\omega x/c_o)[1 - \exp\{-(1-i)\, y'\}] \qquad (C.27)$$

where $$y' = y/\delta_{ac}$$

At this point in the analysis it is necessary to make an additional assumption. It is assumed that the complex coefficient, $u_{12}(x,y)$, is of the form

$$u_{12}(x,y') = X_2(x)\, Y_2(y') \qquad (C.28)$$

and, therefore, equation C.27 becomes

$$Y_2'' + 4\, i\, Y_2 = U_o M_o \sin(2\omega x/c_o)[1 - \exp\{-(1-i)\, y'\}]/X_2 \qquad (C.29)$$

Equation C.29 will be valid only if the function $X_2(x)$ is a constant multiple of $\sin(2\omega x/c_o)$. For simplicity, $X_2(x)$ will be taken as

$$X_2(x) = U_o M_o \sin(2\omega x/c_o) \quad . \tag{C.30}$$

Thus equation C.29 becomes

$$Y_2'' + 4 i Y_2 = 1 - \exp\{-(1-i) y'\} \tag{C.31}$$

where the prime notation represents differentiation with respect to y'. The general solution of equation C.31 is

$$\begin{aligned} Y_2(y') = {} & (c_1 + i c_2) \exp[\sqrt{2}(1-i) y'] \\ & + (d_1 + i d_2) \exp[-\sqrt{2}(1-i) y'] \\ & + i/4 \{1 - 2 \exp[-(1-i) y']\} \quad . \end{aligned} \tag{C.32}$$

Finally, the expression for $\mathrm{REAL}[u_{12}(x,y) \exp(-i2\omega t)]$ becomes

$$\begin{aligned} \mathrm{REAL}[u_{12}(x,y) \exp(-i2\omega t)] = {} & U_o M_o \sin(2\omega x/c_o) \cdot \\ & \{\exp(\sqrt{2} y')[c_1 \cos(2\omega t + \sqrt{2} y') + c_2 \sin(2\omega t + \sqrt{2} y')] \\ & + \exp(-\sqrt{2} y')[d_1 \cos(2\omega t - \sqrt{2} y') + d_2 \sin(2\omega t - \sqrt{2} y')] \\ & + \tfrac{1}{4} [\sin(2\omega t) - 2 \exp(-y') \sin(2\omega t - y')]\} \end{aligned} \tag{C.33}$$

If equations C.24 and C.25 are applied to equation C.33 and if the terms which are of the order of magnitude of $\exp(-a/\delta_{ac})$ or less are assumed to be zero, then the following values for the coefficients c_1, c_2, d_1 and d_2 are obtained:

$$c_1 = c_2 = d_1 = 0 \ , \quad d_2 = 1/4 \tag{C.34}$$

With these simplifications, equation C.33 becomes

$$\begin{aligned} \mathrm{REAL}[u_{12}(x,y)\ \exp(-i2\omega t)] \ = \ & \tfrac{1}{4}\, U_o M_o\, \sin(2\omega x/c_o)\ [\sin(2\omega t) \\ & + \exp(-\sqrt{2}\ y')\ \sin(2\omega t - \sqrt{2}\ y') \\ & - 2\ \exp(-y')\ \sin(2\omega t - y')] \end{aligned} \tag{C.35}$$

and finally, the x-component of the time-dependent velocity to a second approximation in dimensionless form becomes

$$\begin{aligned} u_1'(x',y',t') \ = \ & -\cos(\pi x')\ [\cos(\pi t') \\ & - \exp(-y')\ \cos(\pi t' - y')] \\ & + \frac{M_o}{4}\ \sin(2\pi x')\ [\sin(2\pi t') \\ & + \exp(-\sqrt{2}\ y')\ \sin(2\pi t' - \sqrt{2}\ y') \\ & - 2\ \exp(-y')\ \sin(2\pi t' - y')] \end{aligned} \tag{C.36}$$

It can be seen from equation C.36 that it is unnecessary to determine the time-dependent velocities to a second approximation since the contribution of the second harmonic term is of the order of magnitude of δ in comparison to the first harmonic term.

The y-component of the time-dependent velocity can be determined by subjecting the solution of equation C.11 to the boundary conditions given in equations C.24 and C.25.

LITERATURE CITED

(1) T. W. Jackson, K. R. Purdy and C. C. Oliver, "The Effects of Resonant Acoustic Vibrations on the Nusselt Number for a Constant Temperature Horizontal Tube", Second International Heat Transfer Conference, (August 1961).

(2) Ian Eastwood, T. W. Jackson, C. C. Oliver and K. R. Purdy, "Heat Transfer Threshold Values for Resonant Acoustic Vibrations in a Horizontal Isothermal Tube", ARL Technical Report 62-326, Aeronautical Research Laboratories, (1962).

(3) J. V. Sanders, "A Photomultiplier-Schlieren for Acoustic Measurement and Some Investigations of the Kundt's Tube", Dissertation Abstracts, (February 1962).

(4) R. M. Fand and J. Kaye, "The Effect of High Intensity Stationary and Progressive Sound Fields on Free Convection From a Horizontal Cylinder", WADC Technical Note 59-18, Wright Air Development Center, (1959).

(5) Lord Rayleigh, "On the Circulation of Air Observed in Kundt's Tubes and On Some Allied Acoustical Problems", Philosophical Transactions of the Royal Society of London, 175, Part I, (1883), p. 1.

(6) V. Dvorak, "Ueber einige neue Staubfiguren", Annalen der Physik, 3, (1874), p. 102; and "Ueber die akustische Anziehung und Abstossung", Ann. Physik, 7, (1876), p. 42.

(7) P. J. Westervelt, "The Theory of Steady Rotational Flow Generated by a Sound Field", Journal of the Acoustical Society of America, 25, (1953), p. 60.

(8) E. N. da C. Andrade, "On the Circulations Caused by the Vibrations of Air in a Tube", Proceedings of the Royal Society of London, Series A, 134, (1932), p. 445.

(9) W. Koenig, "Hydrodynamisch-akustische Untersuchungen", Ann. Physik, 42, (1891), p. 353.

(10) Lewis Laboratory Staff, "A Summary of Preliminary Investigations Into the Characteristics of Combustion Screech in Ducted Burners", NACA Report 1384, National Advisory Committee for Aeronautics, (1958).

(11) T. W. Jackson, W. B. Harrison and W. C. Boteler, "Free Convection, Forced Convection, and Acoustic Vibrations in a Constant Temperature Vertical Tube", Transactions of the American Society of Mechanical Engineers, Series C, 81, (1959), p. 68.

(12) C. C. Lin, "Motion in the Boundary Layer With a Rapidly Oscillating External Flow", 9th International Congress of Applied Mechanics, University of Brussels, Belgium, 4, (1956), p. 155.

(13) T. W. Jackson and H. L. Johnson, "Convective Flow Due to Acoustic Vibrations in Horizontal Resonant Tubes", AFOSR Technical Report 60-52, Air Force Office of Scientific Research, (1960).

(14) P. M. Morse, Vibrations and Sound, second edition, New York: McGraw-Hill Book Co., Inc., (1948).

(15) A. P. G. Peterson and L. L. Beranek, Handbook of Noise Measurement, General Radio Company, (1956).

(16) R. M. Rotty, Introduction to Gas Dynamics, New York: John Wiley and Sons, Inc., (1962).

(17) H. W. Liepman and A. Roshko, Elements of Gasdynamics, New York: John Wiley and Sons, Inc., (1957).

VITA

Kenneth Rodman Purdy was born in New Rochelle, New York, on October 16, 1933. He attended elementary schools in New Rochelle and in West Palm Beach, Florida, and was graduated from Palm Beach High School in 1952. He entered the Georgia Institute of Technology in the same year and was graduated in 1956, receiving the degree of Bachelor of Mechanical Engineering. After graduation, he was employed by Georgia Tech as an Instructor in Mechanical Engineering until he received the degree of Master of Science in Mechanical Engineering in 1959. At this time he was promoted to his present position of Assistant Professor.

Mr. Purdy was married in 1954 to the former Nancy Berry Beam. They have a daughter, Linda Leigh, and a son, Kenneth Jeffrey.